

Aggregation-Induced Emission: The Whole Is More Brilliant than the Parts

Ju Mei, Yuning Hong, Jacky W. Y. Lam, Anjun Qin, Youhong Tang, and Ben Zhong Tang*

"United we stand, divided we fall."—Aesop.

Aggregation-induced emission (AIE) refers to a photophysical phenomenon shown by a group of luminogenic materials that are non-emissive when they are dissolved in good solvents as molecules but become highly luminescent when they are clustered in poor solvents or solid state as aggregates. In this Review we summarize the recent progresses made in the area of AIE research. We conduct mechanistic analyses of the AIE processes, unify the restriction of intramolecular motions (RIM) as the main cause for the AIE effects, and derive RIM-based molecular engineering strategies for the design of new AIE luminogens (AIEgens). Typical examples of the newly developed AIEgens and their high-tech applications as optoelectronic materials, chemical sensors and biomedical probes are presented and discussed.

1. Introduction

The *Oxford Dictionary* and *Wikipedia* define "aggregate" as "a whole formed by combining several separate elements" and "a collection of items that are gathered together to form a total quantity", respectively.^[1] Concrete, a widely used building

Dr. J. Mei, Dr. Y. Hong, Dr. J. W. Y. Lam, Prof. B. Z. Tang

Department of Chemistry

HKUST Jockey Club Institute for Advanced Study

Division of Life Science

Institute of Molecular Functional Materials
and Division of Biomedical Engineering

The Hong Kong University of Science

& Technology (HKUST)

Clear Water Bay

Kowloon, Hong Kong, China

E-mail: tangbenz@ust.hk

Dr. Y. Hong, Dr. J. W. Y. Lam, Prof. B. Z. Tang

HKUST Shenzhen Institute

Hi-tech Park, Nansha, Shenzhen 518057, China

Prof. A. Qin, Prof. B. Z. Tang

Guangdong Innovative Research Team

SCUT–HKUST Joint Research Laboratory

State Key Laboratory of Luminescent Materials and Devices

South China University of Technology (SCUT)

Guangzhou 51640, China

Dr. Y. Tang

Centre for NanoScale Science and Technology

Centre for Maritime Engineering, Control and Imaging

School of Computer Science, Engineering and Mathematics

Flinders University

South Australia 5042, Australia

DOI: 10.1002/adma.201401356



material, is an archetypal example of aggregate given by the Dictionary and Encyclopedia.^[1] In scientific study, aggregate often refers to a cluster or an ensemble. In the area of luminescence research, there is a notorious photophysical phenomenon called concentration quenching (CQ): emission from a solution of luminophore is quenched with an increase in concentration. The CQ effect is "common to most aromatic hydrocarbons and their derivatives", as summarized by Birks in his classic book on *Photophysics of Aromatic Molecules*.^[2] In a concentrated solution, the damage (CQ) is normally done through the "formation of aggregates"^[3] of luminophores.^[4–8] Due to its association with the luminophore aggregation, the CQ process has frequently been referred to as aggregation-caused quenching (ACQ).

Fluorescein is a prototypical ACQ fluorophore.^[9] It is soluble in water but insoluble in most organic solvents. Its molecularly dissolved solution in water emits a bright green light (upper panel in Figure 1). Its fluorescence is gradually weakened when a poor solvent (e.g., acetone) is progressively added into water. The poor miscibility of fluorescein with acetone causes an increase in the local fluorophore concentration in the water/acetone mixture. When the fraction of acetone (f_a) is increased to 60 vol%, the CQ effect becomes visually discernible. When f_a is further increased, the solvating power of the water/acetone mixture becomes so poor that many solute molecules form nanoscopic aggregates. Owing to the severe aggregate formation, the light emission of fluorescein gets completely quenched. The planar polycyclic aromatic structure of fluorescein enables its molecules to pack well in the aggregates. The π - π stacking interaction between the solute molecules prompts the formation of such detrimental species as excimers, resulting in the observed ACQ effect. The powders of fluorescein do not emit light at all, showing a marked ACQ effect in the solid state.

The ubiquitous ACQ effect has prevented many lead compounds identified by the solution-screening processes in research laboratories from finding real-word technological applications in an engineering viable and robust form, because a light emitter is practically often used as a whole (aggregate), rather than separate elements (individual molecules).^[9–18] For example, luminophores have been used as sensors to detect bioactive molecules in physiological media and as probes to

monitor ionic species in ecological systems.^[9,11,12] Although polar functional units (e.g., carboxylic and sulfonic acids) can be introduced into hydrophobic chromophores (e.g., polynuclear aromatic rings) to increase their hydrophilicity, the resultant water-miscible luminophores are still prone to form aggregates in the aqueous media, due to the unalterable hydrophobicity of their π -conjugated cores. The ACQ effect is also a thorny problem for the fabrication of efficient optoelectronic devices such as organic light-emitting diodes, in which the luminophores are commonly used in the aggregate state as thin solid films.^[10]

Evidently, ACQ is a harmful photophysical effect in terms of light emission and practical applications. Another photophysical phenomenon associated with chromogen aggregation is aggregation-induced emission (AIE), which is opposite to the ACQ phenomenon.^[19] In the AIE process, weakly luminescent chromogens are induced to emit efficiently by the aggregate formation. A number of luminogenic molecules with propeller-shaped structures have been found to show pronounced AIE effect.^[19–21] Such luminogens with AIE attribute have been referred to as AIEgens (like in the case of liquid crystals, where rod-like molecules showing mesomorphism are named as mesogens). A typical example of AIEgen is shown in the lower panel of Figure 1. Hexaphenylsilole (HPS) is non-emissive when its molecules are dissolved in a good solvent, such as tetrahydrofuran (THF) or a THF/water mixture with a fraction of water (f_w) lower than 80 vol%. Its fluorescence is turned on when f_w reaches ca. 80 vol%. It becomes highly fluorescent at $f_w = 90$ vol%, thanks to the heavy aggregation of the HPS molecules in the aqueous mixture with poor solvating power.

In the AIE system, the aggregates (*the whole*) are more brilliant than the individuals (*the parts*), whereas in the ACQ system the reverse is true—the parts are more luminescent than the whole (cf., Figure 1). Normally, quantity–effect relationship is directly proportional: e.g., a sugar solution with a higher concentration is sweeter. In this sense, the AIE effect follows the general collective quantity–effect rule. Photophysical processes in dilute solutions have been extensively researched; in contrast, luminescence behaviors in aggregate state have been much less studied. The AIE effect provides a large platform for researchers to look into light-emitting processes from luminogen aggregates, from which information on structure–property relationships and insights into working mechanisms of luminescence processes in aggregate state may be gained.^[21–27] Since AIE is a photophysical effect on the luminescence process in the practically useful solid state, AIE research may lead to hitherto impossible technological innovations.

Since ACQ is a detrimental effect, researchers have taken various chemical, physical and engineering approaches to deter luminophore molecules from forming aggregates.^[14–18] For example, bulky cyclics, spiral kinks and dendritic wedges have been covalently attached to luminophore cores to obstruct aggregate formation. These approaches, however, have often ended up with a frustrating outcome: the old issue is partially solved at the cost of creating new problems. In many cases, the aggregation can only be temporarily hampered to certain extents, because aggregate formation is a natural process for the luminogen molecules located in close proximity. In sharp



Anjun Qin received his BS and PhD degrees from Shanxi University and Chinese Academy of Sciences in 1999 and 2004, respectively. He did his postdoctoral research at HKUST and Zhejiang University in 2005–2008. He joined Zhejiang University as an Associate Professor in 2008 and moved to SCUT with promotion to Full Professor in 2013. He was awarded the National Science Fund for Excellent Young Scholars in 2012.



Youhong Tang received his BS and PhD degrees from Wuhan University of Technology and HKUST in 2000 and 2007, respectively. He worked as a Research Associate at HKUST in 2007–2009 and an Associate Professor at SCUT in 2009–2011. After a brief stay at University of Sydney as an ARC-DECRA Fellow, he joined Flinders University as a Lecturer in 2012 and is now a Research Leader of Flinders NanoScale Science & Technology Program.



Ben Zhong Tang received his BS and PhD degrees from SCUT and Kyoto University in 1982 and 1988, respectively. He conducted his postdoctoral work at University of Toronto and worked as a senior scientist in Neos Co., Ltd. in 1989–1994. He joined HKUST in 1994 and was promoted to Chair Professor in 2008. He is serving as a News Contributor to *Noteworthy Chemistry* (ACS) and Editor-in-Chief of *Polymer Chemistry Series* and Associate Editor of *Polymer Chemistry* (RSC).

contrast, AIE is a constructive effect. The AIE effect makes it possible to actively utilize the aggregation process, instead of passively working against it, as people have done about the ACQ effect.

In the past decade, many research groups have enthusiastically worked on the decipherment of AIE mechanisms, design of new AIEgens, manipulation of their morphological structures, and exploration of their technological applications. The dynamic research has resulted in the collection of a wealth of

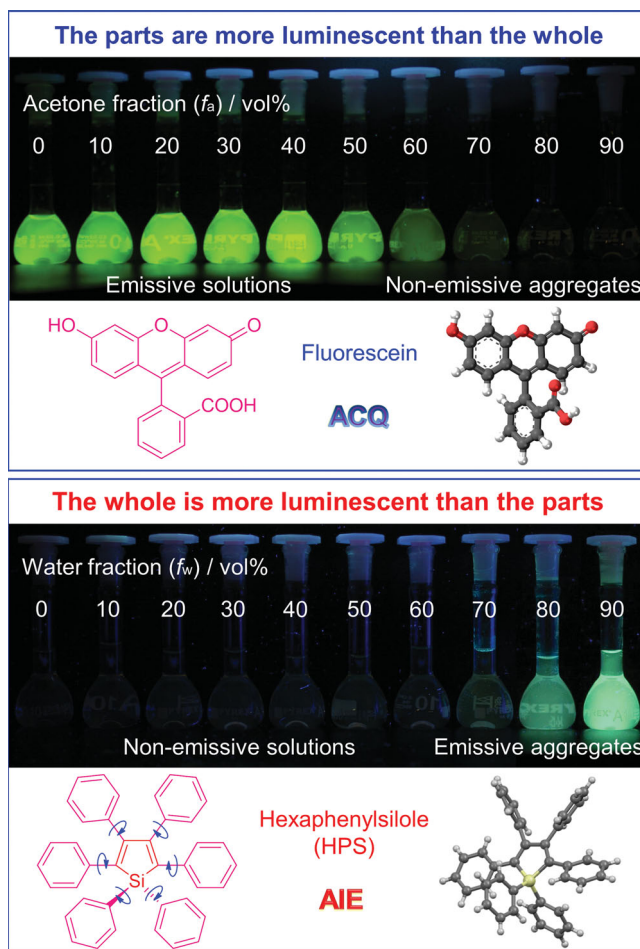


Figure 1. Fluorescence photographs of solutions and suspensions of (upper panel) fluorescein (15 μ M) in water/acetone mixtures with different fractions of acetone (f_a) and (lower panel) hexaphenylsilole (HPS; 20 μ M) in THF/water mixtures with different fractions of water (f_w). The crystal structure of HPS is retrieved free of charge from the Cambridge Crystallographic Data Centre (CCDC-195948) via www.ccdc.cam.ac.uk.

mechanistic insights, development of a variety of new AIEgens, and demonstration of a number of practical applications.^[27–35] In this Review, we will summarize the progress made in the area of AIE research in the recent years. We will first examine the operating hypotheses for the AIE processes, in an effort to clarify and unify their working mechanisms and to derive structural design strategies for creating new AIEgens. We will then present some typical examples of the new AIEgens developed according to the mechanism of restriction of intramolecular motions (RIM), followed by the discussion on potential high-tech applications by making use of the AIE effect.

2. Mechanistic Discussion

A correct decipherment of AIE mechanisms is of crucial importance, for it will help deepen our understanding of luminescence processes and guide our molecular engineering endeavors to develop new AIE systems. An AIE process may mechanistically be associated with such pathways as restriction

of intramolecular rotation (RIR),^[36] J-aggregate formation (JAF),^[2] twisted intramolecular charge transfer (TICT),^[28,29] and excited-state intramolecular proton transfer (ESIPT).^[30–35] In this Section, we will carry out a study of mechanistic comparison. We will try to piece together the scraps of scattered information on various AIE mechanisms proposed by different research teams, in an effort to draw a clear picture on the light emission processes and unify the multifarious hypotheses into a uniform model. Special efforts will be made to learn how the structural aspects, such as conformational and morphological variations, influence light-emitting behaviors of the AIEgens.

2.1. Restriction of Intramolecular Motions

Fundamental physics teaches us that any movement, whether it is microscopic or macroscopic, consumes energy. Molecular motions include rotations and vibrations. As stated above, HPS is an emblematic AIEgen. In this luminogen, six phenyl peripheries are tethered to a silole core. The phenyl rings can dynamically rotate against the silole stator on the single-bond axes.^[36] Tetraphenylethene (TPE) is another well-studied AIEgen (Figure 2), which has an apparently different but intrinsically same configuration as HPS. In TPE, four phenyl rings are linked to a central ethene rod through single bonds. The phenyl rings have great freedom to rotate or twist against the ethene stator. The isolated molecules of TPE in a dilute solution can undergo active intramolecular rotations, which serves as a relaxation channel for the excited states to non-radiatively decay to the ground state. In aggregate state, however, the intramolecular rotations are restricted due to the involved physical constraint, which blocks the radiationless relaxation channel and opens the radiative decay pathway.

The above analysis implies that the RIR process is responsible for the AIE phenomena of molecular rotor systems. To check whether this is true, a series of control experiments have been performed to externally and internally modulate the intramolecular rotations. Using HPS as a model AIEgen, the changes in its luminescence have been studied by carrying out such external control experiments as increasing solvent viscosity, decreasing solution temperature, and pressurizing solid film. It has been found that HPS emits more efficiently in more viscous solvent, at lower temperature, and under higher pressure, which verifies that the RIR process is indeed a cause for the AIE effect of HPS.^[36–38] When the intramolecular rotations of the aromatic rings are hindered by such internal control experiments as introducing sterically bulky groups and cross-locking with tethering units, the emission of the AIEgen is enhanced. Theoretical calculations and simulations on the low-frequency intramolecular motions also support the RIR mechanism.^[39–42]

Although many AIE systems can be readily explained by the RIR mechanism,^[33] some AIE systems, such as the one shown in the lower panel of Figure 2, cannot be fully interpreted by the RIR process, as 10,10',11,11'-tetrahydro-5,5'-bibenzol[*a,d*][7]annulenylidene (THBA or 1) carries no any rotatory elements.^[43] The THBA molecule may be viewed as composed of two flexible parts, in each of which two phenyl rings are connected by a bendable flexure. These two parts are non-coplanar

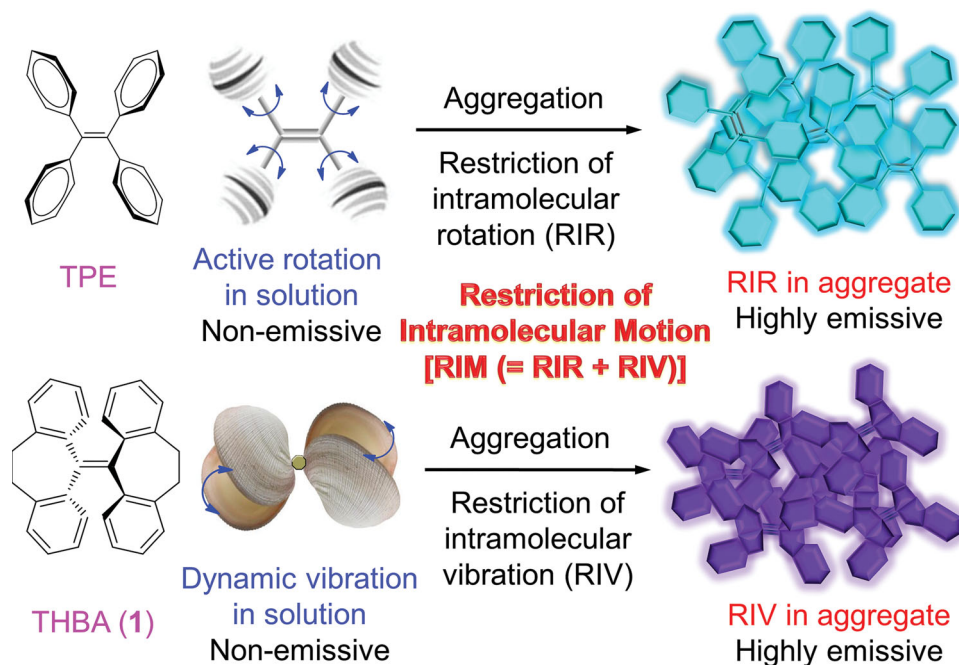


Figure 2. Propeller-shaped luminogen of tetraphenylethene (TPE) is non-luminescent in a dilute solution but becomes emissive when its molecules are aggregated, due to the restriction of intramolecular rotation (RIR) of its phenyl rotors against its ethylene stator in the aggregate state. Shell-like luminogen of 10,10',11,11'-tetrahydro-5,5'-bidibenzo[*a,d*][7]annulenylidene (THBA; **1**) behaves similarly, due to the restriction of intramolecular vibration (RIV) of its bendable vibrators in the aggregate state.

and the whole molecule adopts an *anti*-conformation. The flexibility of the flexure allows the phenyl rings of THBA to dynamically bend or vibrate in the solution state, which serves as a relaxation pathway for its excited states to non-radiatively decay. The intramolecular vibration of THBA is in some sense like the breathing movement of a clam or scallop, as illustrated by the cartoon shown in the lower panel of Figure 2. Upon aggregate formation, owing to the physical constraint associated with the space limitation, the intramolecular vibrations become restricted. As a result, the radiationless pathway is blocked and the radiative decay channel is opened, which renders THBA emissive in the aggregate state.

From the above discussions on the two examples given in Figure 2 and on the basis of the experimental data and theoretical simulations reported in the literature, it can be concluded that the RIR and restriction of intramolecular vibrations (RIV) are the main causes for the AIE phenomena observed in the propeller-shaped and shell-like luminogen systems, respectively. Putting the individual cases together gives a unified general picture that the RIM processes mechanistically account for all the AIE systems developed so far.^[27–35]

For the propeller-shaped AIEgens like silole derivatives that cannot undergo photo-induced *E*-*Z* isomerization (EZI) processes, the active intramolecular rotations of their aromatic rotors undoubtedly plays a major role in quenching their luminescence processes in the solution state. For the AIEgens based on TPE derivatives, however, the case is more complicated. The issue involved here is whether the EZI^[44–48] or RIR^[36] mechanism plays a predominant role in their solution luminescence quenching processes. The EZI mechanism advocates that the excited states of TPE are non-radiatively annihilated by the EZI

process in the solution state and that the decreased probability of the EZI process in the aggregate state sets off an increase in the luminescence efficiency.^[44–48] The RIR mechanism, on the other hand, states that the solution emission of TPE is quenched by the active intramolecular rotations of its phenyl rotors against its ethene stator. The formation of aggregates of TPE molecules suppresses their molecular motions and rigidifies their molecular structure, which activate the radiative decay channel and make the TPE molecules emissive in the aggregate state.

Study of the EZI process needs to use samples of pure *E* and *Z* stereoisomers of an olefinic luminogen, whose synthesis, isolation and purification, however, have been difficult. In an effort to investigate the EZI process, triazole groups are introduced into the TPE skeleton by a facile click reaction to enlarge difference between the conformers and to achieve separability on the macroscopic level (Figure 3a).^[49] The pure stereoisomers (*E*)-2 and (*Z*)-2 were readily obtained by simple silica-gel column chromatography. Like their parent form (TPE), both the isomers exhibit marked AIE effect. In the ¹H NMR spectra, many of the resonance peaks of the *E* isomer are shifted down-field as compared with those of its *Z* counterpart. The most distinguishing spectral difference lies in the chemical shift region of δ 7.04–7.14. The *E* isomer resonates at δ 7.09, where the *Z* isomer is silent. On the other hand, the *Z* isomer displays a large resonance peak at δ ~ 7.06. These spectral differences make it possible to utilize NMR spectroscopy to follow conformational changes of the stereoisomers induced by photoirradiation.

The NMR spectral changes reveal that (*Z*)-2 can be readily generated by irradiation of (*E*)-2 with a high power UV lamp (1.10 mW/cm²). The fraction of *Z*-isomer in the photogenerated

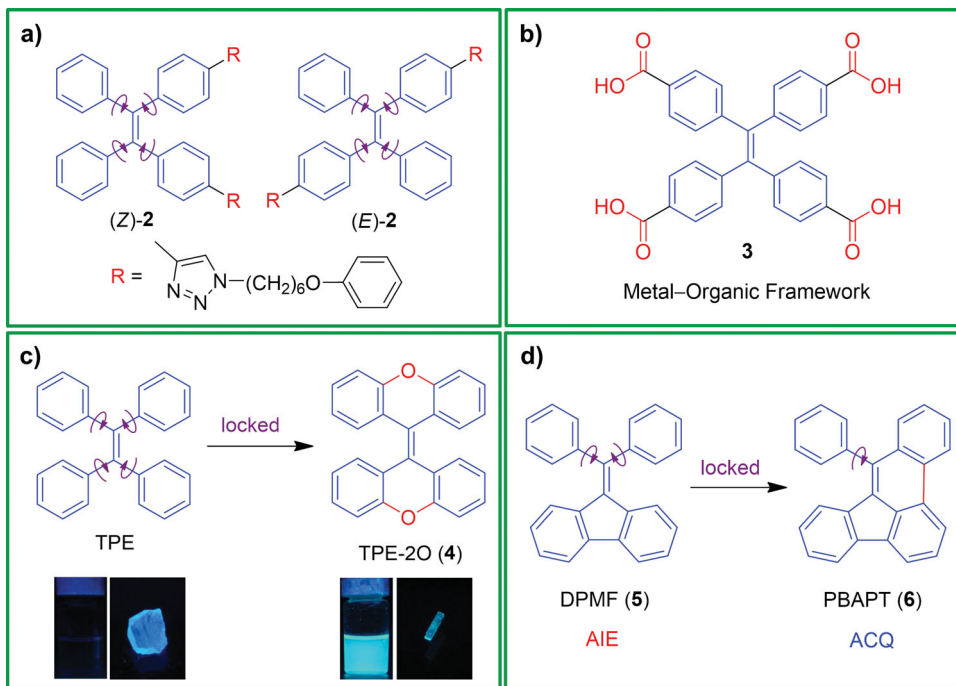


Figure 3. (a) The photoinduced conformational changes of the pure stereoisomers of a TPE derivative (**2**) monitored by NMR substantiate that RIR is a main cause for AIE. (b) The RIR process activated by coordination bonding turns on emission of the metal–organic framework of TPE derivative **3**. (c) Locking the phenyl rotors of TPE by covalent bonding makes it AIE inactive. Reproduced with permission.^[52] Copyright 2012, Royal Society of Chemistry. (d) Locking one of the phenyl rings of 9-(diphenylmethylene)-9H-fluorene (DPMF; **5**) causes the AIE-to-ACQ transformation.

E/Z mixture steadily increases to 35% almost in a linear fashion in the first 50 min irradiation. Afterwards, the EZI process slows down, with the *Z* fraction reaching ~50% at 150 min. The *Z* isomer can also be generated by heating the *E* isomer at a high temperature (203 °C). These data indubitably indicate that the EZI process can be activated by the irradiation with a high power UV lamp irradiation or a high temperature annealing. In a photoluminescence (PL) spectrum measurement, however, a spectrofluorometer is operating at much lower power (~52 μW/cm²) and temperature (room temperature or ~20 °C). To answer the question whether the EZI process takes place under the mild conditions, an (*E*)-**2** solution is exposed to continuous irradiation of the xenon lamp in the spectrofluorometer for 30 min ($\lambda_{\text{ex}} = 332$ nm). The ¹H NMR spectra of the sample before and after irradiation are practically identical, indicating that the EZI process has not occurred. Similar results are obtained for the *Z* conformer.^[49]

The AIE processes of all the AIE systems, including the TPE derivatives, have ordinarily been investigated under the conditions of PL spectral measurement or under the excitation of a xenon lamp with a low power at ambient temperature for a little while (usually less than 1 min). As understood from the data discussed above, the EZI processes of (*E*)- and (*Z*)-**2** do not take place even after being irradiated for a much longer time (i.e., 30 min). Clearly, EZI does not play a role, at least not to an appreciable extent, in the AIE process. The C=C bond can hardly be broken down by the low power of the xenon lamp, and hence the critical initial step for the EZI process cannot occur. Thus the luminescence of **2** in the solution state is not quenched by the EZI process, instead mainly by the photo-

activated intramolecular rotations of the aromatic rotors. The greatly enhanced solid-state light emission is primarily resulted from the restricted motions of the multiple phenyl rotors. In other words, the RIR process is the predominant mechanistic cause for the AIE effects of the TPE-based AIEgens.

In general, AIE arises because rotor-carrying luminogens undergo low-frequency twisting and torsional motions in dilute solutions. These vibrational modes account for the very fast radiationless decay of singlet excited states but are restricted in aggregate state as a result of intermolecular interactions. For example, TPE displays low-frequency phenyl torsion modes which are largely hampered in the aggregates by the steric hindrance between the interfacing hydrogen atoms or the neighboring phenyl rings. Dinca et al. have conducted some studies to uncover the mechanism that induces fluorescence in the metal–organic frameworks (MOFs) based on TPE derivatives (Figure 3b).^[50] The coordination of the phenyl groups with the metal atoms within the MOFs is found to turn on fluorescence of the TPE cores. The metal complex, Zn₂(**3**)(solvent)₂, displays arene···H and Ph···Ph interactions between the neighboring TPE cores whose distances are 1.5 Å longer than those in the molecular TPE nanoaggregates. Though these distances may allow the phenyl rings to rotate or flip, the MOF is still emissive.

Since the carboxylate groups in **3** are in the *para* positions, the flipping of the phenyl rings in **3** may have not been completely restricted. To see whether this is the case, a deuterated TPE-based MOF with analogous structure to Zn₂(**3**)(solvent)₂ is synthesized for the sake of NMR measurement. The ²H NMR spectroscopy and ¹³C cross-polarized magic angle spinning solid-state NMR spectroscopy are employed to investigate the

phenyl ring dynamics of the TPE cores that are coordinately trapped inside a MOF matrix. The energy barrier for a phenyl ring flipping is found to be 43(6) kJ/mol. Evidently, the phenyl ring flipping or torsion energy is not low in this coordination complex. The intramolecular motions are thus partly restricted and a portion of radiationless decay is blocked, which explains why the MOF is emissive.^[50]

The electronic and steric contributions to this flipping barrier are investigated by means of density functional theory (DFT) calculations. The study suggests that the torsion of the phenyl rings and the twisting of the olefinic C=C bond are both involved in quenching the light emission of the TPE derivative. The results build a relation between the two modes of motions: diminution of the C=C twisting angle results in a large steric barrier for the torsion or flipping of the phenyl rings, implying that a relatively large C=C twisting angle or flexible core is required for a low-barrier phenyl ring torsional motion. Such fundamental mechanistic study of the AIE effect of TPE on the basis of MOF is of guiding value for the development of tunable luminescence turn-on porous sensors constructed from AIEgens.^[50]

The construction of MOFs by taking advantage of the coordination effect of functionalized AIEgens and metallic elements can be regarded as a way to activate the RIM processes of the AIEgens. But owing to the relatively large interspaces and free volumes in the MOFs, this approach can only partially restrict the intramolecular motions. In order to provide more solid proof to the RIM mechanism, the motions of AIEgen rotors should be more rigidly controlled. The most direct and effective way to restrict intramolecular motions is to lock the rotors of an AIEgen through covalent bonding.^[51–54] Dong et al. have worked on conveniently locking the phenyl rings of TPE with “O” bridges by McMurry coupling (Figure 3c).^[52] The emission spectrum and fluorescence quantum yield (Φ_F) of the solution of TPE-2O (4) agree well with those of its crystal due to its fully locked phenyl rings and twisted conformation. As shown in Figure 3c, TPE is nearly non-emissive in dilute solution. However, the solution of 4 emits an intense sky blue light in a high Φ_F (30.1%). The greatly increased emission intensity of the isolated species of 4 as compared to TPE is due to the lockage of the phenyl rings of 4 by the “O” bridges, which hinders the radiationless decay caused by the intramolecular rotations of the phenyl rotors.

The steady-state spectral data indicate that the introduction of the “O” bridges greatly alters the dynamics of the excited states of 4. The excited species of 4 in solution relax much more slowly ($\tau = 5.14$ ns) than TPE ($\tau < 0.1$ ns). The crystals of TPE are highly fluorescent ($\Phi_F = 24.6\%$, $\tau = 3.9$ ns), owing to the blockage of its radiationless pathway by the RIR process in the crystalline state. However, the crystals of 4 show a Φ_F value of 30.8%, nearly the same as that of its solution, exhibiting no AIE activity. Because the rotations of its phenyl rings are already locked by the two “O” bridges, the RIR process does not work in the crystalline state and hence its emission is not enhanced. Although the rotations of the phenyl rings of TPE are hindered by the two “O” linkages, the resultant luminophore 4 is not transformed into an ACQ system. This is because 4 still adopts a twisted conformation and its molecules cannot be closely packed to form harmful species such as excimers. AIEgen 5 shown in Figure 3d, however, can be transformed into an ACQ

system when its rotatory units are covalently locked, due to the close interaction between the flat discotic benzo[e]acephenanthrylene plates in the molecules of the resultant luminophore 8-phenylbenzo[e]acephenanthrylene (6).^[23,53,54]

In addition to the experimental data, theoretical calculations and computational simulations have also been used to understand the AIE processes and predict new AIE structures. Using the vibration correlation function formalism coupled with first-principles calculations under displaced/distorted harmonic oscillator approximation, the radiative and radiationless decay processes of AIEgens have been studied.^[39,40] The important role of the mode mixing caused by the Duschinsky rotation in radiationless decay process has been clarified. The solid-state packing effects on the radiative and non-radiative decays have been revealed by a combined quantum mechanics and classical molecular mechanics (QM/MM) study. These investigations provide supportive evidences to the RIM process and clearly define the role of low-frequency motions in the radiationless decay processes.^[55,56] The aggregation tends to significantly slow down the non-radiative relaxation process and populate the radiative decay species.

However, for low-frequency vibration, not only Duschinsky rotation and mode distortion must be considered, anharmonicity should also be taken into account. In addition, microscopic access to detailed motions and interactions from a dynamic point of view is highly desirable. To this end, Shuai's group takes a non-adiabatic dynamic approach based on the incorporation of time-dependent Kohn-Sham (TDKS) and density functional with tight binding (DFTB) methods with Tully's fewest switches surface hopping (FSSH) algorithm to investigate the non-radiative decay processes of the excited states of 5 and 6 in details.^[54] The simulation confirms that 5 shows exotic AIE activity, in sharp contrast to the normal ACQ behavior of 6. From the geometry optimization in the ground (S_0) and excited (S_1) singlet states, it is found that in both 5 and 6, the major bond length modifications appear in the dibenzofulvene ring. Typical dihedral angle changes in 5 are about 20°, whereas in 6 the dihedral angles do not experience any significant alteration. In 5, the major contribution to the reorganization energy from the vibrational mode relaxation is from the low-frequency twisting modes, but the high-frequency stretching modes are more important in 6.

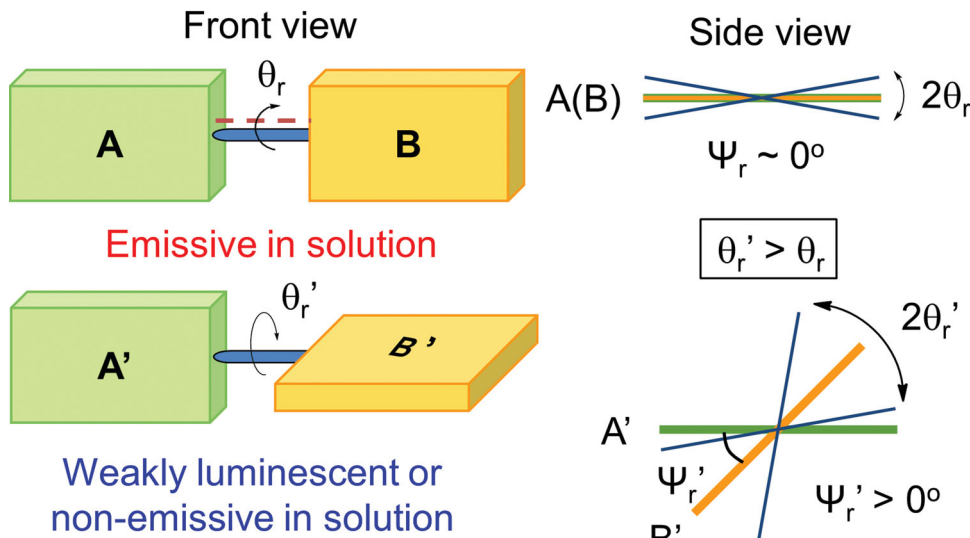
In general, the larger the reorganization energy is, the more important the mode is in terms of consuming energy by the non-radiative decay process. Thus during the radiationless decay process, 5 undergoes larger changes in the energy gap and faster decay rates than 6. In other words, the low-frequency twisting motion in 5 couples strongly with the electronic excitation and dissipates the energy efficiently by a fast decay rate (1.4 ps), while in the locked molecule 6, such motion is hindered by the covalent bond with a much slower decay rate (24.5 ps). On the basis of this theoretical work, it is believed that in the aggregate state, the low-frequency motions of 5 are hampered and the energy dissipation pathway by the non-radiative decay is slowed down, leading to a remarkable AIE effect. The above evidences and insights obtained from the experimental investigations and the theoretical calculations further corroborate the RIM, especially the RIR, process as a main mechanistic cause for the AIE phenomena.^[57–59]

Theoretically, any luminophore molecule can undergo intramolecular rotation, but why is not every molecule AIE active? To answer this question, it is necessary to use the simple model elaborated by us in our previous review article.^[29a] Figure 4a illustrates the correlation among the geometrical planarity, conformational flexibility, intramolecular motion, and light emission behavior. A luminescent molecule is simplified as comprising of two chromophore units A and B through the linkage of a rotatable bond, for example, a C–C single bond. In the diagram, θ_r and Ψ_r denote the extent of intramolecular motion

and the dihedral angle between units A and B, respectively. In other words, θ_r specifies the structural flexibility or rigidity of a molecule, whilst Ψ_r serves as an indicator for its conformational planarity.

For many conventional ACQ molecules, chromophoric units A and B are aligned in almost parallel fashion ($\Psi_r \sim 0^\circ$). Such molecule (A–B) enjoys a maximal electronic conjugation and a minimal potential energy, as shown in Figure 4a. The C–C linkage is endowed with some pseudo-double-bond character by the extended cross-chromophore π -electronic delocalization.

a) Restriction of Intramolecular Rotation (RIR)



b) Restriction of Intramolecular Vibration (RIV)

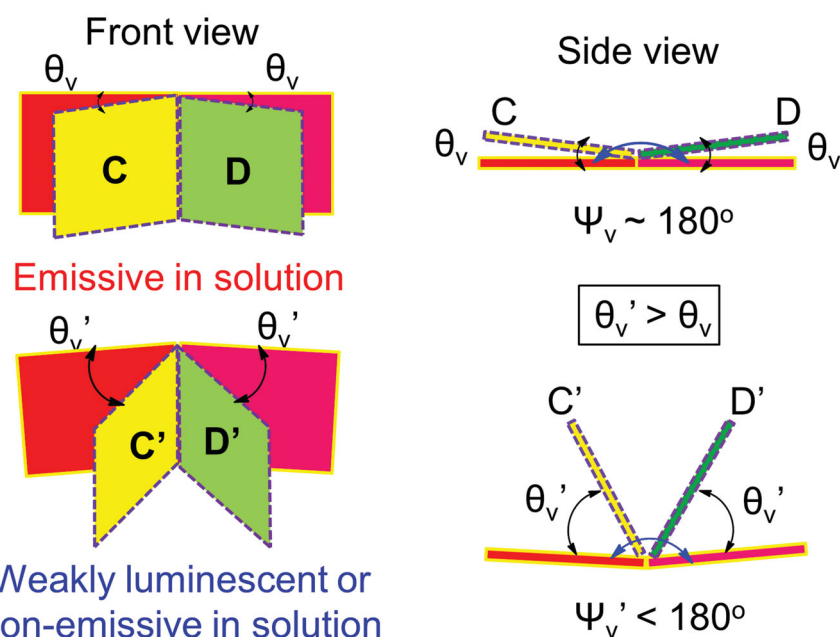


Figure 4. Diagrammatic sketch illustrating the relationships among conformational planarity, structural flexibility, intramolecular motion, and luminescence efficiency, where $\theta_r^{(\dagger)}$ and $\theta_v^{(\dagger)}$ are the rotation and vibration amplitudes, and $\Psi_r^{(\dagger)}$ and $\Psi_v^{(\dagger)}$ are the dihedral angles between chromophoric units A^(†)/B^(†) and C^(†)/D^(†), respectively. The sketch in panel a) is reproduced with permission.^[29a] Copyright 2011, Royal Society of Chemistry.

The molecular conformation is thus stiffened and its resistance against the intramolecular rotations is strengthened. Although the chromophoric units may still swing to a small extent (θ_r), the trifling low-frequency motion is insufficient to quench the luminescence process. The high-frequency vibration thereby becomes the major mode of molecular motion and the potential energy surface becomes steeper. Owing to the rigidity of the conformation, the luminophore has a small overall reorganization energy, which enables it to afford a high Φ_F in the solution state.

In contrast to ACQ molecules, the two chromophoric units A' and B' in an AIE molecule are twisted out of plane due to the involved steric effect. In this case, Ψ_r' is larger than 0° . The overlap between the π -electron clouds of the A' and B' plates becomes smaller and the cross-chromophore π -electronic conjugation becomes weaker. The C-C linkage between A' and B' units thus poses little restraint to the intramolecular rotations. Such motions now require a lower energy, in agreement with the larger contribution of the low-frequency modes to the theoretically calculated molecular motions (e.g., 5 in Figure 3d). The low-frequency energy leads to a shallower potential energy surface, meaning that there exists a little energy barrier to a conformational change. Because the θ_r' value can be varied in a much wider range (theoretically 0° – 90°), the rotational amplitude becomes larger. Much energy is therefore dissipated by the large twisting motions, resulting in a weaker emission of the luminogen in the solution state. According to such a pictorial model, luminescence behavior of a molecule in a solution can be predicted from Ψ_r (planarity) and θ_r (rotatability), where the structural stiffness plays a decisive role. The usefulness of this model has been verified by the studies of a large number of AIEgens.

However, not every AIE system can be explained by the model discussed above, such as luminogen **1** shown in Figure 2. It has no rotatory elements but its luminescence in solution is quenched. This suggests that other low-frequency motion (e.g., vibration) is responsible for the quenching process. Whilst every molecule can vibrate in various modes (e.g., bending, stretching, twisting and shearing),^[60] not every molecule is AIE active. Whether a luminogen shows AIE activity largely depends on its conformational flexibility and vibrational amplitude. To illustrate this point, a diagrammatic model is given in Figure 4b, in which the luminogen is depicted as the chromophoric units C and D linked by a junction such as an aromatic or alicyclic ring. In this graphical model, Ψ_v and θ_v define the dihedral angle between units C and D and the extent of intramolecular vibration, respectively. In other words, Ψ_v and θ_v are used here to indicate the conformational planarity of a luminogen and its structural stiffness, respectively.

When the chromophoric units C and D are coplanar to each other ($\Psi_v \sim 180^\circ$) as shown in Figure 4b, the C-D ensemble enjoys a maximal π -electronic conjugation, an example of which is the non-rotatable disc-shaped benzo[e]acephenanthrylene moiety in **6** (Figure 3d). The cross-chromophore π -electron delocalization between phenylene (C) and 9-methylene-9H-fluorene (D) units rigidifies the conformation and restrains the intramolecular vibration of units C and D. The chromophoric units may still oscillate in a small amplitude (θ_v) but the inappreciable vibration is insufficient to block the radiative decay

channel of excited species in the solution state. Due to the conformational stiffness, the luminophore has a small overall reorganization energy and can thus luminesce brightly in solution. Upon aggregation, the planarity of the C-D ensemble enables compact chromophore packing through π - π stacking interaction, which leads to the formation of deleterious species (e.g., excimers and exciplexes) and the eventual quenching of the luminescence process.

On the other hand, if the two chromophoric units C' and D' are tilted out of plane due to the non-planarity of the interchromophore linkage, as displayed in Figure 4b for the case of $\Psi_v' < 180^\circ$, the overlap between the π -electron clouds of the C' and D' plates becomes smaller and the cross-chromophore π -conjugation becomes weaker. The vibratile junction between C' and D' units imposes little constraint on their intramolecular vibration. The unperturbed motion involves lower energy and leads to a gentler potential energy surface, meaning that there is little energy barrier to a conformational change. The vibrational amplitude will be larger, as the θ_v' value can vary in a wider range. Much energy will thus be dissipated by the vigorous vibration motion, resulting in a weaker emission of the luminogen in solution. When the luminogen molecules are aggregated, the restriction to intramolecular vibration makes the aggregates highly emissive, thus showing an AIE effect.

The examples given in Figure 5 illustrate the usefulness of the models depicted in Figure 4. Luminogen **1** can be viewed as two bendable groups linked by a C=C bond. In the light of the cartoon sketch shown in the lower panel of Figure 4b, each of the two bendable groups of **1** can be regarded as a set of C'-D' unit with a cycloheptane ring as a flexure. The alicyclic flexure is not electronically conjugated with C' and D' units and the dihedral angle (Ψ_v') between C' and D' is $<180^\circ$, which endows the C' and D' units with a dynamic vibratility. In other words, as the conformation of **1** is flexible and the seven-membered cycloheptane ring can easily flip, the chromophoric units and flexure can vigorously vibrate in large amplitudes. These massive low-frequency motions can readily consume excited-state energy, resulting in a weak luminescence in solution state. Indeed, the Φ_F for the solution PL of **1** is as small as $<0.1\%$. In aggregate state, **1** becomes very emissive ($\Phi_F = 23\%$), because its intramolecular vibrations are efficiently restricted by the steric hindrance and intermolecular interaction, as revealed by the X-ray crystallography analysis.^[43]

Luminogen **7** shows the similar emission behavior. Its dilute solution is weakly fluorescent, giving a low Φ_F value of 0.5% (Figure 5). Its solid is highly emissive ($\Phi_F = 30\%$), displaying an obvious AIE effect. The difference between **1** and **7** is the structure of the flexure that hooks up the two vibratile units. The flexure in **7** is cycloheptene, which is electronically partially conjugated with the peripheral phenyl rings, and the intramolecular vibration in **7** is thus somewhat less free than in **1**. The solution of **7** is thus a bit more emissive than that of **1**. In the solid state, its less flexible conformation makes it easier to suppress the intramolecular vibrations. Its emission efficiency in solid state is accordingly increased. Like **1**, luminogen **7** is also twisted in conformation as revealed by the theoretical calculations, which makes it AIE active and ACQ silent.

The non-planar molecular conformations of luminogens **1** and **7** and their pronounced AIE effects suggest that the

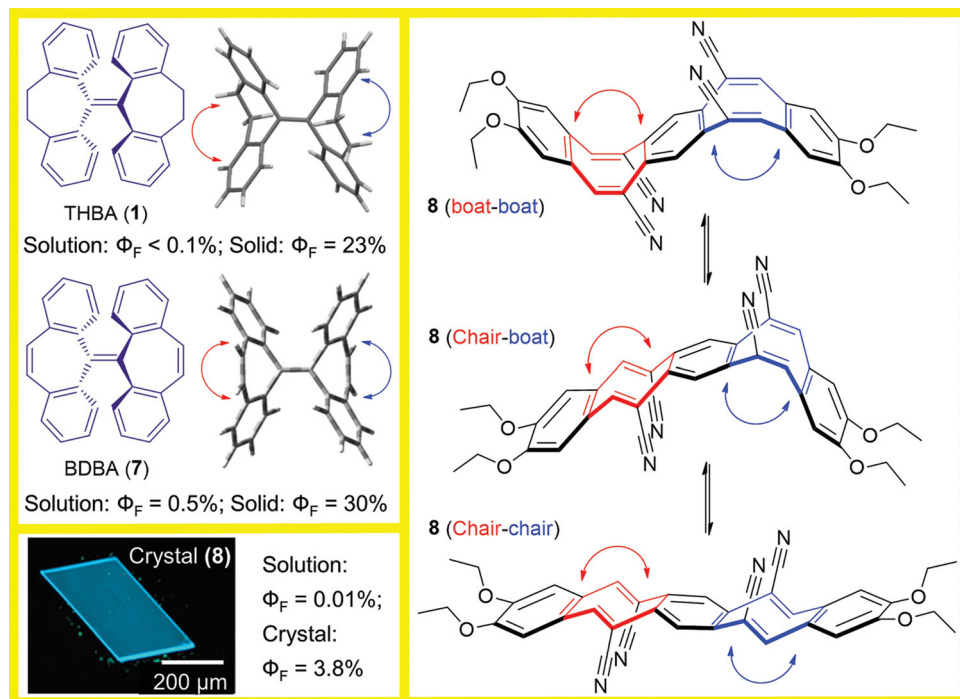


Figure 5. Examples of luminogen molecules whose AIE activities are ascribed to the process of restriction of intramolecular vibrations (RIV). Reproduced with permission.^[67] Copyright 2013, Wiley-VCH Verlag GmbH & Co. KGaA.

introduction of bendable alicyclic flexures into π -electron conjugated chromophores is a promising strategy for generating new AIEgens with 3D scaffolds. 3D π -conjugated systems like saddle-, bowl- and belt-shaped molecules have attracted considerable attention, thanks to their unique structures and properties such as concave–convex interaction and redox activity.^[61–66] Recently, Iyoda et al. have developed 3D molecular tweezers (e.g., 8) of an undulating π -surface with two readily bendable 6,9-dicyanobenzocyclooctatetraene units anchored by a benzene bay (Figure 5).^[67] The most important structural feature of 8 is its conformational flexibility. Theoretically, it has *anti* and *syn* isomeric structures with boat and chair conformations, coexisting in equilibrium in solution owing to the ring inversion of the cyclooctatetraene units. In the crystal packing revealed by the X-ray crystallographic analysis, molecules of 8 experience no π – π stacking interaction because of its bent structure.

The solution of 8 is non-emissive ($\Phi_F \sim 0.01\%$) but its crystal is fluorescent ($\lambda_{em} = 470$ nm). The Φ_F value of the latter is 380-fold higher than that of the former. The amorphous powder of 8, however, emits very weakly. The luminogen therefore shows a crystallization-induced emission (CIE) effect. In the solution state, the conformational flexibility of 8 enables active intramolecular vibrations, which dissipates its exciton energy and quenches its light emission. The *anti-to-syn* or boat-to-chair isomerization is a possible vibration mode that consumes the energy of the excited states. In the amorphous state, the molecular packing is rather loose with large void spaces for conformational changes, owing to the bulky and bent structure of 8. The intramolecular vibration remains active and the solid powder is thus still non-emissive. In the crystalline state, however, the inversions and

vibrations of 8 are effectively restricted due to the close packing, which blocks the radiationless decay pathway and activates its PL process.

It is worth pointing out that the two cyano groups on each cyclooctatetraene wing of 8 play a very important role in adjusting the structural flexibility of the whole luminogen molecule. If one cyano group is taken away from each of the two cyclooctatetraene wings, the resultant bent π system becomes nearly non-luminescent even in the crystalline state, as a result of its unsymmetrical structure and hence larger flexibility and looser packing as compared to its parent form 8. This example, together with the data for luminogens 1 and 7, proves that the RIV mechanism accounts for the AIE systems with non-planar vibrators but without multiple rotors. This opens up a new avenue for the design and development of new AIEgens. It is anticipated that under the guidance of the RIM principle, the territory of AIE systems will be greatly widened and the scope of AIE study will be significantly expanded.

2.2. Comparative Mechanistic Study

It has now become clear that the RIM processes are the major causes for the observed AIE phenomena. Luminescence can also be intensified to various extents by other mechanisms such as JAF, ESIPT and TICT. What are the mechanistic relationships between AIE system and other luminescence enhancement systems? We here discuss some examples operating in different mechanisms, in an effort to understand their differences and correlations.

2.2.1. RIM Versus JAF

Before comparing RIM with JAF, we need to find out what is the authoritative definition for J-aggregate. A literature search results in many hits but the answers are more or less the same.^[68–72] An encyclopedic definition is as follows: “A J-aggregate is a type of dye with an absorption band that shifts to a longer wavelength (a bathochromic shift) with increasing sharpness (higher absorption coefficient) when it aggregates under the influence of a solvent or additive or concentration as a result of supramolecular self-organization. The dye can be characterized further by a small Stokes shift with a narrow band.”^[72] Some researchers have considered that JAF leads to red-shifted and enhanced luminescence, thus showing AIE or aggregation-enhanced emission (AEE) effect. However, according to the definition given in the literatures, (1) a red-shifted and enhanced luminescence is not necessarily associated with J-aggregate, (2) its monomer does not need to be non-emissive, and (3) not every J-aggregate is AIE- or even AEE-active.

Dye **9** given in **Figure 6**, for example, is a perylene bisimide (PBI) derivative that can form J-aggregates under appropriate conditions. Employing temperature-dependent absorption and fluorescence spectroscopy, the optical properties of **9** in the monomeric and aggregative states are studied in different solvents.^[73] The UV-vis spectrum of **9** in dichloromethane

with an absorption maximum (λ_{ab}) of 583 nm is typical of a monomeric tetraaryloxy-substituted PBI chromophore. Its emission spectrum with a λ_{em} of 621 nm is a mirror image of its absorption spectrum. The absorption and emission bands are broad with full-width-at-half-maximums (fwhm) of 2311 and 1780 cm⁻¹, respectively. Its absorption spectrum in methylcyclohexane (MCH), however, displays a sharp, intense band with a bathochromic shift of ~13 nm from the monomer band. Its fluorescence spectrum mirrors its absorption spectrum, with a Stokes shift of merely 11 nm. Meanwhile, the fwhm values of its absorption and emission spectra are greatly reduced to 850 and 786 cm⁻¹, respectively. These spectral features clearly indicate the formation of J-aggregates of **9** in the nonpolar solvent.

In acetone and dioxane, molecules of **9** exist in monomeric form at low concentrations and high temperatures. Organogels, however, are formed in these solvents at considerably high concentrations and low temperatures. The Φ_F value for the monomeric form of **9** in the dilute dioxane solution is very high (100%). When the J-aggregates are formed in MCH, the Φ_F value is decreased to around 82%. In the gel phase in dioxane, the Φ_F value is further reduced to 20%. Therefore, while **9** undergoes JAF process in MCH, the resultant J-aggregates exhibit weaker fluorescence than its monomers. Its emission in the gel phase in dioxane is quenched to a very large extent (viz.,

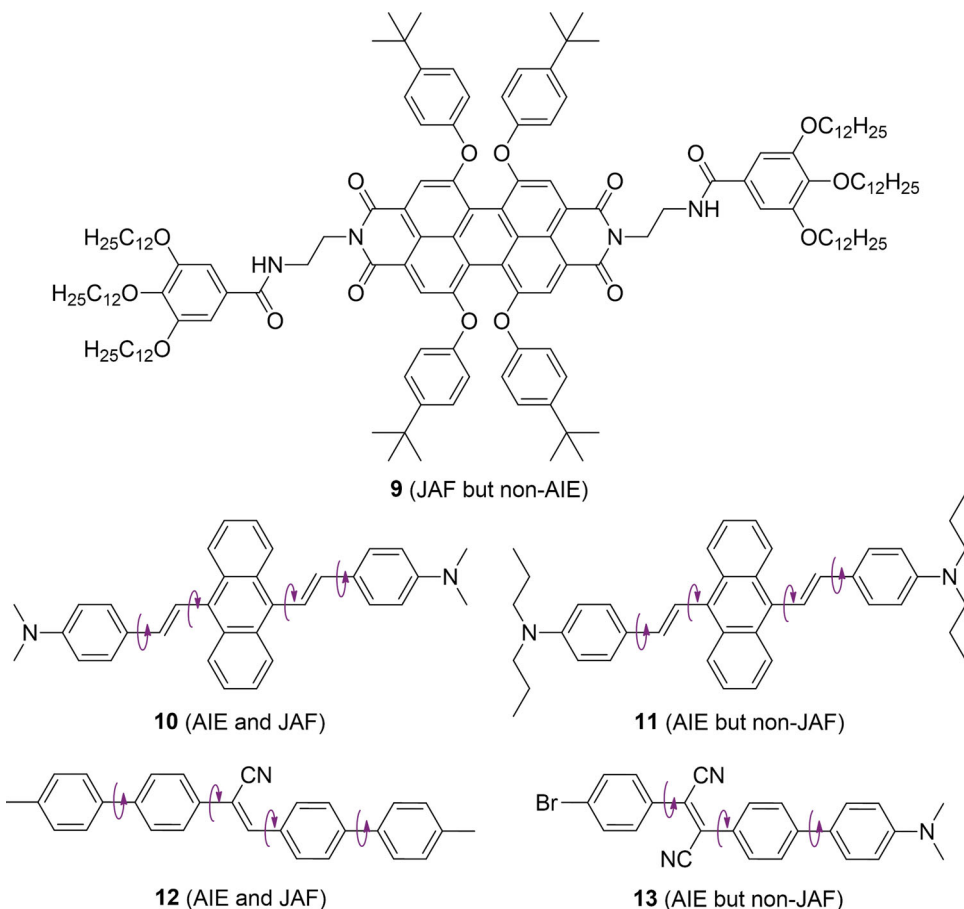


Figure 6. Examples illustrating the relationships between RIM and J-aggregate formation (JAF).

20% of its monomer emission). In other words, **9** is ACQ active but AIE silent, although its molecules form J-aggregates.

Some luminogens do form J-aggregates and meanwhile exhibits AIE activity. 9,10-Bis(*p*-dimethylaminostyryl)anthracene derivative **10** shown in Figure 6, for example, is practically non-fluorescent in solution and shows AIE behaviors.^[74] As proven by its absorption and PL spectra as well as crystal analysis data, **10** takes a specific packing mode in the crystalline state, i.e., J-aggregates. In comparison to its dilute solution and aqueous suspension, the J-aggregates of **10** display red-shifted emission maximum ($\lambda_{\text{em}} = 586$ nm) and high emission efficiency ($\Phi_F \sim 59\%$), thus showing an AIE effect. Luminogen **11** is similar to **10** in that they both have a D–A structure, where D and A stands for electron-donating and electron-accepting units, respectively. However, **11** does not form J-aggregate but shows AIE activity, indicating that JAF is not an intrinsic cause for AIE effect of a luminogen.

Luminogen **12** has been reported to form J-aggregates and show marked AIE activity.^[75] Its molecules are weakly fluorescent but its nanoparticles are strongly emissive, with the Φ_F of the latter being about 700-fold higher than that of the former. Luminogen **13** is a newly developed red light emitter.^[76] It is AIE active, with a solid-state Φ_F of 26.5% (cf., Φ_F for its dilute solution being merely 0.4%). Despite its structural similarity to **12**, luminogen **13** does not form J-aggregates. There exist multiple C–H \cdots π hydrogen bonds but no π – π interactions in its crystals. The H-bonding helps rigidify the molecular conformation and impede the intramolecular motions, hence endowing **13** with AIE activity. Like the case discussed above for luminogen pair **10/11**, the data here for **12/13** once again prove that JAF is not essential to AIE.

Let's try to summarize the differences and relationships between AIE and JAF. The term of aggregate in AIE is defined in a broad sense, referring to "a whole" formed from several "parts", according to the dictionary and encyclopedic classifications.^[1] In the AIE aggregates, the luminogen can be polar or nonpolar, the packing can be ordered or random, the spectrum can be unchanged or red/blue-shifted, and the Stokes shift can be big or small. The scope of J-aggregates, however, is much narrower, because they have customarily referred to a group of specific dyes that carry polar or functional groups with D–A interaction, pack in a highly ordered fashion, undergo red-shifts in absorption or emission spectra, and exhibit very small Stokes shifts. J-aggregates may thus be regarded as a subgroup of AIE systems, if they show AIE activity.

Whether JAF leads to AIE is highly dependent on molecular and packing structures. If a dye has a rigid and planar (core) structure (e.g., **9**), even if its molecules form J-aggregates, it is AIE inactive, due to the quenching effect caused by the strong π – π stacking interaction in the aggregates. On the other hand, if a luminogen is conformationally flexible and structurally twisted, its excited-state energy can be efficiently annihilated by the dynamic intramolecular motions in the solution state, while the energy can be transformed to efficient light emission in the solid state due to the activation of the RIM process by the aggregate formation. Such a luminogen will show AIE activity, no matter whether its molecules can form J-aggregates or not. In the J-aggregates formed by the molecules of such a luminogen, the JAF process serves as an effective means to rigidify

the molecular conformation and to restrict the intramolecular motion. It is thus the RIM process that plays a decisive role in an AIE process. It is worth pointing out that JAF cannot explain why light emission of an AIEgen is quenched in solution state.

2.2.2. RIM Versus ESIPT

ESIPT is an extremely fast photoinduced proton transfer process mediated by intramolecular H-bonding.^[77,78] Like JAF, ESIPT process has been considered to be the AIE mechanism for some particular luminogens, because the light emissions of some ESIPT dyes are enhanced in the aggregate state. Due to their intrinsic peculiar four-level cyclic proton-transfer processes, ESIPT dyes are a family of extensively investigated functional materials.^[79] It is well known that an ESIPT dye is normally more stable as enol (E) and keto (K) forms in the ground and excited states, respectively. A fast four-level (E–E * –K * –K) cycle occurs immediately after photoexcitation of the dye molecule through the intramolecular H-bond. This is accompanied by a very large Stokes shift without self-absorption.^[80] The ESIPT process, however, cannot fully explicate why the luminescence of an ESIPT dye is enhanced in the aggregated state.

An example of AIE-active ESIPT luminogen (**14**) is shown in Figure 7a. As intramolecular proton transfer can be inhibited by the formation of intermolecular H-bond with surrounding solvent, the ESIPT process of **14** is significantly affected by solvent properties.^[81] As a result, its emission behaviors are distinctly different in different solvents. Thus, in an aprotic solvent like methyltetrahydrofuran (meTHF), **14** shows two peaks at ~416 and 538 nm (spectrum I in Figure 7a). These peaks are ascribed to emissions of the E and K forms of **14**, respectively, which are tautomers in equilibrium, due to the moderate polarity of the solvent. In the dilute meTHF solution, no matter which form (E or K) **14** takes, the two emission peaks are very weak (noting that spectrum I has been magnified by 20 times in order to make it visible). In the molecularly dispersed dilute solution, the non-planar molecule of **14** may undergo active conformation change. Its single-bonded rotors can rotate easily and the radiative decay is effectively quenched by this kind of intramolecular motion.

However, when **14** is dissolved in a protic polar solvent like methanol, although it still shows two peaks, the E emission band at 416 nm is overwhelmingly stronger than the K band at 538 nm (spectrum II). In the methanol solution, the intramolecular H-bonding is replaced by the intermolecular H-bonding between molecules of luminogen **14** and solvent. As a result, the intramolecular rotations of **14** become partially restricted. The radiative decay is thus not completely quenched and the E emission becomes stronger than that in the meTHF solution. In an apolar solvent like MCH, only one emission band peaked at about 538 nm is observed. Its emission intensity is very weak (noting the 20-fold magnification of spectrum III). There exists little interaction between **14** and the apolar solvent. The luminogen thus undergoes a full ESIPT process mediated by the intramolecular H-bond and completely changes to the K form. This structure is flexible and twisted and its dynamic intramolecular motions dissipate most of the exciton energy, resulting in the faint fluorescence in the solution.

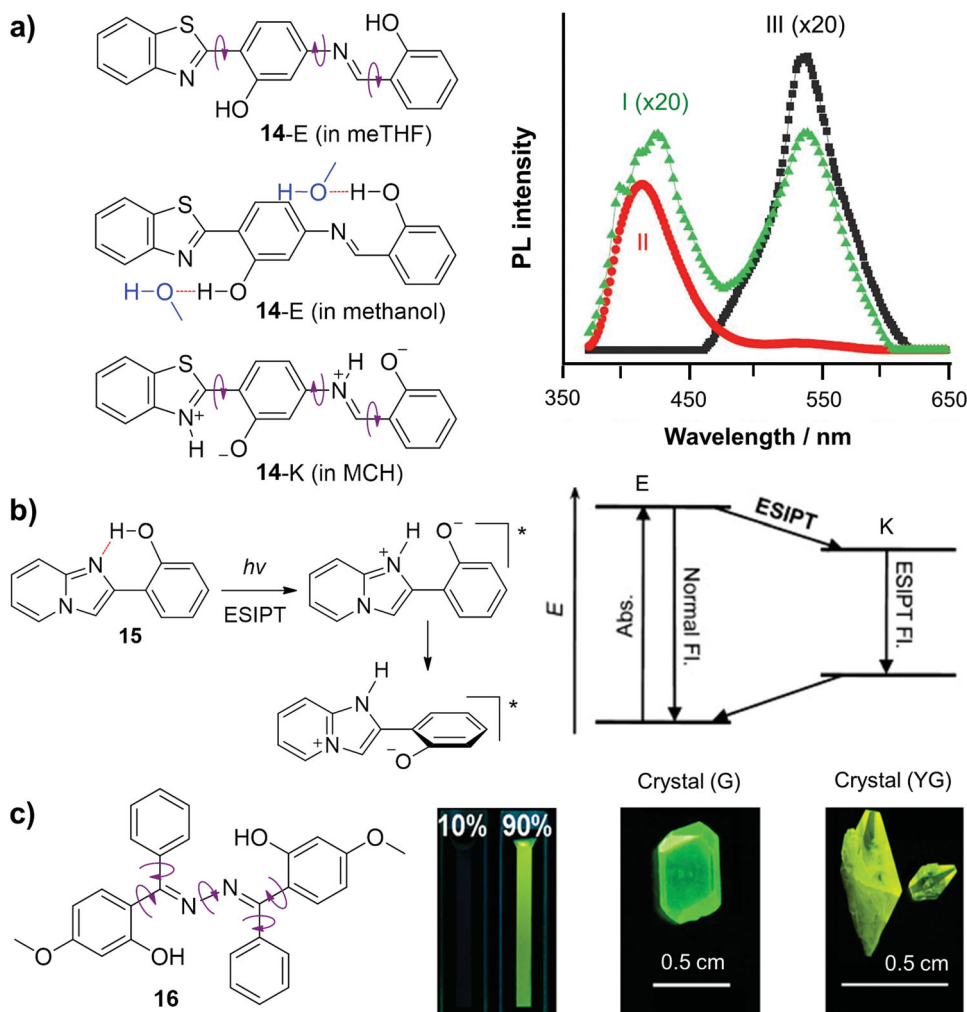


Figure 7. (a) Structures of enol (E) and keto (K) forms of luminogen **14** with excited-state intramolecular proton transfer (ESIPT) characteristics and fluorescence spectra of their dilute solutions (10 μ M) in methyltetrahydrofuran (meTHF; spectrum I), methanol (spectrum II) and methylcyclohexane (MCH; spectrum III) at room temperature. Spectra I and III are very weak and multiplied by 20 fold to make them visible. Excitation wavelength: 355 nm. Reproduced with permission.^[81] Copyright 2011, Elsevier. (b) Proton transfer and subsequent twisting motion of luminogen **15** in excited state and its four-level energy diagram of ESIPT process. Reproduced with permission.^[82] Copyright 2013, American Chemical Society. (c) Structure of AIE-active ESIPT luminogen **16** and fluorescence photographs of its solution ($f_w = 10\%$), aggregates ($f_w = 90\%$), and crystals with green (G) and yellow-green (YG) light emissions. Reproduced with permission.^[84] Copyright 2013, American Chemical Society.

When temperature is decreased, the emissions of the solutions of **14** are intensified in all of the apolar, protic polar, and aprotic polar solvents, including MCH, methanol, and meTHF. For example, when it is cooled from room temperature to 140 K, the solution of **14** in MCH becomes ~28-fold more emissive. This indicates that regardless of the involvement of ESIPT process, the emission of **14** is enhanced as temperature goes down. The ESIPT process thus should not be the essential cause for the AIE effect of the ESIPT luminogen. Because 140 K is close to or below the freezing point of MCH, methanol or meTHF, the solvent should be highly viscous or nearly solidified at this temperature. In such conditions, the intramolecular motions of **14** are significantly obstructed and the radiationless decay channel is effectively blocked, which populates the radiative excitons, leading to a large increase in fluorescence. This proves that the RIM process has played an

important role in enhancing the fluorescence of **14** at the low temperature.

Another example of AIE-active ESIPT luminogen is **15** (Figure 7b), which has been well studied due to its structural simplicity.^[82,83] Similar to **14**, luminogen **15** emits very weakly with a large Stokes shift in an apolar solvent, which is ascribed to the ESIPT emission. Its fluorescence spectrum in THF contains two peaks at 377 and 602 nm with corresponding Φ_F values of 8% and 2%. Its emission in ethanol is peaked at 373 nm with a Φ_F of 11%, while in apolar, aprotic cyclohexane, its emission maximum is at 578 nm with a Φ_F of 4%. However, its two crystal polymorphs emit bright blue-green and yellow lights, with high Φ_F values of 50% and 37%, respectively. Its amorphous powders, blends with polymer matrixes, and frozen dilute solutions all show high Φ_F values (>37%). These experimental data offer further support to the aforementioned RIM hypothesis.

On the basis of the experimental observations and the theoretic calculations on the potential energy surfaces in the S_0 and S_1 states, the AIE effect of **15** can be explained at the single molecular level. The E form of **15** with a planar conformation is the most stable form in the S_0 state due to the stabilization by the intramolecular H-bond between the imino and phenolic groups (Figure 7b). In the S_1 state, the E form is first transformed to a zwitterionic ESIPT species, followed by the conformational twisting along with the rearrangement of surrounding solvent molecules in a fluidic solution, which accounts for the very large Stokes shift. The efficient radiationless decay process of **15** proceeds via the inversion between the E and K forms coupled with the twisting motion. This is the reason for the weak emission of **15** in the solution state. Because such intramolecular motion is largely suppressed in a rigid aggregate, the ESIPT species retains the planar conformation, permitting emissive decay from the K- S_1 state to the K- S_0 state.

From the above discussion, it can be predicted that luminogen **16** in Figure 7c should show more pronounced AIE effect than its ESIPT counterparts **14** and **15**, because it has a higher conformational flexibility.^[84] The experimental results agree with our prediction. The light emission of **16** is dramatically affected by the water content in a water/ethanol mixture. In the low water fraction region ($f_w = 0$ –60 vol%), **16** is non-fluorescent. When f_w is increased from 60% to 90%, its fluorescence is greatly intensified, showing a large AIE effect. At low f_w , the emission of **16** in the solution state is dim due to the radiationless decay of its excited states caused by the active intramolecular rotations of its multiple rotors around the C–C and N–N single bonds. At high f_w , the rotations are suppressed as a result of the close packing in the aggregated state, leading to the observed strong fluorescence. Due to the large conformation flexibility and multiple rotors, the emission of **16** in solution is quenched to a much larger extent as compared to its ESIPT congeners **14** and **15**. Moreover, **16** shows unique morpho- and thermochromisms (Figure 7c), thanks to the easy tunability of the packing structure of its non-planar molecules.

2.2.3. RIM Versus TICT

AIE systems may be categorized into two subgroups, one without D–A structure and another with D–A structure. For a system without D–A structure, the emission quenching in solution is caused by the torsional and vibrational motions, and the AIE effect in aggregates is brought about by the RIM process. For a D–A system, however, its faint emission in solution is often ascribed to a “dark state”, i.e., TICT state, while in aggregates, the AIE effect is thought to stem from the inhibition of transformation from locally excited (LE) state to TICT state.^[85,86] TICT is sensitive to environmental change, particularly polarity variation. Taking luminogen **17** as an example, it is comprised of two pairs of D–A units (Figure 8a). Its solution exhibits a marked solvatochromic effect with its emission red-shifting from green ($\lambda_{\text{em}} = 510$ nm) in hexane (a typical apolar solvent) to red ($\lambda_{\text{em}} = 667$ nm) in dimethyl formamide (DMF; a polar solvent), although the red fluorescence is too weak to observe by the naked eyes.^[86,87]

In the apolar solvent, the planar conformation of **17** is stabilized by electronic conjugation, which confers a sharp fluorescence spectrum on its LE state. The intramolecular twisting in the polar solvent, however, transforms **17** from LE state to TICT state, where a total charge separation between its D and A units occurs. The twisted conformation of **17** is stabilized by the solvating effect of the polar solvent. Elevation of its HOMO level in the polar solvent narrows the band gap, hence bathochromically shifting its PL spectrum. The fluorescence is weakened due to the susceptibility of the TICT state to non-radiative quenching processes. Different from its dilute solution in the polar solvent, the crystal of **17** emits an intense orange-red light at 610 nm with a high Φ_F (31%), clearly manifesting its AIE activity. If the AIE effect in the solid state is simply ascribed to the inhibition of the TICT process, the large shift in the emission wavelength and the great enhancement in the emission intensity of the crystal, as compared to those of the solution, can hardly be fully explained.

Photophysical behaviors of a boron dipyrromethene (BODIPY) derivative (**18**) are studied in THF/water mixtures, in an effort to learn how aggregate formation affects the emission of a TICT luminogen (Figure 8b).^[88] As BODIPY derivatives are generally insoluble in water, the molecules of **18** should form aggregates in the aqueous mixture with a high f_w . The THF solution of **18** emits a red light at 688 nm, which is red shifted and catastrophically weakened when a small amount of water (10%) is added into THF, owing to the increase in solvent polarity and the transformation to TICT state. The fluorescence remains invisible but starts to blue-shift when more water is added. When the f_w is increased beyond 65%, the fluorescence is revitalized. In the aqueous mixtures with high water contents ($f_w > 65\%$), the luminogen molecules are clustered together to form microaggregates. The hydrophobic environment and the restriction to intramolecular motions in the aggregates leads to the observed blue shift in the emission color and enhancement in the emission intensity.

Like **18**, **19** is a TICT dye with a D–A structure. Similar to that of **18**, the emission of **19** is red-shifted in color and decreased in intensity with an increase in the solvent polarity (Figure 8c).^[89] In pure THF, **19** emits a red light with a λ_{em} of 620 nm upon photoexcitation. When a small amount of water is added, its fluorescence is dramatically weakened with the λ_{em} red-shifted to ca. 670 nm. When a large amount of water is added, the molecules of **19** undergo aggregate formation. Although a hydrophobic environment is created inside the aggregates and therefore the TICT effect should be alleviated, the emission is not recovered because of the prevailing ACQ effect. According to the TICT-restriction mechanism proposed by some researchers, **19** should exhibit an AIE effect but in fact it does not. The distinct difference between the PL behaviors of **19** and **18** prompts us to find out the underneath AIE mechanism for a TICT dye and the interrelation between AIE activity and TICT effect.

Among all the TICT dyes (**17**–**19**) discussed above, **19** is structurally most rigid, because the dicyanomethylene-4H-pyran (DCM) core and two styryl wings form a large plane through π -electron conjugation.^[90] As a result, **19** suffers from the ACQ problem instead of showing an AIE effect. This indicates that not every TICT dye is AIE active. Whether a TICT dye shows

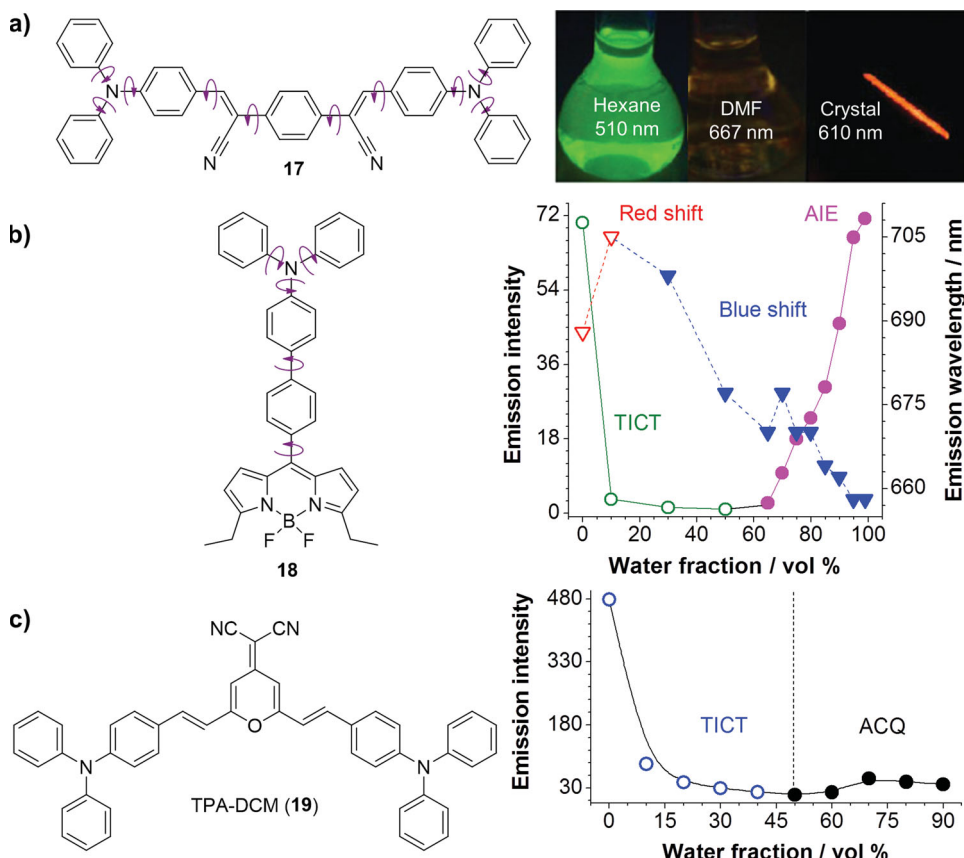


Figure 8. Examples of twisted intramolecular charge transfer (TICT) dyes with (**17** and **18**) and without (**19**) AIE activity. a) Reproduced with permission.^[86] Copyright 2011, Elsevier. b) Reproduced with permission.^[88] Copyright 2009, American Chemical Society. c) Reproduced with permission.^[89] Copyright 2012, Wiley-VCH Verlag GmbH & Co. KGaA.

AIE activity is dependent on the extents of its conformational flexibility and rotational motion. Though rotation or twisting plays an important role in the TICT process, the number of the rotors and their rotation amplitudes do not need to be very large. Moreover, TICT is a process active in the solution state. On the other hand, the intramolecular motions for an AIE luminogen in solution must be vigorous enough to dissipate the excited-state energy and the motions should be restricted to block the radiationless pathway in aggregates. Thus in an AIE-active TICT system, there must be multiple rotors to maximize the emission quenching effect in solution and omnidirectional structural rigidification to restrict the intramolecular motions in aggregates. The TICT-restriction mechanism can only describe the emission behaviors in the apolar solvents, whereas the RIM process can well explain the photophysical phenomena in both solution and aggregate states.

Putting all the experimental data together enables us to draw a clear picture for the emission behavior of an AIE-active TICT luminogen (Figure 9). In an apolar solvent, it takes a planar conformation with a conjugated D–A structure and emits in the short wavelength region in a high intensity from the LE state. When the solvent polarity is increased, the conformation of the luminogen becomes partially twisted and the charge becomes partially separated. Its light emission is red-shifted in color but decreased in intensity due to the LE-to-TICT transition. Upon

further increase in the solvent polarity, the D–A units become more twisted. The large conformational twisting breaks the electronic conjugation and enables easier intramolecular rotation. The complete charge separation is realized, which is stabilized by the surrounding polar solvent molecules. The emission becomes greatly red-shifted and severely quenched, due to the elevation in the HOMO level and the vigorous intramolecular motion, respectively. When the luminogen molecules are aggregated, the local environment becomes less polar and the D–A structure becomes less twisted. The emission thus becomes blue-shifted owing to the TICT-to-LE transition. The aggregate formation substantially hampers the intramolecular motions, hence activating the RIM process and boosting the emission efficiency.

As a summary of this Section on the mechanistic comparison, we may conclude that there exist the following relationships among the different emission enhancement systems operating in different mechanisms: (1) The AIE system partially overlaps with the other luminescence enhancement systems associated with JAF, ESIPT and TICT processes; (2) in all the emission enhancement systems, the RIM process is competing with other intra- and intermolecular forces; (3) if the RIM process prevails in a luminogen system, it shows an AIE effect, but if other competing forces dominate in a system, it becomes AIE inactive; (4) if the competing force involves π – π

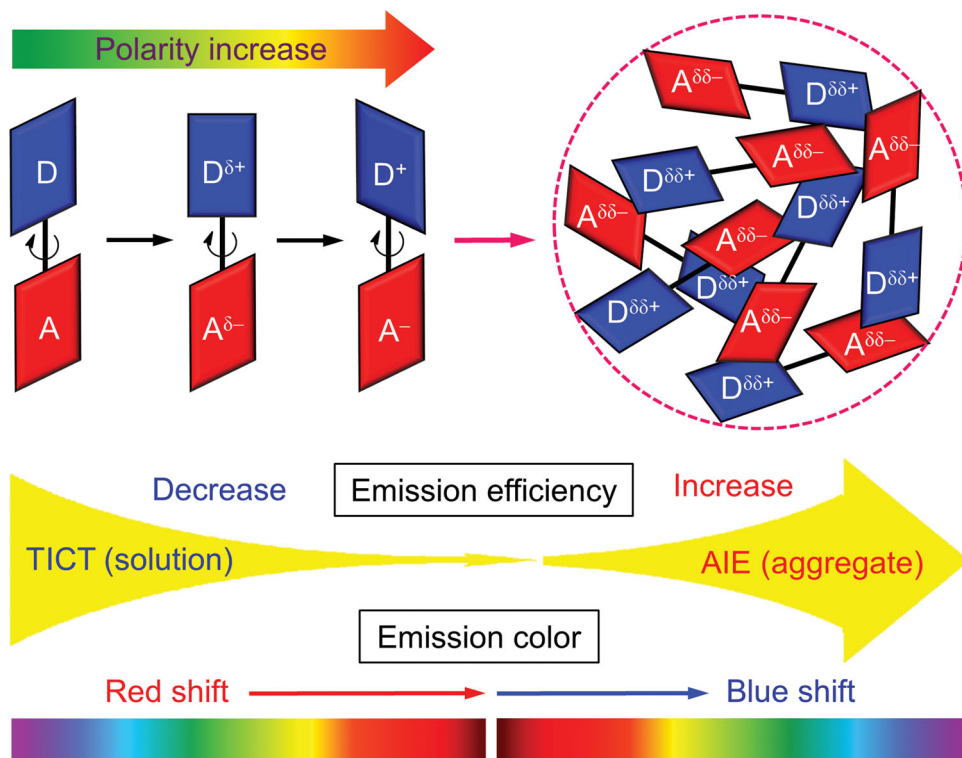


Figure 9. Schematic illustration of TICT and AIE effects on emission behavior of a D–A structured AIE luminogen. Reproduced with permission.^[88] Copyright 2009, American Chemical Society.

stacking interaction followed by excimer formation, the system becomes ACQ active; and (5) regardless of the involvement of a JAF, ESIPT or TICT process, it is the RIM process that endows the system with AIE activity. The essence of the RIM process is the structural rigidification or conformational stiffening.

3. Structure Diversification

The above mechanistic discussions have made the AIE picture clear. Under the guidance of the mechanistic understanding, researchers have designed and synthesized a wide variety of new AIEgens with a structural feature of a central stator bearing multiple rotors or vibrators that can rotate or vibrate to large extents. Since the area of AIE research is fast advancing in recent years, it is difficult for us to cover all the AIE systems developed so far in this review. We thus will not expatiate on technical details but choose some typical examples to illustrate the involved working principles. The examples of the new AIEgens will be grouped together according to their structural characteristics and categorized into hydrocarbon, heteroatom, and organometallic systems.

3.1. Hydrocarbon AIE Systems

Development of pure hydrocarbon AIE luminogens containing no atoms other than carbon and hydrogen is of great importance for fundamental research, such as proof-of-concept study and mechanism decipherment. Moreover, high-performance

hydrocarbon AIEgens can serve as building blocks for the construction of advanced functional materials. TPE, for example, is the best-known AIEgen and has been widely used as a simple model for mechanistic study, a versatile Lego for assembling AIE polymers, and a “magic spell of Lumos” for transforming ACQ dyes into AIE luminogens.^[32,91] In addition to TPE, other hydrocarbon AIE systems have also been generated by various research laboratories in the past decade, examples of which include diphenyldibenzofulvene (5),^[53] 9,10-distyrylanthracene^[92] and substituted 1,4-distyrylbenzene derivatives.^[93] These systems have been discussed in the previous reviews^[27–35] and will not be covered here; instead the newly developed AIE systems will be presented below.

Li et al. have observed a marked AIE effect in 1,2-bis[2-(9-anthracylvinyl]benzene (**20**; Figure 10).^[94] The luminogen is practically non-fluorescent when it is molecularly dissolved in dichloromethane or ethanol. Addition of >20% of water into ethanol causes the molecules of **20** to aggregate and fluoresce. The Φ_F value of the solid powder of **20** is 12%, which is much higher than that of its solution (<1%). It therefore behaves like a typical AIEgen. Its structure is featured with two anthracene units linked to the central phenyl ring through single bonds with vinylene groups as bridges. This structural characteristic suggests that the RIR process is at work in this AIE system. In the ethanol solution, there exists little electronic interaction between the molecules of **20** and solvent, as **20** is apolar and neutral. Its multiple rotating units undergo dynamic twisting motion against its benzene core. The intramolecular motion serves as a non-radiative channel for its excited states to relax. In the aggregate state, the intramolecular rotations are

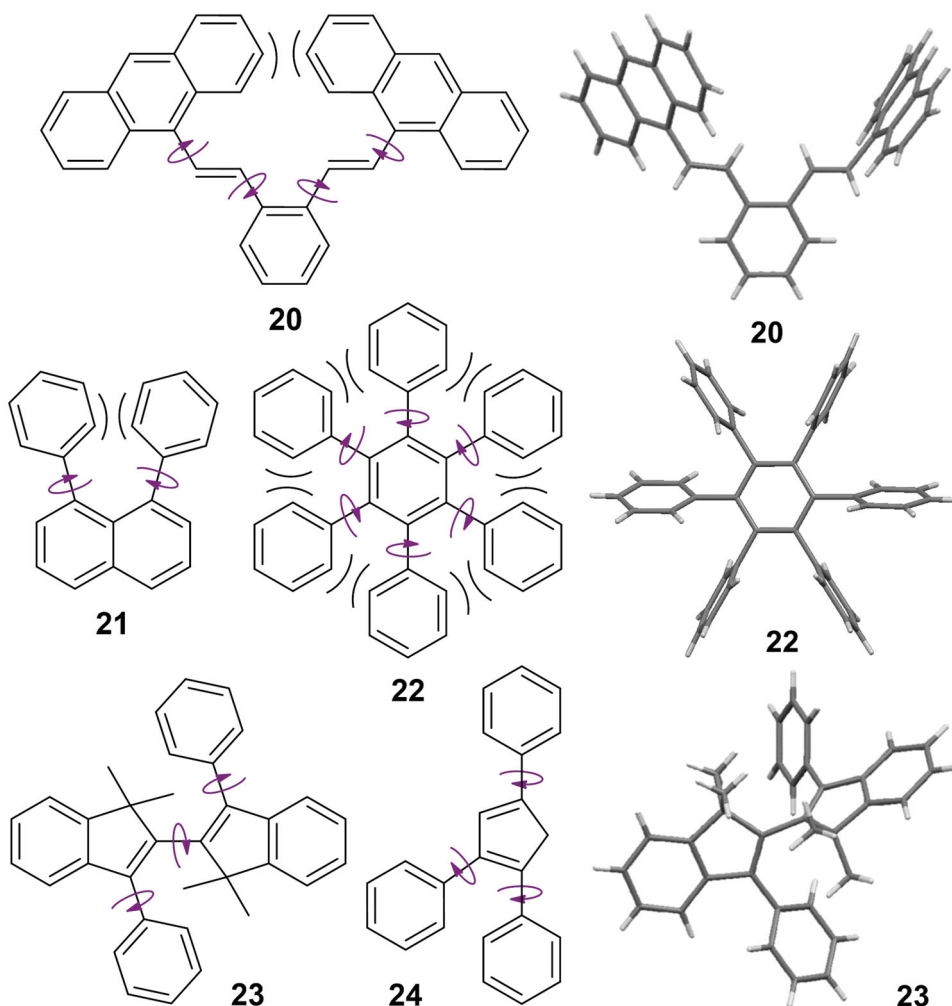


Figure 10. Examples of pure hydrocarbon AIEgens. The crystal structures are retrieved free of charge from CCDC (848984, 633293 and 762612) via www.ccdc.cam.ac.uk.

restricted or the RIR process is activated, and the emission of **20** is thus turned on.

The RIR mechanism is proved by the analysis of crystal structure of **20**. Its molecules are highly twisted with torsion angles in the range of 53.20° – 73.55° , which permits free rotations of its rotors in solution. In the crystal, its molecules pack together with the aid of multiple intra- and intermolecular interaction such as C–H \cdots π bonds, with no involvement of the π – π stacking interaction. The photophysical behaviors of its 1,3- and 1,4-isomers provide further evidence to the RIR mechanism. In sharp contrast to **20** (a 1,2-isomer), both of the 1,3- and 1,4-isomers display marked ACQ effect. Owing to the large steric effect and small electronic conjugation, the bulky rotors in **20** can rotate against the central core to quench the emission in solution. On the other hand, the small steric effect and large electronic conjugation in the 1,3- and 1,4-isomers make the molecules more planar and rigid and hence more difficult to rotate in solution. The strong π – π interaction between the planar molecules facilitates excimer formation and thus turns off their light emissions.

The data for **20** and its regioisomers indicate that the steric interaction between the rotating units affects molecular

conformation, packing arrangement, π – π interaction, and luminescence behavior. This suggests the possibility of creating new luminogen systems through judicious utilization of steric effect between adjacent rotors. Luminogens **21** and **22** are such examples whose photophysical properties are greatly affected by steric interaction.^[95,96] Luminogen **21** emits weakly in cyclohexane with a low Φ_F of 3%. When suspended as nanoaggregates in a THF/water mixture with $f_w = 90\%$, its Φ_F is increased by 7.8 times, thus showing an AEE effect.^[95] Examination of its single crystal data reveals that this U-shaped luminogen is non-planar and the two phenyl rings are twisted out of the naphthalene plane with a dihedral angle of $\sim 60^\circ$ and a splay angle of $\sim 20^\circ$. This twisted conformation favors intramolecular rotations of the phenyl rotors and weakens the light emission in the solution. In the nanoaggregates, the π – π stacking is obstructed, the intramolecular motion is constrained, and the light emission is hence enhanced.

The luminescence behavior of **22**, namely hexaphenylbenzene, is similar to that of **21**.^[96] As mentioned above, conformational planarity and structural rigidity are very important in determining whether a luminogen is AIE active or not. Like

HPS and TPE, **22** is propeller-like in molecular shape, which generates large free volume and impedes intermolecular π - π stacking in the aggregates, as can be understood from its crystal structure shown in Figure 10. However, the peripheral phenyl rings in **22** cannot rotate as freely as those in HPS and TPE, owing to the severe steric repulsion between its neighboring phenyl groups. It is thus an ideal model for studying the effect of rotational freedom on AIE process.

The light emission of **22** in a good solvent (e.g., THF) is weak but readily detectable. In an aqueous mixture with $f_w = 80\%$, its emission is increased by 12 fold. The steric crowdedness in **22** limits the intramolecular rotations of its phenyl rings even when it exists as an isolated species, thus making its emission measurable in the solution state. The steric effect caused by its propeller shape hinders the close packing of its molecules and the formation of detrimental species in the aggregated state. The examination of its single-crystal structure reveals that its phenyl rings are almost perpendicular to the central benzene ring. The dihedral angle between the central benzene core and a phenyl substituent is 102° , from which a twisting angle of 12° is derived. This is much smaller than that in TPE, suggestive of a smaller twisting amplitude of the phenyl rotors in **22**. Theoretical calculation indicates that the energy barrier for the phenyl ring rotation in **22** is two times higher than that in TPE, implying that the rotations of the phenyl rotors in **22** is more difficult. Evidently, the twisting amplitude and steric effect are crucial for the AIE behavior in non-planar luminogens.

Linear aromatic luminophore systems consisting of bridged phenylenevinylene units are of great interest owing to their promising high-tech applications as light-emitting materials.^[97] Tian's team has designed and synthesized a series of biindenyl derivatives (e.g., **23**), in which the C=C double bonds are locked up by five-membered rings (Figure 10).^[98] Solutions of **23** emit faintly, whereas its crystals luminesce intensely with Φ_F up to 76%. In the crystalline state, the 2,2'-biindene skeleton conformation of **23** is far from planar, with the interplane angles between the two indene rings being as large as around 70° . The indene planes and the phenyl substituents are not coplanar either, with their dihedral angles varying from 37° to 70° . This largely twisted propeller-shaped conformation prevents the aromatic rings in **23** from experiencing π - π stacking interaction and hence its crystalline form is highly luminescent. The non-planar conformation contributes to the emission quenching of **23** in the solution state, for it allows active intramolecular rotations, which effectively deactivates its excited states non-radiatively.

Siloles are a family of silicon-bridged cyclopentadiene (Cp) derivatives and are archetypal examples of AIEgens. If RIM is the real mechanistic cause for AIE, other Cp derivatives containing different heteroatoms and even those of pure hydrocarbons should also exhibit AIE activity. This proves to be the case: for example, 1,2,3,4-tetraphenyl-1,3-cyclopentadiene was found to be AIE active in 2007.^[24] Recently, Yang et al. have developed a series of AIE-active triarylcyclopentadiene derivatives (e.g., **24**).^[99] Luminogen **24** is weakly emissive in its good solvents (e.g., acetonitrile) but becomes highly luminescent upon aggregation. Its Φ_F values in solution and crystal are about 1.6% and 32%, respectively. According to the single crystal analysis, there

is large distortion between the neighboring phenyl rings in **24**, which renders the co-facial π - π stacking difficult. The adjacent luminogen molecules with multiple C-H \cdots π interaction stiffens the molecular conformation, which activates the RIM process and makes the crystal of **24** emissive.

3.2. Heteroatom AIE Systems

The hydrocarbon AIEgens enjoy structural simplicity and ready synthetic accessibility. They have served as excellent elementary models for understanding the mechanistic causes of AIE effects and for expounding the structure–property relationships in AIE processes. The scope of their structural variation, however, is limited. Incorporation of heteroatoms into AIEgens will significantly expand the territory of AIE study and enrich the structural diversity. The unique molecular orbitals and electronic conjugations of heteroatoms (boron, nitrogen, silicon, phosphorous, sulfur, etc.) and intramolecular interactions induced by the D/A units based on the heteroatoms may endow the AIE systems with functional properties that are difficult to access by the pure hydrogen systems.^[100–103]

Heteroatom-bridged cyclopentadienes are often referred to as heteroles or metalloles, which have attracted much attention owing to their unique electronic structures and optoelectronic properties.^[104–106] Many heteroles are AIE active. 1,2,3,4,5-pentaphenylphosphole oxide (**25** in Figure 11), for example, shows typical AIE phenomenon.^[107,108] It is faintly fluorescent in a THF solution, while addition of a large amount of water into THF sets off intense emission at ~ 500 nm. When the f_w reaches 90%, its fluorescence intensity is 12-fold higher than that of its THF solution. Like HPS, **25** possesses a propeller-shaped structure and carries multiple aromatic rotors. Its AIE effect should thus also be caused by RIM process. Recently, a series of amphiphilic dithieno[3,2-*b*:2',3'-*d*]phosphole derivatives that combines electronic feature of phosphole with self-assembly attribute of lipids have been developed by Baumgartner et al.^[109] The fused-ring phospholium luminogens show low (0.3–0.5%) and high (9–19%) Φ_F values in solutions and aggregates, respectively. Their AIE activities are also ascribed to the RIM process: the intramolecular rotations of their flexible structural elements are restricted in the solid state.

Germoles are heavier group-14 congeners of siloles. A family of 1,1-disubstituted 2,3,4,5-tetraphenylgermole with AIE characteristics have been reported by Braddock-Wilking and coworkers in 2011.^[110] Luminogen **26** is discussed here as a representative of the germoles. Its single crystal structure has a highly distorted conformation with the phenyl substituents twisted out of plane with respect to the gerhole ring core. The average dihedral angles for the phenyl substituents at the 2,5- and 3,4-positions are about 38° and 63° , respectively, quite close to those of tetraphenyl-substituted siloles. As a result of this structural similarity, the electronic and optical properties of **26** are similar to those of siloles. It is weakly fluorescent with an emission peak at 483 nm and a Φ_F of 0.4% in the dilute solution of acetone. With addition of 90% water into acetone, its Φ_F is boosted to 26%. Its AIE effect is rationalized to originate from the lack of intermolecular π - π stacking interaction and the RIM process in the aggregates.

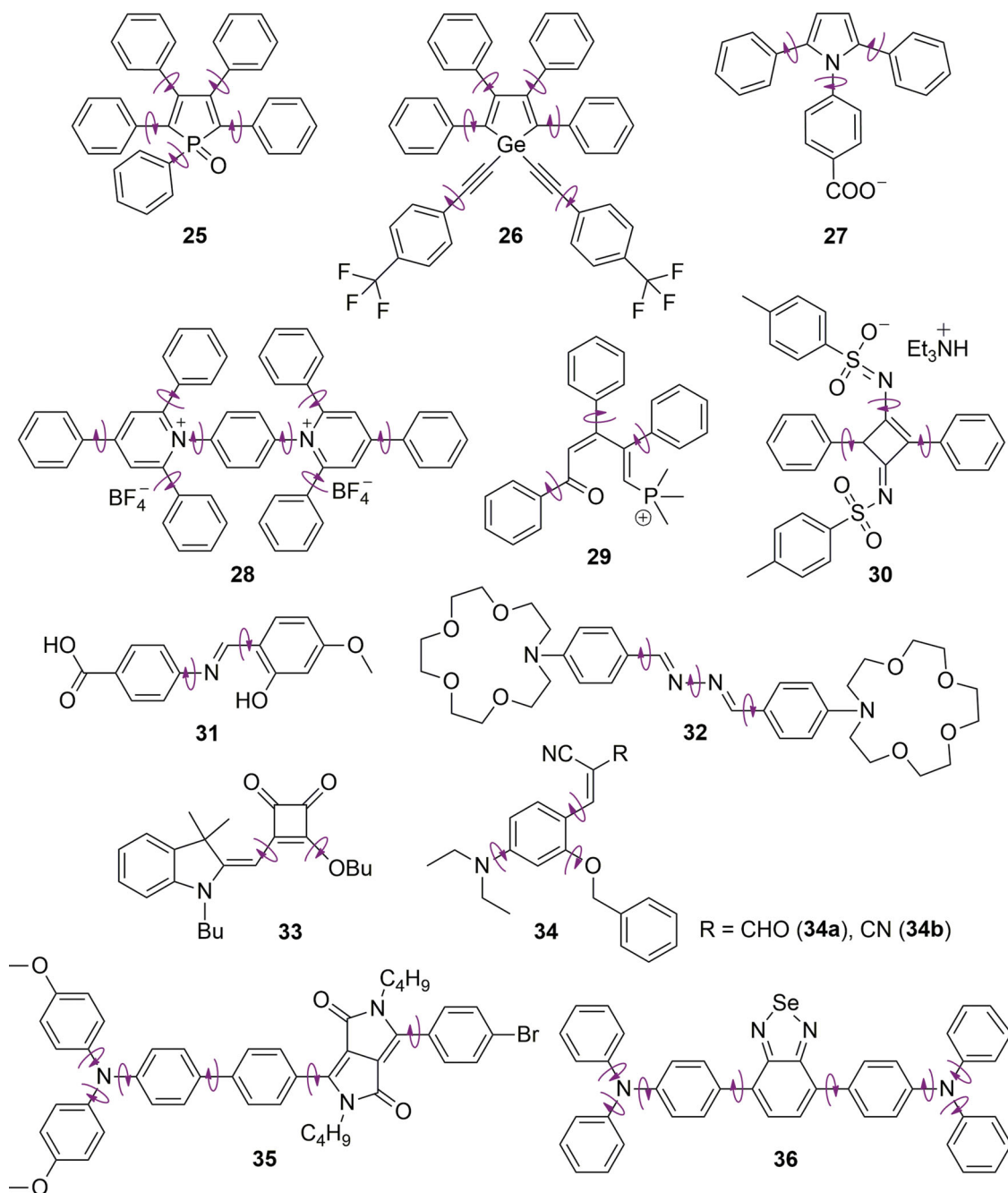


Figure 11. Examples of heteroatom-containing AIEgens whose AIE phenomena are mainly caused by RIR process.

A series of aryl-substituted pyrrole derivatives have recently been designed and synthesized by Dong's team.^[111,112] The conformational twisting, morphological packing and structural rigidification have been found to play essential roles in the photophysical processes of the pyrroles. The prevention of parallel packing of the conjugated chromophores by the twisted conformation and the activation of the RIR process by the aggregate formation are the main causes for the AIE phenomena of the pyrroles. Luminogen 27 is an example of AIE active pyrrole, whose light emission is greatly enhanced by the chromophore aggregation.^[111] The highly twisted conformation

with large torsion angles between its pyrrole core and phenyl substituents as well as the aromatic C–H···π interaction in its aggregates have collectively contributed to its AIE process. The luminogen is water soluble, rendering it promising for an array of technological applications, for example, as chemosensors and bioprobes in aqueous media.

For biomedical applications, AIEgens have often been decorated with hydrophilic groups on their peripheries to make them miscible with aqueous media, which, however, requires additional functionalization procedures. Direct syntheses of water-miscible ionic AIEgens are thus of great interest. Our

laboratories have developed a new AIEgen (**28**) containing cationic 1,2,4,6-tetraphenylpyridinium units according to the RIR mechanism.^[113] The luminogen is propeller-shaped with multiple phenyl rotors. Its solution in dimethyl sulfoxide (DMSO) is practically non-fluorescent. When its molecules are aggregated, the light emission is boosted by 85 fold. This luminogen is facilely prepared by a one-step reaction in a one-pot procedure. It is miscible with aqueous media and has the potential to find biological applications.

A new conjugated phosphonium salt (**29**) has been synthesized by Gong, Ning, et al. from a phosphine-triggered ring-opening reaction of 2,4,5-triphenylpyrylium ring.^[114] When **29** is dissolved in acetonitrile at a concentration of 10 μM, almost no fluorescence is noticeable ($\Phi_F \sim 0.1\%$). Increasing the solution concentration of **29** in acetonitrile dramatically intensifies its fluorescence, implying an AIE effect. Its AIE feature is further confirmed by the fluorescence behaviors of **29** in water/acetonitrile mixtures. When water is added into acetonitrile, the molecules of **29** form nanoscopic aggregates. When f_w is >40%, its suspension in the aqueous mixture becomes somewhat turbid and its Φ_F is increased to 5%. The AIE activity of **29** is rationalized to result from the RIR process: the motions of its aromatic rotors around the single bond consume the excited-state energy in solution and the intramolecular rotations are limited due to the space constraint in aggregated state.

Pitchumani et al. have prepared a class of bis-*N*-sulfonylcyclobutene derivatives by Cu(I)-catalyzed cycloaddition cascade reactions.^[115] These cyclobutenes are found to exhibit AIE properties. Taking **30** as an example, the emission from its chloroform solution is very weak. When hexane is added into chloroform, its emission is enhanced. When the hexane fraction reaches 99%, its emission becomes very bright, with a spectral shift to the blue region. Single crystal analysis offers supportive evidence for its AIE mechanism. In addition to the multiple rotatory elements, the bond lengths of the imine groups in **30** are found to be longer than those of "normal" imines, which are attributed to the effective delocalization of the electrons between the two sulfonyl groups in the opposite diagonal of the cyclobutene ring. This means that the photoisomerization is easier than unconjugated C=N bonds. The photoisomerization of the C=N bonds and the subsequent intramolecular rotation of the rotors become the major non-radiative decay channels of the excitons of **30** in solution. In contrast, the molecules of **30** are tightly packed in the solid state as a rigid supramolecular network. The intramolecular rotations are greatly suppressed and the fluorescence is thus turned on. As **30** is in ionic form, it is partially soluble in water and is responsive to pH variation.

Tong's team has prepared a number of *p*-carboxyl-*N*-salicylideneaniline derivatives.^[116] With two planar π-conjugated units linked by a rotatable C–N single bond in the molecular structure, these derivatives are AIE active, emitting bright light in solid state. For example, the Φ_F values of **31** (Figure 11) in the solution and solid states are 1% and 17%, respectively. Its RIR mechanism is supported by the enhancement in the emission of its solution with an increase in the viscosity of the solvent, because high viscosity slows down the intramolecular rotations. The intramolecular H-bonding between the O–H and C–N groups of **31** and the intermolecular H-bonding between its carboxylic acid groups greatly rigidifies the molecular

conformation, making its molecules difficult to undergo intramolecular rotations in crystalline state. Luminogens with similar molecular structures, e.g., pyrene- and anthracene-containing Schiff bases, also exhibit marked AIE activity, with emission enhancements up to 630 and 101 times, respectively.^[117]

Luminogen **32** has been designed and synthesized by Zhou and co-workers in 2012.^[118] This structural design has the following unique features: it contains rotatable N–N single bond and its substituents at terminals are big aza-crown-ether rings. Luminogen **32** fluoresces very weakly in THF but becomes a strong emitter in a water/THF mixture with an f_w of 95%. The 89-fold enhancement in emission is a notable AIE effect. X-ray structural analysis reveals massive molecular interactions, such as C–H···C and C–H···N H-bonds, in the crystalline aggregates, which considerably restrict the intramolecular vibrations and rotations. The molecules thus become conformationally stiff. Furthermore, the big aza-crown-ether rings restrain the π–π stacking interaction. These all contribute to the AIE effect through a RIM process.

In addition to the flexible C–N and N–N linkages, other rotatable linkages like C–O bond also annihilate excited states non-radiatively through their twisting motions. Indolenine semi-squarylium dye **33** is such an example.^[119] It shows an obvious AIE effect: the Φ_F values of its solutions and solids are <1% and ca. 21%, respectively. This suggests that the dynamic rotation of the C–O bond and the vibration of the semi-squarylium ring of **33** are hampered in the aggregate state. This is verified by the single-crystal analysis. There exist C–H···π and C–H···O H-bonds, instead of π–π stacking interaction, in the crystals of **33**. The H-bonding hinders the intramolecular motions of the OBu group and semi-squarylium ring of **33**, hence turning on its fluorescence. As discussed below, the intramolecular rotation of the C–O band in **34** has also contributed to the non-radiative decay of its excitons in the solution state.^[120]

Many AIEgens are comprised of multiple aromatic rings and/or polycyclic skeletons; as a result, they often emit blue and green lights. AIEgens with red emissions are relatively small in number. To broaden the scope of high-tech applications of AIEgens, their emissions need to be bathochromically shifted. One effective strategy to realize red emission is to introduce D–A units into AIE systems. Much work has been done along this line, an example of which is a pair of intramolecular charge transfer (ICT) luminogens based on 2-benzoyloxy-4-diethylaminobenzaldehyde with formylacrylonitrile (**34a**) and malononitrile (**34b**) as electron acceptors.^[120] The luminogens are soluble in organic solvents (e.g., ethanol) but immiscible with water. In ethanol, **34a** and **34b** emit weakly with emission maxima at 480 and 485 nm, respectively. In an ethanol/water mixture with $f_w = 95\%$, they show bright emissions peaked at 582 and 603 nm, respectively. The Φ_F values of the crystals of **34a** and **34b** are 11% and 13%, which are respectively 112- and 137-fold higher than those of their solutions. Single crystal analysis reveals that multiple H-bonding (e.g., C–H···π, C–H···O and C–H···N) and dipole–dipole (e.g., J-aggregate) interactions exist in the crystals. These interactions restrict the rotations of the rotors and block the radiationless processes, thus enhancing the emission efficiency of **34** in the aggregation state.

Although triphenylamine itself is not AIE active, its electron-donating attribute makes it a versatile building block for the

construction of AIEgens, whose emission color can be tuned through judicious combination with other electron-accepting groups. This design strategy is well illustrated by the AIEgens containing D–A pairs of triphenylamine–diketopyrrolopyrrole (DPP; **35**)^[121] and triphenylamine–benzoselenodiazole (**36**).^[122] Hua et al. have synthesized **35** in pursuit of highly efficient red emitters.^[121] With a large D–π–A structure, two-photon absorption (TPA) is also expected. Luminogen **35** is weakly fluorescent in a THF solution, but its intensity is increased by ~29 fold in a THF/water mixture with $f_w = 90\%$. The AIE mechanism of **35** is rationalized as a result of the restriction of intramolecular vibrations and rotations or RIM in the aggregated state. As expected, **35** shows TPA activity. As measured by the open aperture Z-scan technique, the aggregates of **35** give a TPA cross-section (δ) of 188 GM and emit an intense red light when excited with a near infrared light (800 nm). The high AIE and TPA activities make **35** an appealing material for biophotonic applications.

Ishi-i and coworkers have combined triphenylamine with benzoselenodiazole to construct a family of D–A systems.^[122] Luminogen **36** is a member in such a family. It shows TICT and AIE effects in THF/water mixtures. When it is dissolved in THF, it gives an intense emission peaked at ~650 nm with a Φ_F of ~30%. When water is added into THF, its emission is red shifted to ~680 nm and its PL intensity is decreased with its Φ_F reduced to almost zero. This is a TICT effect caused by the increase in the solvent polarity. When a large amount of water ($f_w > 50\%$) is added, its fluorescence recurs, which gradually intensifies with increasing f_w . An efficient red light-emitting system is thus created based on the aggregate formation of the D–A luminogens in the water-rich aqueous mixtures. It is worth mentioning that the red light emission of **36** can also be generated by a two-photon excitation using a near-infrared laser beam. Other D–A systems with multiple rotors, such as Huang's conjugated asymmetric D–A luminogens, show similar TICT and AIE effects.^[123]

The examples given in Figure 11 are the systems comprising of aromatic stators or planar cores and their AIE properties are mainly associated with RIR processes. In comparison to the RIR-dominated AIE systems, RIV-dictated systems are less known. Some examples of the AIEgens with great involvement of RIV process are shown in Figure 12, in addition to the three such luminogens already discussed in Section 2.1 (i.e., **1**, **7** and **8** shown in Figure 5). Boron diketonate derivatives are an important class of organoboron complexes owing to their excellent photophysical properties, such as large molar absorptivities and high Φ_F values.^[124] Many of them, however, suffer from ACQ effect. Boron ketoiminate is an analogue to boron diketonate with an unsymmetrical boron-chelating ring. Such a structure may impart AIE activity to the boron complex. A group of AIE-active boron ketoimimates with hydrogen or alkyl substituents on the nitrogen atom have been developed by Chujo's team.^[125] The Φ_F values of **37**, for example, are 1% and 76% in the solution and solid states, respectively. Increasing solvent viscosity or lowering solution temperature brings about an increase in the emission efficiency.

Scrutiny of the X-ray crystal structures of **37** and its analogue boron diketonate derivative offers useful insight to its AIE mechanism. The structure of **37** has a larger contribution from

the enolimine core than that from the enaminoketone core in the diketonate system. The BF_2 unit in **37** is off-center to the O–N line, while its B–N bond is longer than its B–O bond. Its boron-chelating ring should therefore be more active in the vibrational motion than that of boron diketonate, because of its unsymmetrical structure and ring distortion. The dynamic intramolecular vibration of its non-planar and non-aromatic boron-chelating ring, in addition to the rotation of its aromatic substituents (i.e., the two methoxyphenyl rings), has weakened its light emission in the solution state.

The strategy to endow a luminogen with AIE activity may boil down to a design principle of increasing structural flexibility and ensuring intramolecular motion as a molecular species. Luminogens **38**–**40** are the examples of AIE systems with non-planar vibrant rings.^[126–128] 11,11,12,12,-Tetracyano-9,10-antraquinodimethane (TCAQ) takes a boat-like conformation. It has been widely studied as a conducting material and used as a building block to construct D–A systems.^[129] Hu's research team has chosen TCAQ as a functional unit to build new AIE systems with twisted conformation.^[126] The 2,6-diphenyl substituted TCAQ derivative (**38**) prepared by the researchers shows a Φ_F value lower than 0.5% in a dilute acetonitrile solution. Addition of water into acetonitrile boosts its PL intensity by ~33 fold. Crystal analysis reveals that the molecules of **38** are compactly packed with the aid of many short contacts in the solid state, with the intermolecular C–H···N H-bonds playing an important role in restricting the intramolecular motions.

TCAQ itself also shows an emission enhancement when water is added into its solution, although the increment is only 2 times. In other words, TCAQ (without any rotors) is AIE active. Owing to its flexible boat-like conformation, the molecule, especially its central non-planar anthraquinodimethane ring, can vigorously vibrate in the solution state. The vibration is hampered in the aggregate state because of the molecular stacking. The RIV process has thus contributed to its AIE property. As uncovered by single crystal analysis, one kind of H-bonds in TCAQ is similar to that in **38** in nature but longer in distance, indicating that the molecular packing of TCAQ is looser. As a result, the AIE effect of TCAQ is not as big as that of **38**. The AIE activity of **38** is thus a collective effect of RIR + RIV: in the solution state its molecules substantially vibrate and its phenyl substituents actively rotate, whereas in the aggregate state the compact molecular packing and multiple short contacts constrain the intramolecular vibration and rotation.

Tetrasubstituted olefins have attracted much attention due to their potential applications as photo-responsive materials in molecular devices as well as in the realm of bioengineering.^[130] Perumal's group has developed a facile method for the synthesis of tetrasubstituted olefinic xanthene derivatives via palladium-catalyzed intramolecular carbopalladation followed by C–H activation of substituted 2-bromobenzyl-N-propargylamines.^[127] This method has generated luminogens with new core structures, some of which have been found to show marked AIE effects. They do not emit light on the TLC plates under illumination of a UV lamp when they have been taken out from the developing tanks. After the solvents are evaporated and their spots on the TLC plates are solidified, the luminogens become highly emissive. This “off-on” process can be repeatedly switched, indicative of a typical AIE behavior. Take

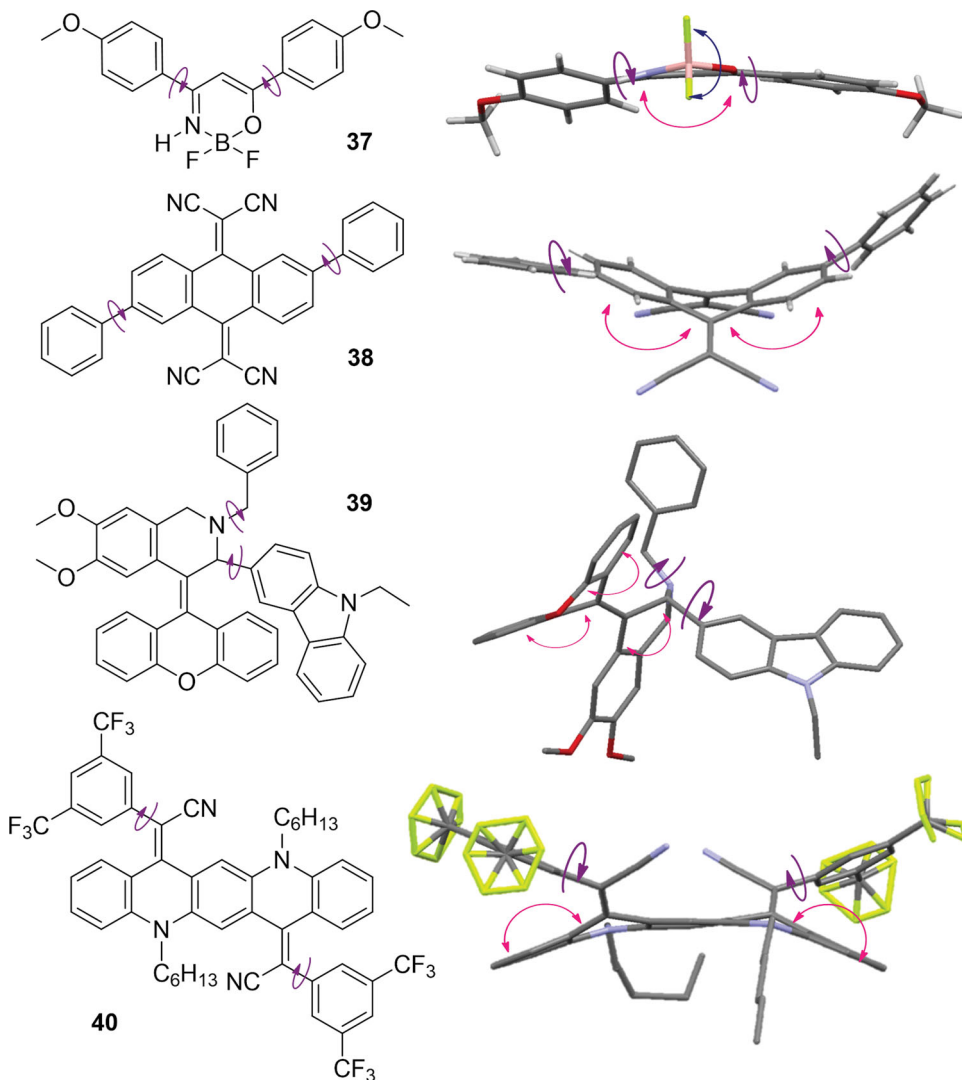


Figure 12. Examples of heteroatom-containing AIEgens whose AIE phenomena are caused by RIM process. The crystal structures of **37–39** are retrieved free of charge from CCDC (905566, 905986 and 899105) via www.ccdc.cam.ac.uk, while that of **40** is obtained from the Supporting Information of Reference 128 free of charge via <http://pubs.acs.org>.

luminogen **39** as an example, its acetonitrile solution is non-emissive. Addition of a non-solvent (e.g., water) makes the suspension visually luminescent, with an emission enhancement up to 28 times. Its aggregates, powders and crystals are all highly luminescent.

Luminogen **39** takes a twisted propeller-like conformation. The packing of its molecules is stabilized by the intermolecular C–H···O H-bond with a distance as short as 2.529 Å, which makes its structure very rigid in the crystalline state. The severe steric hindrance caused by the presence of the *N*-benzyl and carbazole groups at the adjacent positions of the ring further stiffens the molecular structure. Close inspection of the single crystal structure of **39** finds that its tetrahydroisoquinoline and 9-methylene-9*H*-xanthene rings are considerably deviated from planarity, which allows intramolecular vibrations in the solution state. Clearly, besides the intramolecular rotations, the active intramolecular vibrations of the non-planar flexible rings

also participate in the photophysical process in the solution of **39**. Its AIE activity is thus ascribed to the collective effects that rigidify its molecular conformation and encumber its intramolecular motions in the aggregates.

Wang et al. have successfully prepared a number of new quinacridone derivatives with AIE activity.^[128] The emission from a THF solution of **40**, for example, is very weak. However, when a non-solvent like water is added into THF, its luminescence is dramatically boosted. Its Φ_F in the THF solution is ~0.02%, which is increased to 9% in a THF/water mixture with an f_w of 50%. Its thin solid film gives a Φ_F of 9.9%. Although alkyl-substituted quinacridone derivatives do not show any AIE activity, their 2-[3,5-bis(trifluoromethyl)phenyl]acetonitrile-substituted congeners with a twisted conformation exhibit pronounced AIE effects. Molecule **40** is a quinacridine-cored A–D–A luminogen and is an AIE-active red emitter. Its emission at –196 °C is 18-fold higher than that at –108 °C.

In the single-crystal structure, the central quinacridine core of luminogen **40** is significantly bent from the planarity and its molecule adopts a highly twisted conformation. This twisted structure is stabilized by intermolecular interactions including C–H···N and C–H···F H-bonds. The multiple H-bonds lock the rotating units, barricading the intramolecular rotation. Like in **39**, the intramolecular vibration of the non-planar central quinacridine core in **40** contributes to the emission quenching process in the solution state. In the aggregate state, the vibration of the quinacridine core is restricted. Moreover, the buckled shape of the core skeleton prevents the molecules of **40** from face-to-face packing through π – π stacking. All the above processes collectively confer the AIE activity on **40**.

As discussed above, various H-bonding interactions help rigidify molecular conformation. The intramolecular H-bonding aided ESIPT^[131,132] and intermolecular C–H··· π and C–H···X (X = O, N, F, etc.) H-bonding interactions all facilitate AIE processes. For the luminogens containing carboxamide units, H-bonding is essential.^[133–135] Some representative examples of such luminogen systems are discussed in **Figure 13**. *N*-[4-(Benzodioxazol-2-yl)phenyl]-4-*tert*-butylbenzamide carrying hydroxyl group is a widely used structural motif for ESIPT systems. To understand the AIE mechanism of the luminogens with analogue structures, the hydroxyl group is eliminated and the photophysical properties of the resultant parent form (**41**) are studied.^[133] In common organic solvents, **41** is soluble and shows almost no luminescence, whilst remarkably enhanced emissions in the aggregates/solids are observed. The measured Φ_F for the solid powder of **41** is 50.3%, which is 229-fold higher than that of its THF solution.

The optimized conformation of an isolated molecule of **41** is significantly twisted, with a dihedral angle of 60° between the benzoxazole and 4-*tert*-butylphenyl rings. Its structure in the crystalline state, however, becomes almost coplanar, with a dihedral angle of 173°. The structural stiffening in the crystals impedes the rotational motions of the C–N bond between the two subunits, which is essential for the blockage of the radiationless decay channels. Four molecules of **41** per unit cell are cross-stacked through two types of H-bonding interactions, i.e., C–H··· π and C=O···H bonds. Two molecules of **41** are cross-stacked in an edge-to-edge fashion to form an X-shaped dimer via H-bonding between the 4-*tert*-butylphenyl hydrogen and the carbonyl oxygen atoms. Two X-dimers are then edge-to-edge connected with each other through a C–H··· π bond. The two molecules with the C–H··· π interaction adopt an L-shape aggregation mode and the two X-dimers form a #-shaped tetramer. The #-aggregation is further developed to a 3D network by another kind of H-bond between the two #-aggregates formed between the nitrogen atom in the oxazole ring and the neighboring hydrogen atoms of the two cross-linked molecules. The AIE effect of **41** is thus caused by the H-bonding aided RIR mechanism.

Benzene 1,3,5-tricarboxamide (BTA) is a structural motif for supramolecular hierarchical assembly.^[136,137] Albuquerque, Schmidt, et al. have studied self-assembly behaviors of a polar BTA derivative (**42**) in aqueous media.^[134] Its assemblies in the bulk and gel states show a strong blue emission. The luminescence arises from its molecular aggregation via H-bonding. Its aggregation behavior in aqueous media is controllable by pH

variation. When it is admixed with sodium hydroxide, it turns into a water-soluble salt. Upon acidification, the carboxylates get protonated and its solubility in water is reduced, resulting in the formation of hydrogel. Accompanying with the solubility change, its luminescence is intensified. DFT calculation, along with the experimental data, indicate that massive H-bonds in the hydrogel have helped rigidify the supramolecular structure, leading to the AIE effect with a strong blue emission.

Besides the above discussed one- (**41**) and three-armed (**42**) carboxamide derivatives, there are yet multi-armed derivatives that can be used to build AIE systems with the aid of H-bonding. For example, **43** is a multi-armed luminogen that underpins the formation of supramolecular hydrogel with strong luminescence.^[135] Temperature-dependent luminescence measurement has confirmed its AIE activity. It emits very weakly in a hot solution and the light emission is intensified as temperature is decreased from 150 °C to 25 °C. Similar to other carboxamide derivatives, the AIE process of **43** is ascribed to the strong multiple intermolecular H-bonding interactions that rigidify the molecular conformation and constrain the intramolecular motions. The gel of **43** selectively responds to F[–] ion among various ionic species (Cl[–], Br[–], I[–], AcO[–], etc.). The response can be observed by the naked eyes: upon addition of F[–] ion, the gel is changed into precipitates and the emission is further enhanced by the N–H···F interaction.

Development of room temperature phosphorescence (RTP) has attracted much interest due to its fundamental importance and potential applications.^[138,139] Pure organic RTP systems have been rare because of the thermal deactivation and quenching during the long lifetime of triplet excitons. We have observed a phenomenon of crystallization-induced phosphorescence (CIP) in a series of pure organic luminogens at room temperature.^[140] These luminogens do not emit in solution and amorphous states but show efficient phosphorescence in crystalline state. Effort has been directed to the development of new CIP luminogens and understanding of general design principles.^[141–143] Luminogenic molecules containing carbonyl groups with non-planar conformation have been found to be promising candidates. Benzil derivatives (e.g., **44** and **45**) have such structural feature and are thus expected to be CIP-active.^[142] Neither of their solutions in oxygen-free solvents nor their spots on TLC plates under dry nitrogen are emissive at room temperature. However, the solutions emit brilliant light when cooled to 77 K. At room temperature, the molecules undergo active intramolecular motions such as phenyl rotation and carbonyl vibration. At the cryogenic temperature, the deactivation pathways by the intramolecular motions are restricted and the luminogens thus become emissive.

As can be seen from the photo shown in **Figure 14a**, the crystals of **44** emit bright green light. This implies that in the crystalline state, the intramolecular motions of **44** are impeded by the ordered molecular packing and specific intermolecular interactions, such as C–H···O bonding. The long lifetime of 0.142 ms indicates that the light emission from the crystals is phosphorescence in nature. Similar luminescence phenomena are observed in other benzil derivatives such as **45**. The incorporation of more carbonyl groups red-shifts the emission color from green (520 nm for **44**) to orange (584 nm for **45**), owing to the more extended effective conjugation length, the

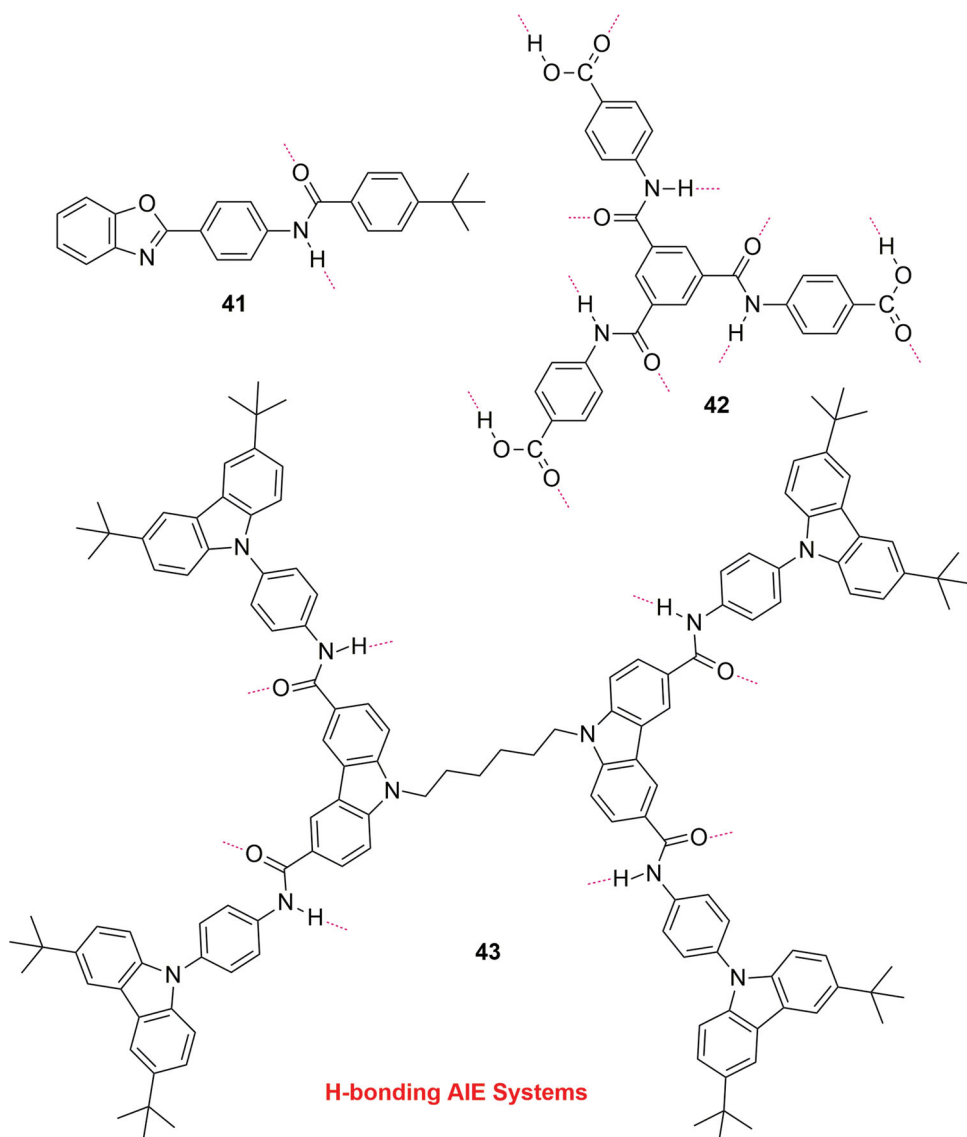


Figure 13. Examples of AIEgens with their structures stiffened by multiple intermolecular hydrogen bonds in the aggregate state.

more enhanced spin-orbit coupling and the lowered energy gap between the T_1 and S_0 states. By combining the following factors, i.e., aromatic carbonyl unit, heavy atom effect and H-bonding interaction, Kim and coworkers have successfully developed new CIP systems based on halogenated aromatic aldehydes.^[143]

Is crystallization a prerequisite for RTP? We know that crystallization is just a physical means to rigidify molecular conformation and hold molecules together through non-covalent interactions. Therefore, if small molecules are connected or confined by covalent bonds or supramolecular forces, their products may also display RTP properties, even if they are not perfectly crystalline. Polymers are formed by linking up numerous small-molecule building blocks. It is very difficult to get perfectly crystalline macromolecules. They are often semi-crystalline, consisting of both crystalline and non-crystalline (amorphous) parts. Many natural products, such as rice, starch, cellulose and bovine serum albumin (BSA), are such semi-crystalline

biopolymers. Although they are everywhere in our life, no light has shed on their luminescent properties, especially phosphorescent behaviors. Driven by the craving for new RTP systems, we have recently looked into luminescence processes in these semi-crystalline biomacromolecules.^[141]

Amazingly, rice emits a bright blue light under illumination of a handy UV lamp (Figure 14b). Its emission spectrum shows a peak and a shoulder at 382 and 433 nm, with lifetimes of 1.72 ns/2.91 μ s and 1.78 ns/5.26 μ s, respectively. The spectral data indicate a dual emission of fluorescence and phosphorescence. It is intriguing that the rice emits such efficient blue phosphorescence at room temperature, for RTP has seldom been observed in pure organic systems under ambient conditions. As mentioned above, molecular interactions are effective in decreasing vibrational dissipation of excited states and are helpful for light emission. In the rice, there exist strong molecular interactions in the form of multiple H-bonds, because the biomacromolecular chain contains numerous oxygen atoms

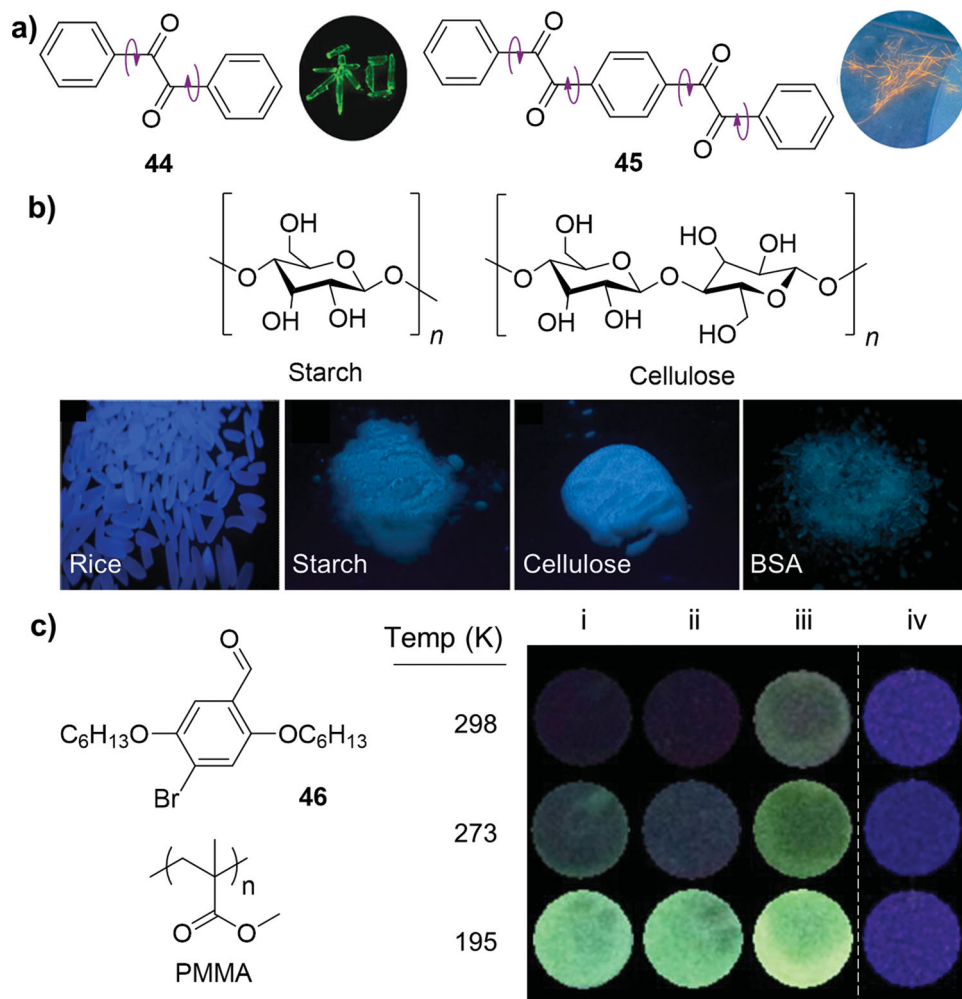


Figure 14. Examples of luminogen systems showing rigidification-induced phosphorescence: (a) benzil derivatives (reproduced with permission;^[142] Copyright 2013, Science China Press and Springer-Verlag), (b) natural products (reproduced with permission;^[141] Copyright 2013, Science China Press and Springer-Verlag), and (c) *p*-bromobenzaldehyde/PMMA mixtures. Inset in panel c: photographs for films of mixtures of **46** with PMMA with different tacticity [atactic (i), syndiotactic (ii) and isotactic (iii)] and for a film of pure **46** (iv) taken under the illumination of a UV light (365 nm) at 195–298 K (Reproduced with permission.^[144] Copyright 2013, American Chemical Society).

and hydroxyl groups. The semi-crystalline morphology of the rice helps fix its chain conformation, which in turn decreases the thermal deactivation and promotes the light emission.

It is known that the major component of rice is starch and we have thus investigated the luminescence behaviors of pure starch. Whereas its aqueous solution is non-luminescent at room temperature, it emits a blue light when the solution is cooled to 77 K. This indicates that its excitons undergo active non-radiative relaxation in the solution state under ambient conditions. Its powders, however, are luminescent even at room temperature. Cellulose is a carbohydrate consisting of a large number of glucose units linked up by glycosidic bonds, whose luminescence properties are comparable to those of starch. BSA also shows similar luminescence behaviors. The emissions from the solid powders of the natural polymers are all visible to the naked eyes. The light emissions are all phosphorescence in nature, as proved by their long lifetimes.

The observation of RTP in the pure organic materials has encouraged us to further explore new luminogen systems. As a

result, many other biopolymers, including chitosan and dextran, have been found to be RTP active.^[141] These natural products are only semi-crystalline, some of which actually have rather low crystallinity. It is thus not so accurate to refer all of these RTP systems as CIP. In the solutions of the biomacromolecules at room temperature, their triplet excitons are non-radiatively deactivated by the dynamic intramolecular motions. In the solid state, multiple structural factors, such as covalent linkage, chain crystallization, and non-covalent interaction, function collectively to rigidify the molecular conformations and activate RIM processes. As a result of the strong suppression of the vibrational dissipations, the light emissions are enhanced even at room temperature. Therefore, in a broad perspective, the CIP concept may be extended to rigidification-induced phosphorescence (RIP). In other words, in principle, any chemical and physical means that can stiffen conformational structure to a great extend can intensify light emission.

Film-forming materials, such as synthetic polymers, are more suitable for real-world high-tech applications. Dispersing

luminogen molecules in a rigid polymer matrix, even if it is in an amorphous state, may well constrain the molecular motions of the luminogens and realize their RTP potentials. Kim et al. have succeeded in suppressing the vibrational dissipations of the triplet excited states by embedding small molecules of **46** in glassy films of poly(methyl methacrylate) (PMMA).^[144] Whereas the microcrystalline films of **46** emit blue fluorescence ($\lambda_{\text{em}} = 425 \text{ nm}$), its PMMA-blended films emit green phosphorescence ($\lambda_{\text{em}} = 520 \text{ nm}$; Figure 14c). The phosphorescence emission is a result of the suppression of the vibrational motions by the glassy PMMA matrix. Theoretically, the more rigid the polymer matrix is, the stronger the vibration suppression would be. The tacticity of PMMA chain thus should strongly affect the quantum yield (Φ_p) of **46**, because it is a structural parameter for chain stereoregularity. This proves to be the case: Φ_p of **46** is progressively increased when the tacticity of PMMA is changed from atactic to syndiotactic to isotactic.

When the isotacticity of the PMMA chain is increased from 0% to 100%, an exponential increase from 0.7% to 7.5% in Φ_p of the PMMA-blended film of **46** is observed. This is associated with the β -relaxation of the macromolecular chain. For PMMA, the β -relaxation is related to the onset of the rotational motion of its ester group, appearing in the temperature region of ~285–300 K (~12–27 °C). The β -relaxation in PMMA is weakened with an increase in its chain isotacticity. At high isotacticity, the loss peak for the β -relaxation is vanished. This is understandable, for the polymer chains with higher isotacticity can pack better, which should hinder the carbonyl vibration to a higher extent. When the temperature is decreased to 195 K (~78 °C), the deep blue fluorescence of **46** itself does not change much but the green phosphorescence of its PMMA-blended film is enhanced. At the low temperature, the β -relaxation is considerably restricted. The phosphorescence is greatly boosted, as a result of suppression of the β -relaxation. Utilization of the amorphous but rigid polymer matrices to stiffen luminogen molecules is on par with the effect generated by the crystallization process, that is, the intensification of the phosphorescence emission.

In addition to polymer matrix, host–guest interaction has also been exploited as a means to rigidify molecular conformation. Adachi et al. have designed and synthesized aromatic guests containing no heavy atoms (e.g., metals and halogens), for such atoms often shorten lifetimes of the triplet excitons.^[145] In their guest–host systems, the aromatic guests are surrounded by amorphous rigid hosts. The guests include amino-substituted deuterated fluorenes, while the hosts include hydroxyl steroids. The light emissions in these systems can be quenched by the radiationless deactivations of the guests and the diffusional motions of the hosts. The heavy deuteration of the aromatic hydrocarbon guests can minimize their non-radiative deactivations, while the conformational rigidity and oxygen barrier of the steroid hosts can suppress the emission-quenching processes. The synergistic effects of the guests and hosts have brought about efficient persistent RTP in air at room temperature. Clearly, the structural rigidification has played an essential role in these RIP processes.

The natural products shown in Figure 14b contain no traditional chromophores, such as π -conjugated double bonds and aromatic rings. It has been reported that some synthetic non-aromatic macromolecules, such as poly[(maleic anhydride)-*alt*-(vinyl

acetate)]^[146] and vinyl polymers carrying succinic anhydride terminal groups,^[147] are also highly luminescent. Apart from these big macromolecules, some small molecules without classical chromophores have been found to show AIE activity.^[148–150] Zhu et al., for example, have synthesized a class of tetrahydropyrimidine derivatives with AIE characteristics.^[149] Luminogen **47**, for instance, is non-emissive in solutions but becomes highly luminescent when aggregated. Its molecular structure is conformationally flexible but rigidified by the multiple intra- and intermolecular forces such as C–H··· π and C–H···O interactions in the crystalline state (Figure 15a). In **47**, the three phenyl rings are attached to a non-aromatic ring through single bonds, which are not conjugated as they are almost perpendicular to each other, as revealed by the crystal structure analysis. Such a luminogen may emit in the UV region, but experimentally its aggregates are found to luminesce in the visible region. What is then the emitting species responsible for the visible luminescence in this unorthodox luminogen system?

Careful examination enables extraction of some common structural and behavioral features in these non-conventional luminogen systems. Although the luminogens contain no classical chromophores, there are numerous electron-rich heteroatoms (oxygen, nitrogen, etc.) with lone-pair electrons in their molecular structures. They become highly luminescent when their conformations are rigidified by covalent bonding, non-covalent interaction, cryogenic cooling, ordered packing, host blending, polymer doping, and so on. On the basis of the experimental results and theoretical simulations, a working mechanism for this kind of non-conventional luminescence processes (including both fluorescence and phosphorescence) is proposed, which is illustrated in panel b of Figure 15.

When molecularly dispersed, the electron-rich luminogens are non-emissive, because of the lack of chromophores with extended electronic conjugations and the quenching by rotational and vibrational motions of the groups carrying the rambling lone-pair electrons. On aggregate formation, the luminogenic molecules become conformationally rigidified. In the aggregates, the electron-rich atoms may form clusters of various sizes, in which their electron clouds are overlapped and shared, thus generating “cluster chromophores” with smaller energy gaps and more extended electronic conjugations, in comparison to those of the isolated molecules. In the meanwhile, the molecular and electronic interactions in the aggregates considerably block the radiationless deactivation channels, thereby rendering the cluster chromophores emissive. The larger the cluster is, the brighter and redder the luminescence would be. This kind of luminescence may therefore be termed as rigidification-induced emission (RIE). A number of natural products, including chitosan, dextran, glycogen, glucose, xylose and galactose, have been found to show RIE effect (vide ut supra), proving the generality of the phenomenon.^[141] RIE may offer a new clue to the underlying causes for the auto-luminescence in biological systems.

3.3. Organometallic AIE Systems

The above discussions are all about the emission enhancements in the pure organic luminogen systems. Most of the

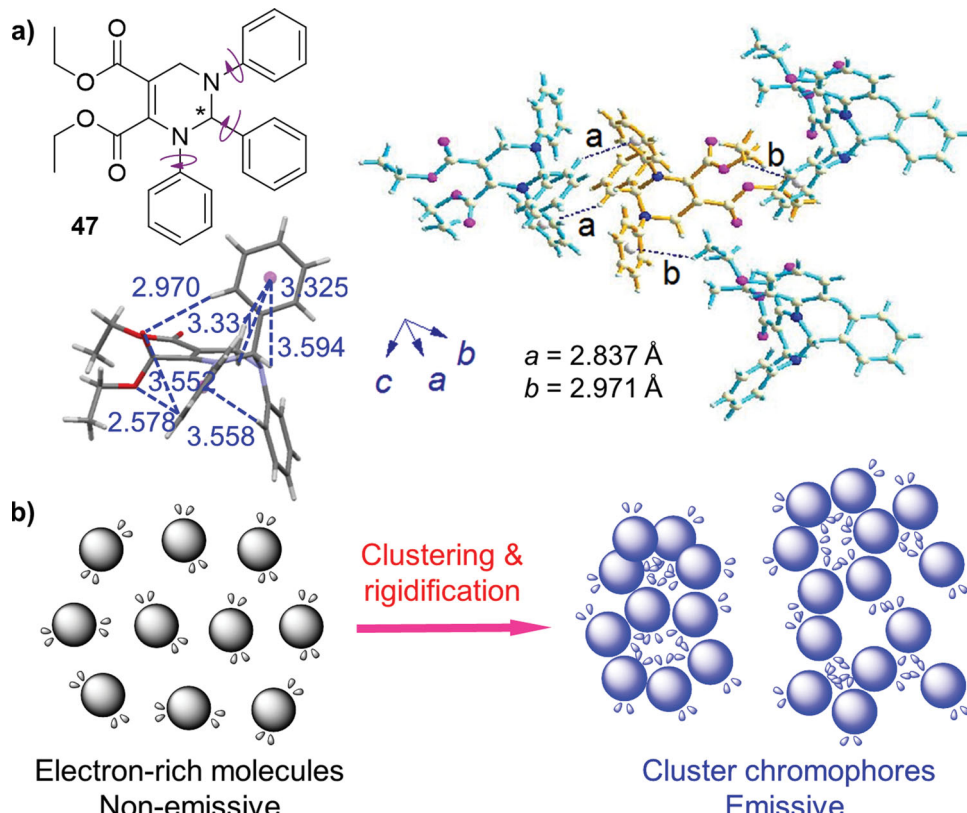


Figure 15. (a) Molecular and crystal structures of a non-conventional tetrahydropyrimidine-based AIEgen (**47**). Reproduced with permission.^[149] Copyright 2013, Wiley-VCH Verlag GmbH & Co. KGaA. The crystal data are retrieved free of charge from CCDC (818027) via www.ccdc.cam.ac.uk. (b) Diagrammatic representation of proposed working mechanism for a heterodox luminogen system.

systems are fluorescence, because their radiative decays are associated with transitions of singlet excited states.^[28,29] In organometallic systems, phosphorescence is readily achievable, thanks to their metallic components. However, similar to many organic systems, phosphorescence emissions of organometallic luminophores are also often weakened with increasing solution concentration and quenched by aggregate formation.^[7] In other words, many organometallic luminophores suffer from severe ACQ effects. Delightfully, AIE effects have also been observed in organometallic phosphorescence systems, which has been referred to as aggregation-induced phosphorescence (AIP).^[29a,151–164] This has helped broaden the area of phosphorescence research. Some emblematic examples of organometallic AIP systems are presented in Figure 16.

Iridium(III) complexes have been extensively investigated as organometallic phosphors but many of them suffer from ACQ effects. The well-known tris(2-phenylpyridine) iridium(III) complex [$\text{Ir}(\text{ppy})_3$], for example, shows typical ACQ behavior: its solution Φ_p is as high as 97%, but its film Φ_p is merely 3%.^[165] Su's group have designed and synthesized a series of AIP-active cationic Ir(III) complexes with different ligands.^[153–156] Complex **48** is a cationic Ir(III) complex bearing a dendrimer-like ligand.^[156] It can be considered as one of the three phenylpyridine ligands of $\text{Ir}(\text{ppy})_3$ being substituted by multiple carbazole units. In sharp contrast to its parent form $\text{Ir}(\text{ppy})_3$, its solution emission is so weak that its Φ_p cannot be accurately determined. When a small amount of water ($f_w =$

10%) is added into acetonitrile, weak phosphorescence starts to appear. At $f_w = 90\%$, the emission of **48** is 90-fold higher than that at $f_w = 10\%$. The long lifetime (3.6 μs) of its solid film manifest its AIP character. The RIR mechanism has been verified to be the main cause for this AIP system by means of structural and temperature controls as well as quantum calculations.

Schiff base complexes of Zn(II) are promising emitters for OLED applications. A group of organozinc Schiff base complexes have been developed by Su's team.^[152] Diphenylamino and carbazole groups are incorporated into the structures of Zn(II) complexes, in anticipation that the introduction of aromatic rotors gives rise to new AIP luminogens. All the organozinc complexes prepared by the researchers show remarkable enhancement in PL efficiency upon aggregate formation. A solution of **49** in dichloromethane, for example, is weakly luminescent with a Φ_p of 3.0%, whereas its powder shows a Φ_p of 21.4%, indicative of an AIP effect. A Zn(II) Schiff base complex without aromatic rotors is prepared as a control. This complex is highly luminescent when dissolved in a good solvent. Its emission is sharply decreased upon aggregate formation due to the ACQ effect. The AIP behaviors of **49** and its congeners are interpreted as the result of RIR processes. In the solution state, their aromatic rotors undergo dynamic intramolecular rotations, resulting in the weak emission. The aggregate formation effectively suppresses the molecular motions, thus making the complexes highly emissive.

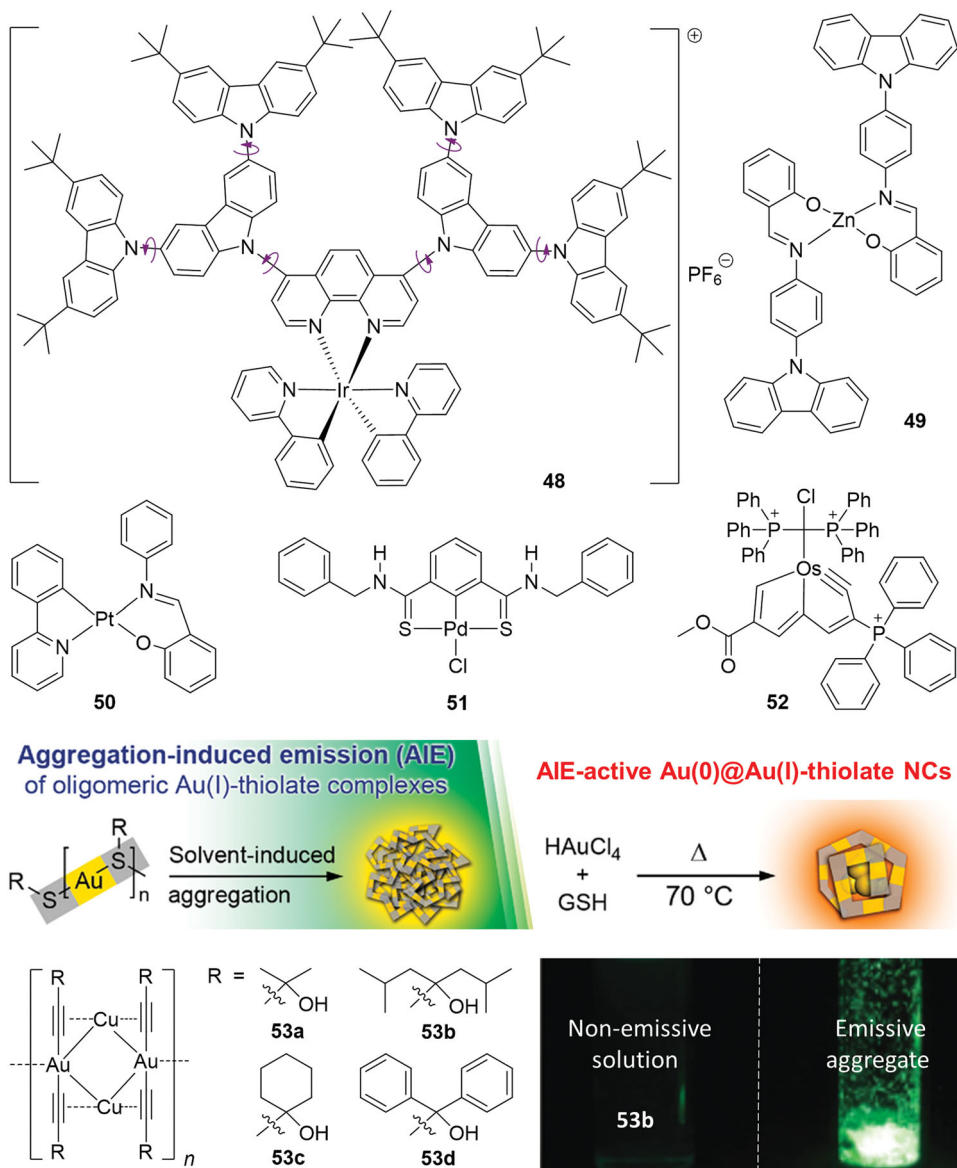


Figure 16. Examples of organometallic AIE systems. Scheme reproduced with permission from American Chemical Society (Copyright 2012),^[159] while photographs reproduced with permission from Wiley-VCH Verlag GmbH & Co. KGaA (Copyright 2013).^[162]

Zhao, Huang, et al. have synthesized a class of new Pt(II) complexes and studied their AIP behaviors.^[158] Their emission colors can be tuned from yellow to red by changing the ligand structure. Among the complexes, **50** emits the strongest luminescence in the crystalline state with a Φ_p of 38%. Whilst its emission in THF is very weak, its phosphorescence in a mixture of THF/water with $f_w = 87.5\%$ is two orders of magnitude stronger. The time-dependent DFT calculations reveal that in the S_0 ground state of the complex, its chelating plane is almost coplanar. In the T_1 excited state, however, the six-membered chelating ring between the Pt center and $N\wedge O$ ligand is significantly distorted. The intramolecular vibration caused by the structural distortion facilitates the non-radiative decay in the solution state. As learned from the X-ray diffraction data, the crystal structures of the complexes are close to those optimized

geometries in the ground state. No evident $Pt\cdots Pt$ and $\pi\cdots\pi$ interactions are detected. There exist multiple $C-H\cdots\pi$ interactions, which rigidify the molecular conformations and hamper the photoinduced structural distortions. Clearly, the AIP activity of the Pt(II) complexes is associated with the RIM processes.

Kanbara and coworkers have prepared a thioamide-based pincer Pd(II) complex (**51**).^[163] It has two thioamide units as H-bonding donors and a chlorine ligand as an H-bonding acceptor. Neither the solutions of **51** nor its powders are luminescent at room temperature. At a low temperature (77 K), it emits a green light in a dichloromethane/THF glass matrix with a Φ_F as high as 65%. The molecules of the organopalladium complex coexist with solvent molecules in the crystals of different densities. The emissions of the crystals are dictated by

the packing arrangements. The zigzag arrangement is found to be unfavorable for emission because of the loose packing of the organopalladium molecules in the crystals, whereas strong luminescence is emitted from the crystals with dense packing arrangement strengthened by the H-bonding at room temperature. The high packing density and strong H-bonding interaction have largely suppressed the distortive motions of the Pd(II) complex in the excited state, resulting in the efficient light emission.

Cyclic alkynes are challenging synthetic goals due to the involved ring strain. Xia's group have successfully synthesized a number of stable osmapentalyne complexes.^[164] With these complexes, the concept of aromaticity is extended to five-membered rings containing metal-carbon triple bonds. These novel metal-aromatic complexes show unusual optical properties, such as near-IR emission with large Stokes shifts (up to 320 nm), long lifetimes (0.1 to 1 μ s), and AIE behaviors. Complex **52**, for example, emits weakly at room temperature in common organic solvents. Addition of a large amount of water into its ethanol solution causes a clear enhancement in its emission intensity. Intense red emission is emitted from its crystals. This is attributed to the stabilization of its excited states by the aggregate formation, in which the intramolecular rotations and vibrations as well as the intermolecular collisions are greatly restricted by the physical constraints.

Au-thiolate nanoclusters (NCs) are ultrasmall gold nanoparticles ($d < 2$ nm) protected and stabilized by thiolate ligands.^[166] Xie's group has recently reported AIE systems based on Au-thiolate NCs.^[159] As depicted in Figure 16, the non-emissive oligomeric Au(I)-thiolate complexes can become luminescent, whose emission intensity and wavelength are tunable by the degree of aggregation. Adding ethanol to an aqueous solution of an Au-thiolate complex disrupts the hydration shell, resulting in charge neutralization and aggregate formation. The aggregation promotes intra- and intercomplex interactions between the metal centers. The formation of the aurophilic bonds in turn gives impetus for further aggregation, leading to the formation of denser and more rigid aggregates. The strong multiple intra- and intercomplex interactions including van der Waals force and aurophilic interaction in the aggregates restrain the complexes from undergoing intramolecular vibrations and rotations. The RIM processes hinder the radiationless relaxations and boost the radiative decays. Similar AIE effects have been observed by Liu et al.^[160] and Tsutsumi et al.^[161] in other Au(I) complex systems.

Apart from the above organometallic complexes with single metal centers, some complexes with multiple metal centers have also been found to display AIE feature. A series of novel AIP-active homoleptic alkynyl complexes $\{[\text{Au}_2\text{Cu}_2(\text{C}_2\text{R})_4]_n$ (**53**) $\}$ have been developed by an international research collaboration team led by Koshevoy and Chou (Figure 16).^[162] These complexes are virtually non-luminescent in the solution state but highly emissive in the solid state. The solid-state Φ_p of **53d**, for example, is as high as 95%. The unique arrangement of the metal ions forces the gold-dialkynyl units to take a significantly twisted conformation, giving a helix-like polymeric chain –Cu–Au–Cu–Au– through the metallophilic interaction in the aggregated state. In addition to the metallophilic attraction and the π -C≡C–Cu bridging coordination of the alkynyl ligands, the $[\text{Au}_2\text{Cu}_2(\text{C}_2\text{R})_4]$ units are

stabilized by the O···H–O H-bonding. The AIP character of these complexes has been concluded by the researchers as the result of a synergistic effect of the array of the metallic chain upon aggregation, which greatly enhances the possibility of spin-orbit coupling and subsequently the phosphorescence emission.

4. Exploration of High-Tech Applications

Technological applications of luminescent materials are often realized in the solid state as thin films, which has motivated scientists to direct their research efforts towards the development of efficient solid emitters. The generation of the AIE materials does not only fit the bill but also provide a new platform for hitherto impossible technological innovations. In some sense, the practical applications of the AIE materials are endless, whose scope is probably limited only by our imagination. In principle, the AIE materials can be used wherever a RIM process is involved. The AIE materials are highly emissive in the solid state and are thus promising for OLED applications. The AIE effect offers exhilarating possibilities for developing new sensing systems that operate in a luminescence turn-on mode, which should outshine their turn-off counterparts based on traditional ACQ materials, in terms of sensitive detection and less likelihood of generating false-positive signals.^[167] In the past decade, the AIE materials have found a wide variety of high-tech applications, with a large number of optoelectronic devices and sensory systems being invented.^[28,29] In this Section, we will briefly discuss some recent progresses in the area, with an emphasis on those accomplished after the publication of our previous review in 2011.^[29a]

4.1. Optoelectronic Devices

4.1.1. Organic Light-Emitting Diodes

Due to their high potentials in display and lighting applications, OLEDs have attracted much interest among scientists and technologists.^[168] Despite the great success achieved by some commercial luminophores in the area, a barricade to the realization of full-color displays is the poor performances of blue light emitters, because their wide band gaps make it very difficult to inject charges into the active layers in the devices.^[169,170] A number of blue light-emitting materials based on anthracene, fluorene and styrylarylene derivatives have been reported.^[171–173] However, when fabricated into thin solid films in the OLED devices, many of them suffer from the notorious ACQ effect, which deteriorates the device performances to great extents. AIE-active luminogens are expected to provide a solution to this problem.^[28,29,174–178]

Using TPE as a building block, many blue emitting AIEgens have been prepared through smart design and facile synthesis, some examples of which are shown in Figure 17.^[174–177] Attaching multiple TPE units to a carbazole core affords a new AIEgen (**54**) with a high solid-state emission efficiency ($\Phi_F = 100\%$).^[174] A multilayer electroluminescence (EL) device is fabricated from this AIEgen, which emits a sky blue light ($\lambda_{em} = 488$ nm)

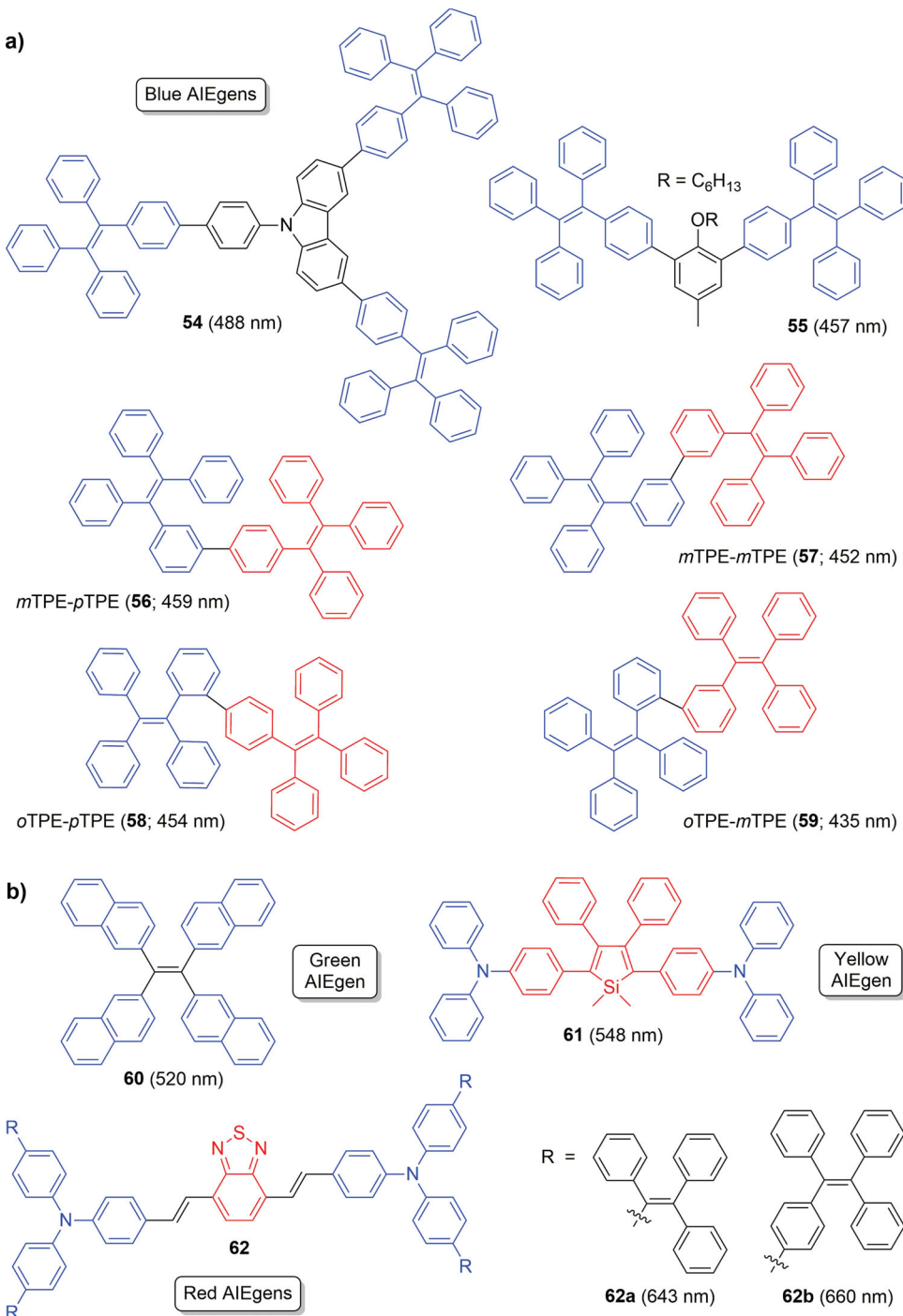


Figure 17. Examples of TPE-based AIEgens showing excellent OLED performances with (a) blue and (b) green, yellow and red light emissions.

with current (η_C), power (η_P), and external quantum efficiencies (EQE) of 3.8 cd A⁻¹, 2.1 lm W⁻¹, and 1.8%, respectively. Because carbazole is a well-known hole-transporting (HT) unit, a simpler EL device without an extra HT layer is fabricated. It emits a similar sky blue light ($\lambda_{em} = 490$ nm) in higher efficiencies ($\eta_C = 6.3$ cd A⁻¹, $\eta_P = 4.1$ lm W⁻¹, and EQE = 2.3%). A fly in the ointment is that the EL emission of **54** is not pure blue.

Li et al. have worked on the development of pure blue AIE emitters.^[175–177] The researchers, for example, have combined TPE and spirofluorene moieties together.^[175] Through striking a balance between blue emission and electronic conjugation, the researchers have succeeded in the fabrication of a non-doped EL device that emits a blue light of 466 nm in an efficiency of 3.33 cd A⁻¹. In Section 2.1., we have discussed a CIE system. A CIE luminogen is known to emit a blue-shifted stronger light

in the crystalline state than in the amorphous state.^[28,29a,67] The researchers have utilized this CIE effect and prepared a group of AIEgens by decorating a benzene core with multiple TPE units.^[176] The conformational twist between the TPE units and the benzene core acts as a buffer to mitigate the π -conjugation extension, preventing the emission color from being too red-shifted. This design rationale is well demonstrated by the EL device performance of the benzene-cored AIEgen **55**. The non-doped OLED using **55** as an active layer emits a pure blue light ($\lambda_{\text{em}} = 457 \text{ nm}$) with a Commission International de l'Eclairage chromaticity coordinate of (0.16, 0.15).

When two TPE units are hooked up through a *para* linkage, the resultant bisadduct (BTPE or *p*TPE-*p*TPE) emits a redder light, although in a higher efficiency, than does its parent form (TPE), due to the more extended π -conjugation in the AIEgen. Li's group have prepared a series of new bis-TPE adducts, i.e., *m*TPE-*p*TPE (**56**), *m*TPE-*m*TPE (**57**), *o*TPE-*p*TPE (**58**), and *o*TPE-*m*TPE (**59**), by different combinations of *ortho*-, *meta*- and *para*-linkages, instead of the *para*-only linkage, in an effort to control the extent of π -conjugation and to achieve the desired blue emission.^[177] When fabricated into OLEDs as emitters, all of the AIEgens (**56–59**) emit blue light in the wavelength region of 459–435 nm with chromaticity coordinates of (0.16, 0.16), (0.15, 0.11), (0.16, 0.14) and (0.16, 0.14). The well-controlled π -conjugations in these AIEgens have enabled them to emit in higher efficiencies (1.8–2.8 cd A⁻¹) than TPE (0.45 cd A⁻¹).

Through utilization of the RIM principle, AIEgens with emission colors covering the whole visible spectral region can be readily designed and generated, which are promising candidate materials for full-color optical display applications.^[28,29,179–181] A green AIEgen (**60**) has been built by replacing the phenyl rings of TPE with naphthalene rings. It shows an enhanced light emission upon aggregation, with a Φ_F of 22.4% in the film state. The device performance of its multilayer OLED is superior to that of TPE. Its EL emission is peaked at 520 nm, with a maximum luminance of 8840 cd m⁻². Thus, although naphthalene is a conventional planar luminophore suffering from the ACQ effect in the solid state, the propeller-like architecture of **60** endows it with marked AIE activity, thanks to the involved RIM process.

Triphenylamine is well-known for its fast hole mobility and has been widely used to make HT materials. Silole is an excellent material for the fabrication of OLEDs, owing to its high solid-state emission efficiency. Fusing triphenylamine with silole in a single molecule may generate a new AIEgen for the fabrication of OLEDs with simple device configurations.^[180] Luminogen **61** is such a fusant. It exhibits a high solid-state Φ_F (74.0%) and a high thermal stability ($T_d \sim 390 \text{ }^\circ\text{C}$). It serves the dual roles of light emitter and hole transporter, which help simplify device structure without sacrificing EL performance. Without using an additional HT layer, an OLED based on **61** emits a yellow light ($\lambda_{\text{em}} = 548 \text{ nm}$) in high luminescence (14308 cd m⁻²) and EQE (2.26%), which are comparable to those of the multilayer EL device with an extra HT layer.

Red emitters with high EL efficiency and thermal stability are scarce and are hence in great demand. Red luminophores are usually big molecules with extended π -conjugation and planar conformation or D- π -A molecules with strong charge transfer character, which often suffer from ACQ effect.^[182] Chi, Xu,

et al. have prepared red emitters with AIE attribute through decorating D- π -A cores (e.g., D = triphenylamine and A = thiadiazole) by AIE units (e.g., TPE and triphenylethene).^[181] These AIEgens (e.g., **62**) show very high thermal stability ($T_d \sim 513$ –529 °C). The multilayer OLEDs based on **62** are turned on by low voltages (down to 3.3 V). The EL device of **62b**, for example, affords a maximum luminance of 13535 cd m⁻², with η_C , η_P , and EQE being 6.81 cd A⁻¹, 4.96 lm W⁻¹, and 2.88%, respectively. These superb device performances put **62b** on the list of the most efficient red emitters for non-doped OLEDs. Du, Wang, et al. have synthesized a group of near-IR AIEgens by integrating TPE moieties into [1,2,5]thiadiazolo[3,4-g]quinoxaline and benzo[1,2-c;4,5-c']bis[1,2,5]thiadiazole structures.^[183] Non-doped OLEDs constructed from these AIEgens emit near-IR light with peak wavelength up to 864 nm in EQE up to 0.89%.

4.1.2. Light-Emitting Liquid Crystals

Integration of luminogens with mesogens is of great interest, because such amalgamation may result in the formation of light-emitting liquid crystals (LELCs) that meld the best parts of the two types of components. The LELCs may find an array of technological applications in such areas as anisotropic OLEDs,^[184] polarized organic lasers,^[185] optical information storage, one-dimensional semiconductors,^[186] chemical sensors, and liquid-crystal displays (LCDs).^[187,188] The optoelectronic devices built from the LELCs may possess a number of advantageous features. For example, an LCD based on an LELC will have simple device configuration, low manufacture cost, and greatly enhanced brightness, contrast, efficiency, and viewing angle.^[189] More importantly, the power-hungry extra backlight will be eliminated. Despite these thrilling prospects, the development of LELCs remains to be a challenging proposition. As mentioned above, the conventional luminophores often suffer from the ACQ effect in the solid state. Aggregation or self-organization is an intrinsic process for the formation of a mesophase, which explains why it has been so difficult to incorporate the traditional chromophores into the mesogenic structures while retaining their luminescent and mesomorphic properties.^[190] The AIEgens are non-conventional systems and are promising candidates for the development of novel LELCs, because aggregation is required for the activation of the RIM processes and the realization of their light emissions.

Three examples of such LELCs are presented in Figure 18. Lai et al. have developed two silole-based gelators containing amide units and carrying alkoxy chains (**63**).^[191] In addition to the gelation ability, the tetraphenylsilole cores of **63** can self-assemble into liquid-crystalline phases over a wide temperature range with the aid of the amide units and the alkoxy chains. The scanning calorimetric analyses of **63** reveal two sets of phase transitions, one for the crystal-to-LC transition (59 °C for **63a** and 54 °C for **63b**) and another for the LC-to-liquid transition (206 °C for **63a** and 176 °C **63b**). The textures of **63a** observed under polarized optical microscope (POM) at 112.4 °C and 60.6 °C correspond to smectic mesophases (Figure 18a). The microphotographs of **63b** taken by the POM at 127.2 °C and 67.6 °C are optically anisotropic but texturally atypical,

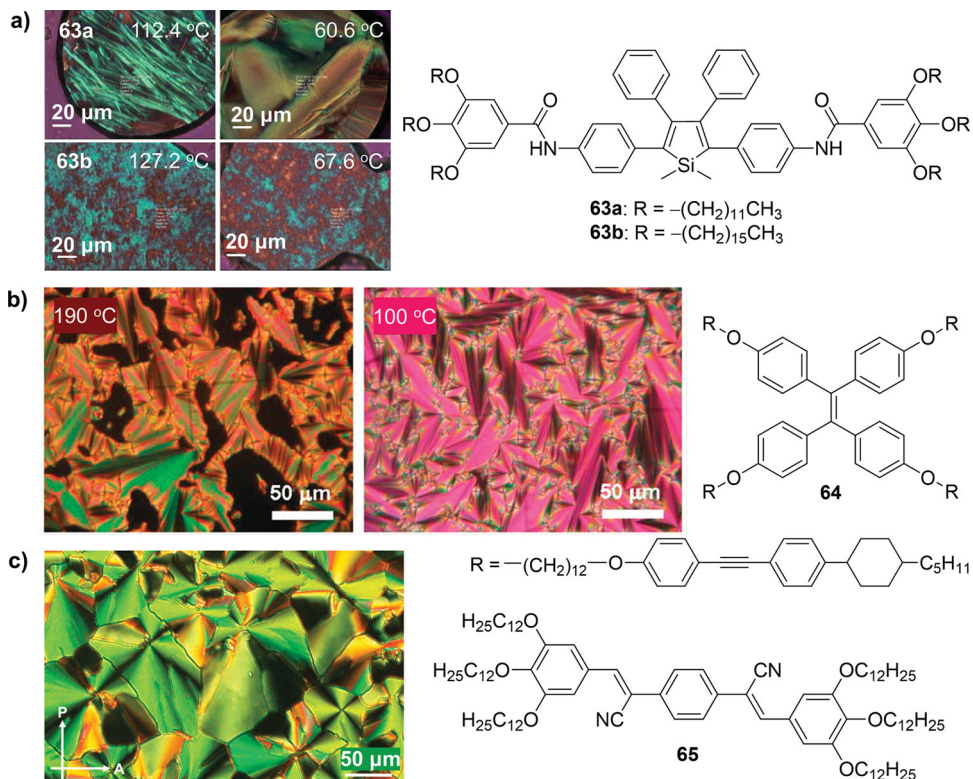


Figure 18. (a) Optical micrographs of **63**, a light-emitting liquid crystal (LELC), between crossed polarizers: mesomorphic textures of **63a** observed at 112.4 °C and 60.6 °C and **63b** at 127.2 °C and 67.6 °C. Reproduced with permission.^[191] Copyright 2010, Royal Society of Chemistry. (b) POM images recorded on cooling LELC **64** to 190 °C and 100 °C from its isotropic liquid state. Reproduced with permission.^[192] Copyright 2012, Royal Society of Chemistry. (c) Pseudo focal-conic fan-shaped texture of LELC **65** observed under POM in the Col_h phase at 40 °C. Reproduced with permission.^[194] Copyright 2012, Wiley-VCH Verlag GmbH & Co. KGaA.

indicating that the mesomorphic packing arrangements of **63** are sensitively affected by the subtle change in the length of the alkoxy chain.

The AIE feature is well preserved in the LELC systems, no matter whether the core is silole, TPE, or another AIEGen. LELC **64**, for example, is AIE active, exhibiting a solid-state Φ_F as high as $67.4 \pm 5\%$.^[192] It consists of a TPE core and four mesogenic pendants. When **64** is cooled from its isotropic liquid state to 190 °C, a fan-shaped mesomorphic texture emerges from the homotropic dark background (Figure 18b). When it is further cooled to 100 °C, a focal conic texture is formed. Thus, although the TPE cores are twisted in conformation, they are still capable of columnar packing in the LC state. The peripheral mesogens self-assemble into a tetragonal smectic structure that is orthogonal to the TPE column, resulting in a unique biaxially oriented packing arrangement. Intriguingly, the bromo-substituted derivative of the peripheral mesogen of **64** has recently been found to be AIE active by Yu and coworkers.^[193] It shows a mesophase transition sequence of nematic-smectic C-smectic B during the cooling process.

Park et al. have recently reported a new phasmidic AIEGen (**65**), which forms a hexagonal columnar LC phase at room temperature (Figure 18c).^[194] The terminal trisdodecyloxy units are attached to the dicyanodistyrylbenzene core to facilitate the mesomorphic organization. As revealed by the POM observation, **65** displays a pseudo focal-conic fan-shaped texture of a

hexagonal columnar (Col_h) phase at 40 °C. It emits intense green and yellow lights in the LC and crystalline states, in contrast to the complete absence of light emission in the isotropic melt state. The AIE feature and dual-color thermochromic fluorescence of **65** are attributed to the peculiar intra- and intermolecular interactions of its dipolar cyanostilbene units. The RIM mechanism activated by the specific molecular stacking processes in the LC and crystalline phases are found to be responsible for the AIE effect. On the basis of these nice examples, it may be concluded that judiciously decorating an AIEGen with appropriate mesogenic units is a rational approach to an LELC with efficient luminescence in the LC state.

4.1.3. Circularly Polarized Luminescence and Optical Waveguiding Effect

Apart from the advanced materials for the OLED and LCD applications, other optoelectronic and photonic materials with functional properties including circularly polarized luminescence (CPL)^[195] and optical waveguide effect have also been constructed from AIE-active building blocks.^[116,196–198] CPL reflects the chirality of a material in the excited state. Chiral materials with efficient CPL are useful for biosensing and optoelectronic applications, e.g., stereoscopic optical information processing, display and storage.^[199–201] Realization of these applications

require materials with high CPL performances. Two essential parameters have been used to evaluate the performances of CPL materials: one is the luminescence dissymmetry factor [$g_{\text{em}} = 2(I_L - I_R)/(I_L + I_R)$] and the other is the luminescence efficiency. A common strategy to π -conjugated chiral systems is to synthesize molecules with planar π -conjugated luminophores in the cores and chiral groups at the peripheries. However, the notorious ACQ effect causes low emission efficiency and poor spectral stability in the conventional luminophore systems.

To tackle this problem, we put forward a strategy to create high-performance CPL-active materials that meet the requirements of high luminescence efficiency and large g_{em} value in the solid state. Luminogen **66** is designed according to the strategy, which is comprised of an AIE-active silole core and two chiral sugar pendants, as shown in Figure 19a.^[195] It shows neither circular dichroism (CD) nor light emission in solution, whereas upon aggregation, its molecules readily self-assemble into hierarchical helical structures and display simultaneous aggregation-induced CD and AIE, affording absolute Φ_F and g_{em} values of 81.3% and ~ 0.32 , respectively. It should be stressed that the g_{em} value of **66** is several orders of magnitude higher than those of previous systems ($g_{\text{em}} \sim 10^{-5}$ – 10^{-2}).^[195] Luminogen **66** is the first example of AIE-active CPL material

with high emission efficiency, dissymmetry factor, and spectral stability. Further study in the area will generate a class of advanced functional materials with efficient CPL in the solid state, widening the territory of CPL research.

Luminescent materials with optical waveguiding effects are an important class of functional materials.^[202] A series of AIEgens with optical waveguide effects spanning almost the whole visible spectral range have been developed.^[196–198] Zhang et al., for example, have reported the waveguide effect of an AIEgen named di(*p*-methoxyphenyl)dibenzofulvene (**67**; Figure 19b).^[196] It displays polymorph-dependent fluorescence, with two crystalline forms emitting strong blue (**67a**) and green (**67b**) lights. On the basis of the crystal structure analyses, the AIE effect of **67** is attributed to the RIR process and the difference in the fluorescence colors between **67a** and **67b** is ascribed to the molecular conformation variation. The microrods of **67a** and **67b** show excellent optical waveguiding behaviors. The light emissions from the two terminals of their microrods are very strong, whereas those from their rod bodies are relatively weak. The microrods are excited with a focused laser beam down to the diffraction limit at different locations. The optical losses for the microrods of **67a** and **67b** are estimated to be 76.5 and 56.7 dB mm⁻¹, respectively.

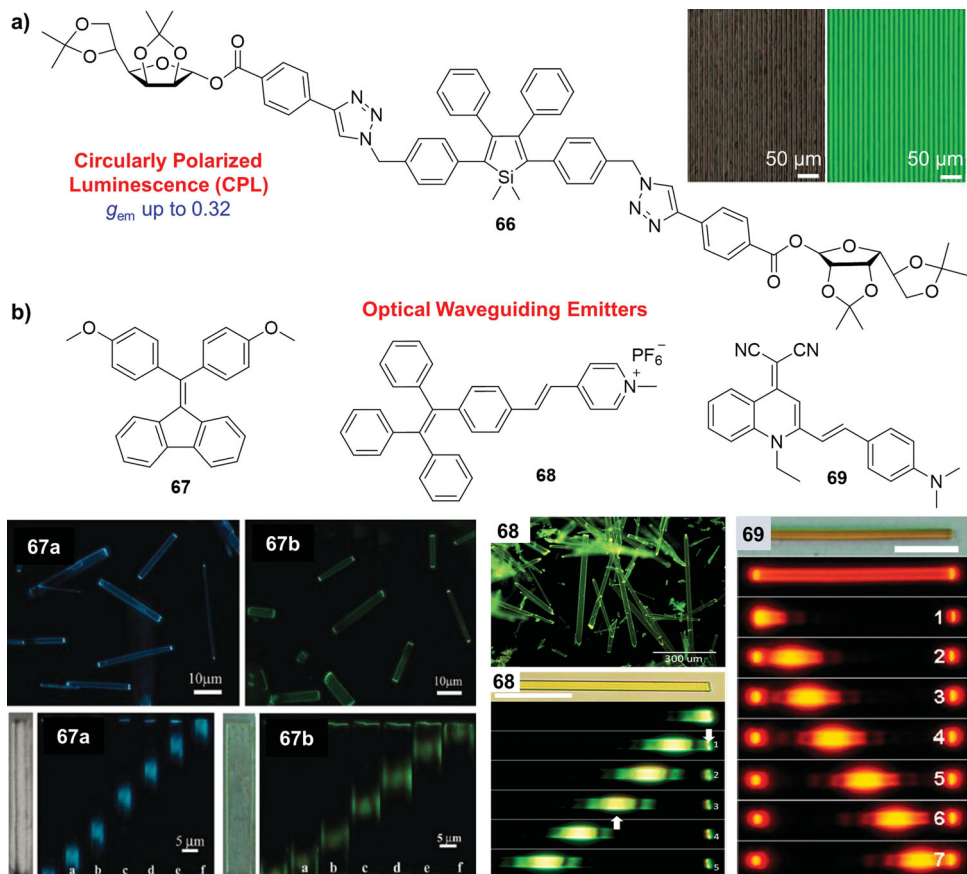


Figure 19. (a) Chemical structure of chiral AIEgen **66** and microphotograph of morphological structures formed upon evaporation of its dichloromethane/toluene solution in microfluidic channels. Image reproduced with permission.^[195] Copyright 2012, Royal Society of Chemistry. (b) Fluorescence images of crystalline microrods of AIEgens **67**–**69** excited on the whole microrods and at different positions along the microrods. Images for **67**: Reproduced with permission.^[196] Copyright 2012, Wiley-VCH Verlag GmbH & Co. KGaA. Images for **68**: Reproduced with permission.^[197a] Copyright 2013, Royal Society of Chemistry. Images for **69**: Reproduced with permission (for **69**).^[198] Copyright 2013, American Chemical Society.

Our group have recently designed and synthesized a heteroatom-containing AIEgen (**68**) by attaching a pyridinium salt unit to a TPE skeleton through a vinyl linkage.^[197] The crystalline microrods of **68** show obvious optical waveguide effect, thanks to the large Stokes shift and well-ordered packing arrangement. As can be seen from the microphotograph taken under the fluorescence microscope, the two ends of the microrods emit brighter green light. A distance-dependent fluorescence image of a single microrod measured on a near-field scanning optical microscope clearly shows that the green light is emitted at the end of the rod, when a spot of its body is photoexcited. It can thus be classified as an active waveguide material as the light is generated from the luminescence process. The optical loss coefficient has been determined to be as low as 32 dB mm⁻¹.

The development of solid-state red light emitters, particularly those with one-dimensional microstructures, is of great interest. A quinolinemalononitrile-based red light-emitting AIEgen (**69**) has been created by Zhao, Zhu, and coworkers through dexterously modifying molecular structure of a conventional ACQ fluorophore called 4-(dicyanomethylene)-2-methyl-6-(4-dimethylaminostyryl)-4H-pyran, which is commonly known as DCM.^[198] The molecules of **69** can self-assemble in a variety of solvents and form “waving ribbons” with a length of 6 mm and a diameter of 10 μm. The self-organized microstructures show excellent optical waveguide performances with low optical losses, thanks to their smooth surfaces and flat facets. Other AIEgens with ordered one-dimensional microstructures have also been found to exhibit optical waveguide effects. For example, fluorescence emissions from the microrods of *p*-carboxyl-*N*-salicylideneanilines propagate along the longitudinal direction with strong emissions coming out from the rod tips.^[116]

4.2. Luminescent Sensors

The concept of AIE has emerged to be a powerful and versatile strategy for the design of new luminescent probe systems. A large variety of AIEgens have been successfully utilized for the development of various optical sensors.^[27–29,33] For example, AIEgens have been used as chemical sensors for the assays of pH,^[203] explosives,^[204] carbon dioxide,^[205] amines^[206] and ions^[207] and as biological probes for the detections of intracellular pH,^[208] amino acids, peptides, proteins,^[209–211] nucleic acids,^[212] and glucose^[213] as well as for electrophoresis gel visualization^[214] and real-time monitoring of DNA/protein conformational changes.^[215] In comparison with the conventional luminophore systems, the AIEgen-based optical sensing systems offer such advantages as facile fabrication, ready functionalization, excellent stability, high signal-to-noise ratio, and low detection limit. Especially, the newly developed bioassays feature label-free and luminescence “turn-on” recognition owing to the AIE effect. The recent advancement in the area has greatly expanded the scope of analytical applications of AIEgens.

4.2.1. Chemical Sensors

Exploration of chemosensors for trivalent metal cations (M^{3+}) is of importance because of their biological significance and

environment implications. We have developed an AIE-based strategy for selective and ratiometric detection of M^{3+} ions in a new working mechanism.^[207] Pyridinyl-functionalized TPE derivative **70** is an AIEgen soluble in ethanol but insoluble in water. It is used to assay trivalent ions in an ethanol/water mixture ($f_w = 0.5\%$). Its solutions containing mono- and divalent ions emit very weak blue light, but those containing trivalent ions emit strong red light (Figure 20a). The suspensions with M^{3+} ions are yellow in color, while the solutions with M^+ and M^{2+} ions are colorless, indicative of colorimetric responses. Thorough analyses reveal that the ratiometric fluorescent and colorimetric responses are associated with protonation of **70**. The protonated **70** is poorly soluble and form aggregates in ethanol, leading to the emission enhancement. Meanwhile, the extended conjugation and the strong D-A interaction of the protonated **70** bring about the red shift in the emission color. The selectivity of **70** to M^{3+} ions over M^{2+} and M^+ ions is ascribed to the high hydrolyzability of M^{3+} , which releases more protons in the polar media.

Specific recognition of K^+ ion is of great value due to its critical roles in the physiological processes.^[216,217] Zhang, Liu, et al. have integrated the concept of AIE with supramolecular recognition of K^+ ion by crown ether to develop effective fluorometric K^+ probes.^[216] A crown ether-functionalized TPE derivative (**71**) is prepared by a facile thiol–ene click reaction. As depicted in Figure 20b, the TPE core and benzo-15-crown-5 peripherals in **71** serve as the AIE-active motif and supramolecular K^+ -recognizing units, respectively. The emission of **71** in THF is turned on by the addition of K^+ because of the luminogen aggregation caused by the K^+ -mediated cross-linking through the formation of K^+ /crown ether supramolecular complex in a sandwich manner. The aggregate formation restricts the intramolecular rotations of **71** and populates its radiative decays. Luminogen **71** thus functions as a highly sensitive and selective fluorometric K^+ probe.

Cyanide anion (CN^-) is one of the most poisonous ions.^[218] According to the World Health Organization (WHO), the highest allowable level of CN^- in drinking water is 1.9 μM. It is thus highly desirable to develop efficient and simple sensing systems for CN^- . Zhang's group have reported a new fluorescence turn-on system for the detection of CN^- in aqueous media by a TPE derivative carrying a positively charged indolium group (**72** in Figure 20c).^[219] The indolium moiety renders **72** water-soluble and as a result, it is weakly emissive in the aqueous solution. The indolium group readily reacts with CN^- to afford **73**, which has a low solubility in aqueous media. Aggregation thus occurs, which turns on the emission of the TPE unit in virtue of its AIE feature. The AIEgen shows high selectivity toward CN^- over other anions. Its detection limit is 91 nM, which is 50-times lower than the maximum level permitted by WHO. The potential of this sensing scheme for practical application is demonstrated by a paper test strip. After exposure to a CN^- -containing aqueous solution, the emission color of the paper strip coated with **72** is quickly switched from orange to blue.

In addition to the above discussed three examples, there are many other AIEgens designed for the detections of ionic species.^[111,112,135,220–225] For example, a water-soluble fluorescence turn-on chemosensor based on AIEgen **27** has been developed

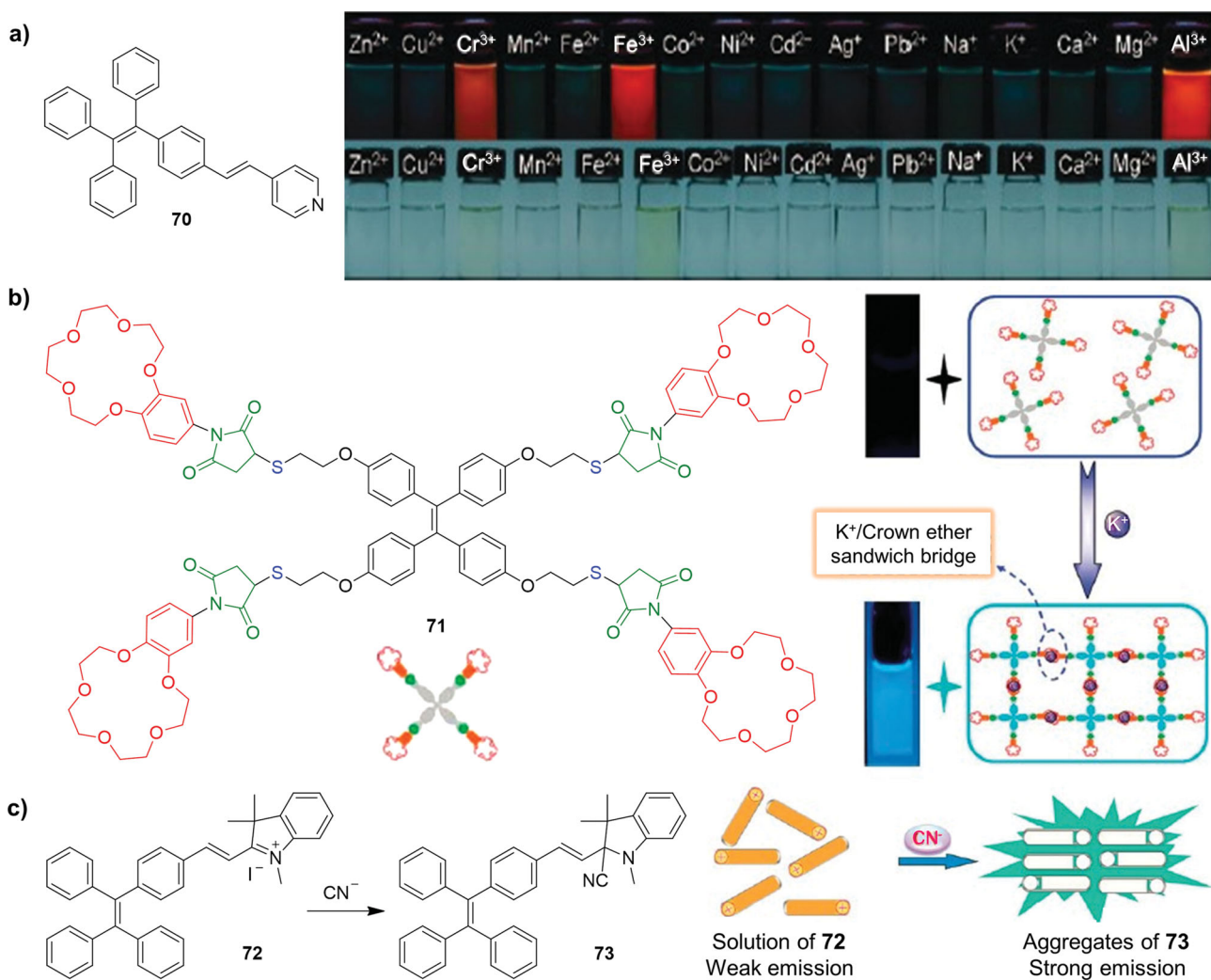


Figure 20. (a) Colorimetric and ratiometric detections of trivalent cations by protonation of pyridinyl group of **70**. Reproduced with permission.^[207] Copyright 2013, Royal Society of Chemistry. (b) A “lighting-up” K^{+} chemosensor based on crown ether-functionalized TPE derivative **71**. Reproduced with permission.^[216] Copyright 2012, Royal Society of Chemistry. (c) Fluorescence turn-on detection of cyanide ion due to the AIE behavior of **72** activated by nucleophilic attack of CN^{-} to its indolium group. Reproduced with permission.^[219] Copyright 2012, Royal Society of Chemistry.

by Tong and Dong's research laboratories.^[111,112] It shows rapid response and excellent selectivity and sensitivity to Al^{3+} . Chemosensors for the recognition and quantitation of other cationic species such as Fe^{3+} ,^[220] Cu^{2+} ,^[221] Hg^{2+} ,^[222] Zn^{2+} ,^[223] and Ag^{+} ^[224] and anionic species including F^{-} ,^[135] and HSO_4^{-} ^[225] have also been constructed from various AIEgens according to the RIM mechanism.

Detection of explosives in groundwater and seawater has become an important issue owing to its antiterrorism implications.^[226] AIE systems have showed great promise in the area of fluorescence sensing of explosives, due to their amplification or superamplification effect in the aggregate state.^[29,227] We have recently introduced TPE into mesoporous silica through covalent bonding and applied the AIEgen-decorated silica for the detection of explosives in water, using 2,4,6-trinitrophenol or picric acid (PA) as a model system (Figure 21a).^[204] PA rapidly and sensitively quenches the light emission of the AIE system due to photoinduced electron transfer and energy transfer. The

quenching constant of this system is up to $2.5 \times 10^5 \text{ M}^{-1}$ and its detection limit is down to 0.4 ppm, much superior to the TPE parent. Importantly, the mesoporous chemosensor is recyclable and reusable after simple washing with a proper solvent.

Latent fingerprints (LFPs) at the scenes of criminal acts are important clues for forensic investigations, thanks to the uniqueness of LFPs defined by their ridge characteristics.^[228] In the forensic tests, different combinations of “development” treatments are used to visualize LFPs. Commonly used procedures for LFP visualization involve brushing magnetic powders or inks, which may destroy the fingerprint details^[229] and pose health hazards to examiners. This calls for the development of effective methods for visualizing LFPs in a simple, rapid, and friendly way. Taking advantage of the AIE character of TPE, a smart protocol for LFP recognition has been developed by Su's team (Figure 21b).^[230] In the protocol, a sebaceous fingerprint is pressed on a substrate, which is put into a TPE solution in an acetonitrile/water mixture under stirring for 5 min. The

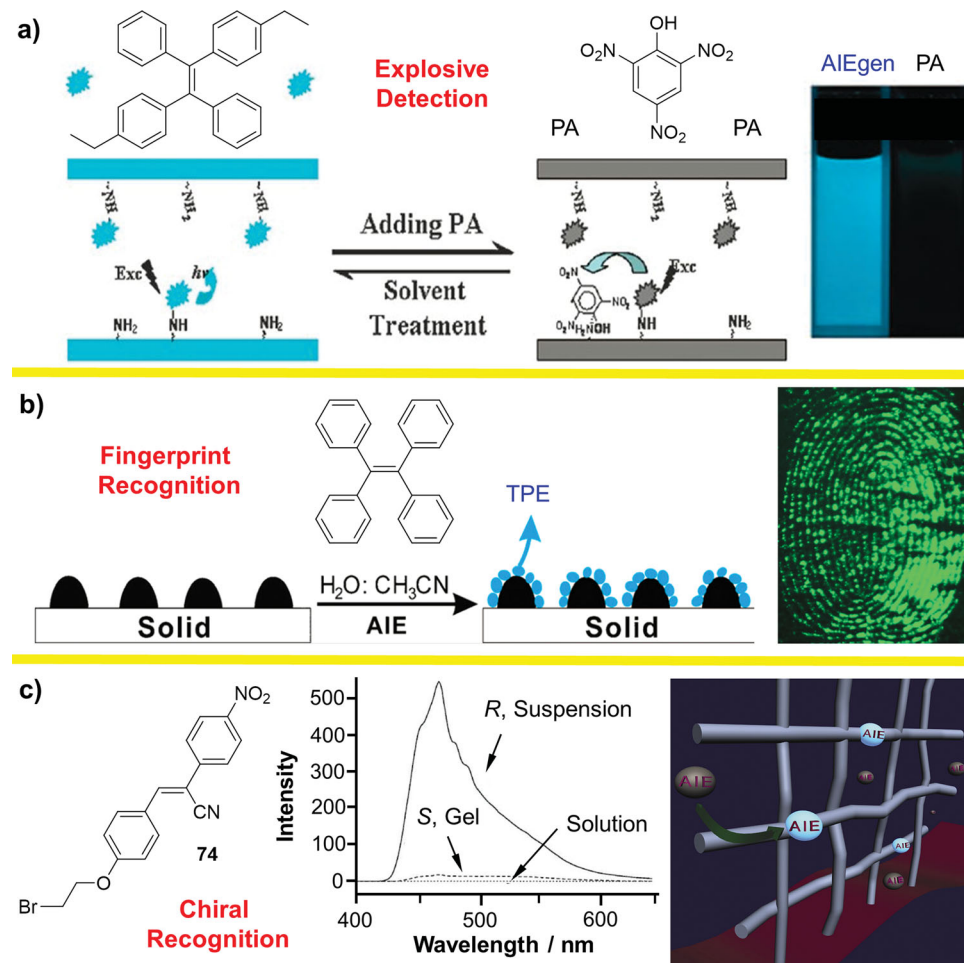


Figure 21. (a) Reversible fluorescence on-off detection of explosives such as picric acid (PA) by recyclable AIE-active mesoporous materials. Reproduced with permission.^[204] Copyright 2012, Royal Society of Chemistry. (b) Fingerprint recognition utilizing AIE characteristics of TPE. Reproduced with permission.^[230] Copyright 2012, Royal Society of Chemistry. (c) Fluorescence spectra of **74** in turbid suspension of (*R*)-mandelic acid and (*S*,*S*,*R*)-2-amino-1,2-diphenylethanol (ADPE; solid line), transparent gel of (*S*)-mandelic acid and ADPE, and solution obtained by heating the gel (dotted line). Reproduced with permission.^[233] Copyright 2011, Royal Society of Chemistry.

substrate is then rinsed with water, dried under an argon stream, and put in a dark box for photographing. The TPE aggregates adhere preferentially to the fingerprint ridges, due to the hydrophobic interaction between the hydrophobic aggregates and the fatty residues in the ridges. The adsorbed nanoaggregates fluoresce strongly under UV illumination with great contrast, realizing clear visualization of the fingerprint pattern.

Chiral recognition is of critical importance for drug synthesis, column enantioseparation, asymmetric catalysis, and so on. Although AIE effect has been utilized for chiral recognition and enantiomeric determination,^[29,231,232] complicated chiral receptors need to be synthesized. To overcome such drawback, simple AIEgens with varying emission intensities in the forms of gel, suspension and precipitate in 1,2-dichloroethane have been developed by Zeng and coworkers and applied to fluorescence switches and quantitative determinations of enantiomer compositions.^[233] AIEgen **74**, for example, is virtually non-luminescent in 1,2-dichloroethane solution (Figure 21c). 2-Amino-1,2-diphenylethanol (ADPE) is used as a base or co-analyte in the analytic protocol. Its (*S*,*S*,*R*) isomer not only forms gel with a

chiral carboxylic acid but also shows enantioselectivity towards enantiomers of the acid.

For example, when (*S*,*S*,*R*)-ADPE is admixed with (*S*)-mandelic acid in a 1:1 ratio, an optically transparent gel is formed, whereas admixing (*S*,*S*,*R*)-ADPE with (*R*)-mandelic acid gives rise to a suspension. Luminogen **74** in the gel formed from the (*S*,*S*,*R*)-ADPE/(*S*)-mandelic acid mixture is practically non-emissive. In contrast, its emission in the suspension of (*S*,*S*,*R*)-ADPE/(*R*)-mandelic acid is very strong. The fluorescence intensity ratio (I_R/I_S) of **74** in the suspension and gel of the two enantiomers of mandelic acids is as high as 32. In the solution obtained by heating the gel, **74** shows no fluorescence at all. This difference in the PL intensity is attributed to the different degrees of aggregation of **74** in the mixtures due to the involved specific steric effects and chiral interactions. By making use of the (*S*,*S*,*R*)- and (*1*,*R*,*S*)-enantiomers of ADPE, enantiomeric compositions of different chiral carboxylic acids are quantitatively determined. The similar results are obtained when other simple AIEgens, such as TPE derivatives, are used for chiral analysis.

Study of the dynamics of polyelectrolyte chains in aqueous media is of great value for both fundamental research and practical applications.^[234] DNAs, for example, are polyelectrolyte chains. The dynamic processes for the formation and stabilization of the biomacromolecule chain conformations remain to be understood. Numerous research efforts have been devoted to investigations of polyelectrolyte chain dynamics, many of which are limited to only dilute solutions.^[235] A fluorescent probe of cationic TPE derivative (**75**) has been developed by us for the investigation of dynamic processes of polyelectrolyte chains in relatively concentrated solution (1 g/L).^[236] Poly(acrylic acid) (PAA) is used as a model polyelectrolyte, taking into consideration that its chain conformation changes with the variation in pH in

aqueous solution (Figure 22a). The AIE effect of **75** caused by the IIR mechanism allows us to investigate the dynamic processes of the PAA chains in a wide range of pH (from 1.78 to 12.06).

In the high pH region (12.06–6.0), the anionic carboxylic groups play a dominant role and the PAA chains take an extended conformation. The molecules of **75** are well dispersed in water without aggregation and are thus non-fluorescent. In the lower pH region (6.0–3.86), part of the carboxylic groups are protonated. This decreases the negative charge density on the polymer chains, causes the formation of intra- and inter-chain H-bonds, and induces the PAA chains to take a coiled conformation. Electrostatic interaction attracts some of the AIE molecules to the PAA chains, with some of them being

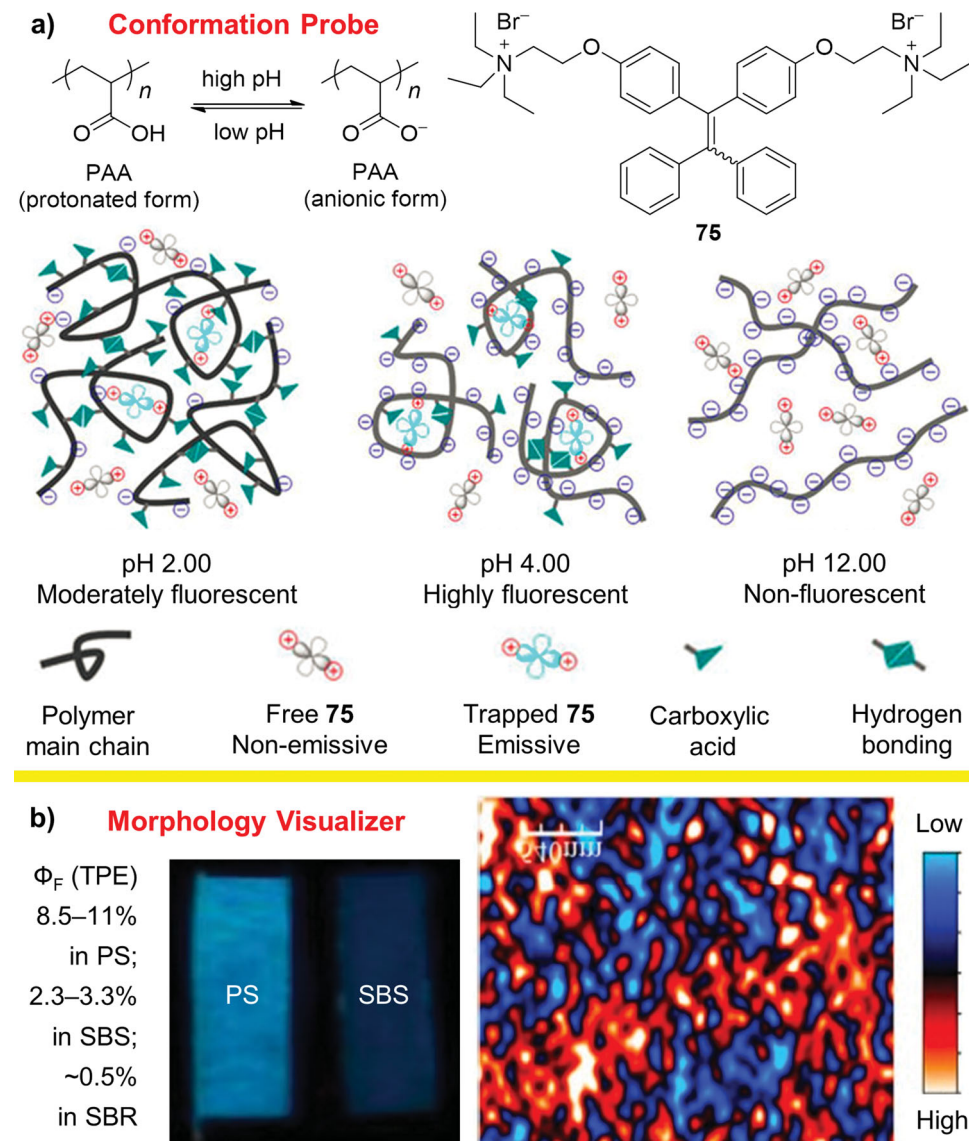


Figure 22. (a) Dynamic changes in poly(acrylic acid) (PAA) chain conformation at different pH values and corresponding fluorescence variation of luminogen **75**. Reproduced with permission.^[236] Copyright 2013, Science China Press and Springer-Verlag. (b) Fluorescent images of different styrene-based polymers containing 0.01 wt% of TPE and near-field optical map recorded during the scan of a TPE-doped SBS film. PS = polystyrene, SBS = styrene–butadiene–styrene (a block copolymer), SBR = styrene–butadiene rubber (a random copolymer). Reproduced with permission.^[237] Copyright 2012, AIP Publishing LLC.

even wrapped by the coils due to the hydrophobic effect. The intramolecular rotations of the phenyl rings in **75** are restricted to certain extent and its emission is thus turned on. Further decreasing the pH value (3.86–1.78), the fluorescence becomes weakened. In the low pH region, the protonated carboxylic groups are dominant, leading to reduced electrostatic interaction between the PAA chains and the AIE probes. The enhanced intra- and interchain H-bonding results in more compact polymer conformation, hampering the AIE molecules from entering the PAA coils and hence causing a decrease in the PL intensity. Distinct from previous studies on polymer chain dynamics, our work is conducted in more concentrated solutions and reveals more process details.

In addition to probing dynamic processes of polyelectrolyte chains in the solution state, the investigations of conformational and morphological structures of polymers as well as their miscibility and phase separation in the solid state are also of great importance. For example, microphase separations in block copolymers and polymer blends significantly affect their self-assembling structures and mechanical properties. However, up till now, examples of using aggregatochromic dyes inside polymer materials for the preparations of built-in temperature and deformation sensors have been extremely rare, owing to the lack of effective and versatile aggregatochromic luminogens. AIEgens are promising for this kind of applications, because their light emission behaviors are distinctly different in dispersed and aggregated states. Pucci and coworkers have done truly ingenious work in the application of AIEgens, such as TPE and its derivatives, as aggregatochromic morphological probes for a variety of commodity plastics with commercial importance.^[237]

The AIEgens are doped into the thermoplastic polymers at various concentrations (0.01–1 wt%) by processing in the melt. When TPE is blended with a polymer featured by a glass transition temperature above ambient temperature, the AIEgen shows more intense emission, owing to the restricted motions of their phenyl rotors. As shown in Figure 22b, progressively increased emission is observed on passing from a butadiene-styrene random copolymer (SBR) to a styrene–butadiene–styrene block copolymer (SBS) and to a styrene homopolymer (PS) at a doping concentration of 0.01 wt% TPE. The Φ_F values of TPE in these polymers are ~0.5%, 2.3–3.3% and 8.5–11%, respectively. A closer scrutiny of the near-field optical microscopy map of the AIEgen-doped SBS reveals fine sub-structures in the TPE emission, which are related to the nanostructures in the SBS matrix. The local variation in the emission intensity thus reflects the distribution of the AIE molecules in the B (butadiene) and S (styrene) phases, which in turn indicates the microphase separation in the SBS copolymer. With the exciting results obtained from TPE and its structural congeners such as bis(benzoxazolyl)stilbene,^[237a] a new application territory is opened. The AIEgens, especially those with mechanochromic characteristics, have great potentials to be developed into visualizers for examining polymer morphologies.

4.2.2. Biological Probes

Life science and biological research call for the development of water-soluble luminescent bioprobes with high sensitivity and

selectivity towards targeted analytes in aqueous media. Polyelectrolytes of biological origin undergo aggregation and assembly in the presence of polyelectrolytes, multivalent organic molecules, and inorganic nanoparticles with opposite charges owing to the involved electrostatic interactions. Amine groups can be caged by carbamate functionalization and selectively decaged on request. Taking advantage of the facile cage-decage reactions, Zhang, Liu and coworkers have designed charge-generation polymers (CGPs) carrying carbamate-masked amine functional pendants, which can undergo transition from the initially neutral state to a charged state in the presence of a specific analyte when triggered by stimuli.^[238] The charge-generation process is coupled with the induced aggregation of a TPE derivative bearing four anionic carboxyl groups (**76**), affording a CGP-based fluorogenic probe with improved detection sensitivity and great designing flexibility (Figure 23a).

The aqueous fluorogenic sensing system for an analyte of interest consists of the CGP and the negatively charged AIEgen **76**. Initially, the mixture shows no fluorescence because the AIEgen does not experience any interactions with the uncharged amine-caged copolymer. When a triggering analyte is added, the uncharged CGP is transformed into a polyelectrolyte carrying multiple positive charges via chemoselective cleavage of the carbamate protecting groups. This transformation encourages aggregate formation of the molecules of negatively charged **76** and thus turns on their light emissions. This fluorogenic probing platform proves effective to biologically relevant species, such as hydrogen peroxide and thiol. It can also be used for detections of glucose and D-glucose 6-phosphate. In virtue of the versatile designs and facile syntheses of CGPs bearing different analyte-specific charge-generation units, this strategy offers a general strategy towards engineering a variety of fluorogenic bioprobes with diverse sensing functionalities.

Through rational structural design, AIEgens can be tailored to serve different purposes. For example, a series of bioprobes for discriminating structurally similar mercapto amino acids, cysteine (Cys) and homocysteine (Hcy), have been developed by decorating AIEgens (e.g., TPE and silole) with aldehyde groups.^[210] Taking silole derivative **77** as an example, it is non-emissive in a DMSO/4-(2-hydroxyethyl)piperazine-1-ethanesulfonic acid (HEPES) mixture (6/4, v/v). When **77** is added into a Cys solution, the reaction between them readily takes place at room temperature and produces a thiozalidine derivative through a Schiff base intermediate (Figure 23b). The response of **77** to Cys is reflected as an increase in the emission intensity, a blue-shift in the emission color, and the formation of white precipitate. The reaction of Hcy with **77** is much slower: it takes three days to cause an observable change, whereas Cys reacts with **77** instantaneously. This large difference in the reaction kinetics permits Cys and Hcy to be readily differentiated. It has been found that many dialdehyde-functionalized AIEgens can discriminate Cys from Hcy. Their probing performances can be modulated by changing their molecular structures and hydrophobicity.

The detection of very low level of protein by sodium dodecyl sulfate-polyacrylamide gel electrophoresis (SDS-PAGE) remains to be a challenge. Many dyes are available for protein assays by SDS-PAGE, among which Coomassie brilliant blue

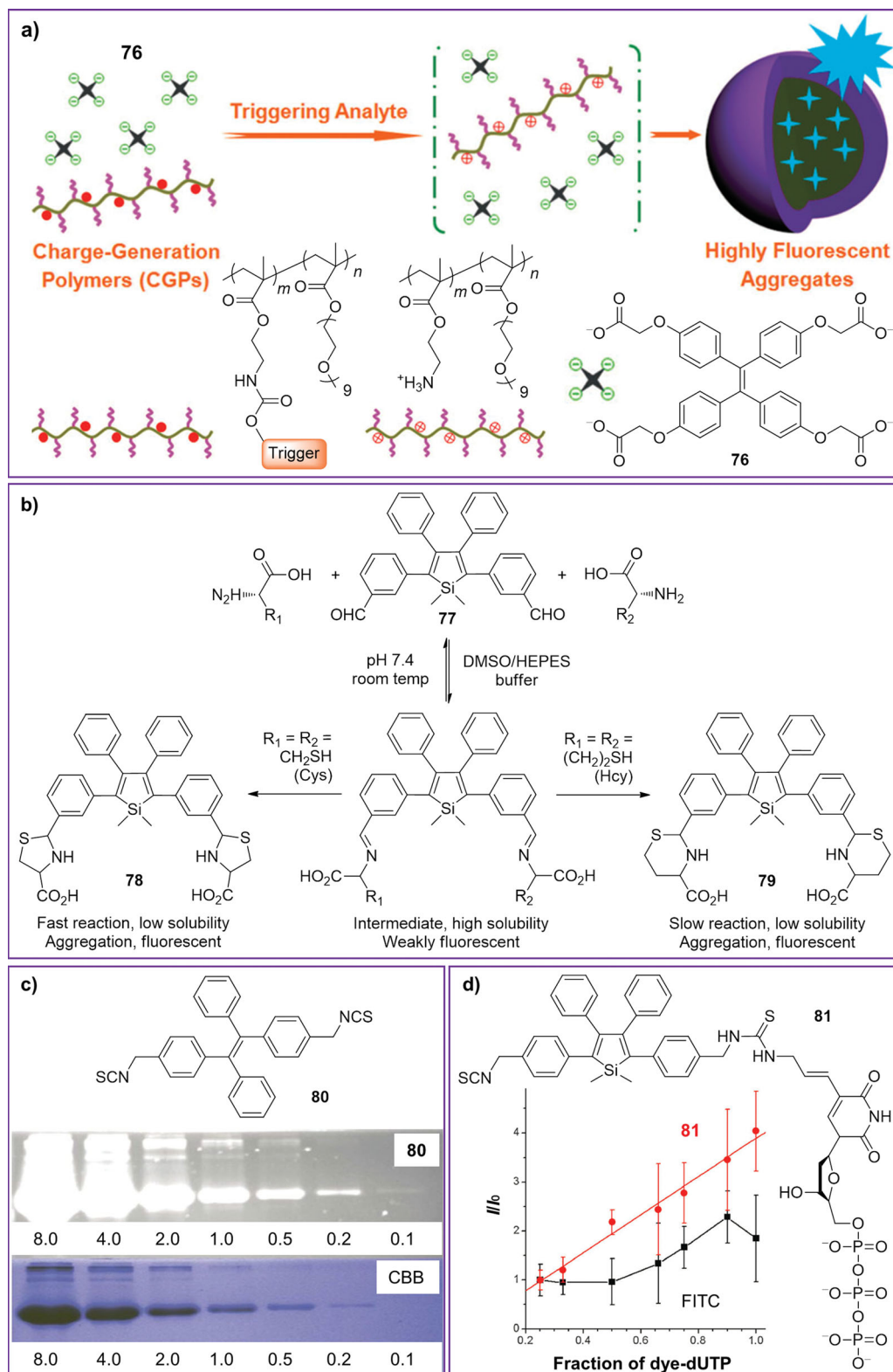


Figure 23. (a) Construction of biosensor through integration of negatively charged AlEgen **76** with amine-caged charge-generation polymer (CGP). Reproduced with permission.^[238] Copyright 2012, Wiley-VCH Verlag GmbH & Co. KGaA. (b) Differentiation between cysteine (Cys) and homocysteine (Hcy) by aldehyde-functionalized AlEgen **77**. (c) SDS-PAGE fluorescence image of BSA (in unit of μg) post-stained with **80** and optical image of the same gel re-stained with Coomassie brilliant blue (CBB). Reproduced with permission.^[214] Copyright 2012, Royal Society of Chemistry. (d) Plot of emission intensity of fluorescent DNA versus fraction of dye-dUTP conjugate. Reproduced with permission.^[242] Copyright 2012, Royal Society of Chemistry.

(CBB) is the most widely used post-staining dye. CBB, however, suffers from poor sensitivity, low signal-to-noise ratio, and troublesome multistep analysis procedures. We have developed an AIEgen-based visualizing agent (**80**) for protein assay.^[29,214] The amine-reactive TPE derivative can be used to detect very low level of protein by SDS-PAGE, because all proteins contain amine groups in their lysine residues. The pre-stained and pure BSA samples are loaded onto two different gel lanes. The pre-stained lane is highly emissive just after electrophoresis owing to the presence of covalently bound AIEgen in the BSA chain, while the pure BSA in another gel lane is non-fluorescent. The pure BSA can be made emissive by post-staining. The visualization by the post-staining is much more sensitive (with detection limit down to 0.1 µg) than the CBB staining (Figure 23c). The AIE visualizer can overcome the problems of CBB staining and eliminates the restraint in the fluorogen/protein ratio, allowing the use of high concentrations of fluorogen in pre- and post-staining systems. The non-fixation staining protocols enable the transfer of the labeled proteins to nitrocellulose membranes for further analyses.

Fluorescent DNA segments have attracted much attention due to their potential applications as bioprobes for gene detection and analysis via fluorescent hybridization *in situ* or in solution with target nucleic acids.^[239] The two main approaches to fluorescent DNA segments are the solid-phase oligonucleotide synthesis and enzymatic incorporation. Each of the pathways has its own drawbacks, such as the necessity of using protecting groups,^[240] requirement of highly selective reactions under mild conditions, poor labeling efficiency, and/or suffering of ACQ effect.^[241] An amine-modified 2'-deoxyuridine-5'-triphosphate (dTTP) is labeled with 1,1-dimethyl-2,5-bis[4-(isothiocyanatemethyl)phenyl]-3,4-diphenylsilole and the resultant adduct **81** is subsequently incorporated into DNA chain through nick translation, random priming, or polymerase chain reaction (PCR; Figure 23d).^[242] Whereas the fluorescent DNA products obtained from the nick translation and random priming have acceptable degrees of labeling (DOLs), the PCR products show very high DOLs (up to theoretical limits) without suffering from the ACQ effect when a large amount of **81** is used to replace dTTP. Unlike the FITC-labeled DNA, the fluorescence intensity of the **81**-labeled DNA is increased linearly with an increase in the fraction of the AIEgen.

Bioprobes with specific targeting capability are highly desirable. We have designed and synthesized an AIE bioprobe for the detection of alkaline phosphatase (ALP) and evaluation of its enzymatic activity by functionalizing TPE with phosphate groups.^[243] In the presence of ALP, the phosphate groups in the bioprobe are cleaved by enzymatic hydrolysis, affording a highly fluorescent product as a result of activation of the AIE process.^[243a] This light-up probe exhibits excellent selectivity towards ALP among a number of different proteins. In a buffer solution, the detection limit of the AIE bioprobe is 11.4 pM or 0.2 U L⁻¹ with a linear working range of 3–526 U L⁻¹. The assay can also be carried out in diluted serum with a linear working range up to 175 U L⁻¹, suggesting its potential applications in clinical analyses of ALP levels in real samples. AIEgens have also been utilized to develop bioprobes working in a fluorescence turn-on or light-up mode for the detection of ATP,^[244] analysis of lectin–oligosaccharide interaction,^[245] examination

of histone deacetylase activity,^[246] sensing of cholera toxin,^[247] testing of biogenic amines,^[248] real-time monitoring of cell apoptosis,^[209] visualization of intracellular location and DNA origami,^[249] and assaying of other biological species.^[208–215]

4.3. Biomedical Imaging

Many AIEgens are featured with strong photobleaching resistance, high emission efficiency in the form of aggregates, and good biocompatibility or little cytotoxicity. These advantages make them promising bioimaging materials.^[27–29] Thanks to the enthusiastic research efforts in recent years, the AIEgens have found a broad range of biomedical applications in the areas of cell, tumor, tissue, organism and animal imaging.^[33,250–278]

4.3.1. Cellular Imaging

Fluorescent bioprobes have been routinely used for visualization and tracking of cellular events.^[250] A large variety of organic and inorganic, natural and synthetic materials have been utilized as markers or reporters for differentiation of cellular morphology,^[251] among which organic fluorophores are dominant, because they are rich in variety and easy to use. Many of the organic fluorophores, however, contain large fused polynuclear rings, which are prone to aggregate when dispersed in aqueous media, suffering from the notorious ACQ problem. AIE materials provide a way out for organic fluorophores in the area of cell imaging. Aggregates of AIEgens, for example, have been successfully used for long-term cellular tracing.^[252] Iron oxide-AIEgen nanoparticles with core–shell structures as well as efficient fluorescence and strong magnetization have been fabricated and used for cell imaging.^[253] Recently, a number of new AIEgens have been designed for specific imaging within cells.

Intracellular pH (pH_i) is an essential parameter that regulates and controls many cellular behaviors and processes, such as proliferation and apoptosis as well as enzymatic activity and protein degradation.^[254] An abnormal variation in pH_i may result in dysfunction of cellular organelles. Anomalous pH_i is a sign of many common diseases. Sensing and monitoring pH changes inside living cells therefore count a great deal for studying cellular metabolisms and gaining deeper understanding of physiological and pathological processes.^[254,255] Techniques based on fluorescence are the most powerful tools for tracking intact and subcellular pH, due to their extremely high sensitivity and unequaled spatiotemporal resolution. The existing pH_i bioprobes, however, are hard to achieve full-range pH_i sensing. Recently, we have designed a pH-responsive fluorogen called TPE-Cy, which consists of TPE and cyanine (Cy) units.^[203] It exhibits a large Stokes shift (>185 nm) and shows AIE behaviors, overcoming the limitations of conventional ACQ fluorophores. The well-defined reactivity of TPE-Cy with OH⁻/H⁺ ions enables it to sense pH_i in a wide range the broadest so far.^[203]

TPE-Cy shows red emissions with strong-to-medium and weak-to-nil intensities at pH 5–7 and pH 7–10, respectively, and nil-to-strong blue emission pH 10–14. There exists a nearly linear dependence of its fluorescence intensity on pH in the physiological region of pH 5.0–7.4, rendering it a promising fluorescent indicator for pH_i (Figure 24a). TPE-Cy can also be

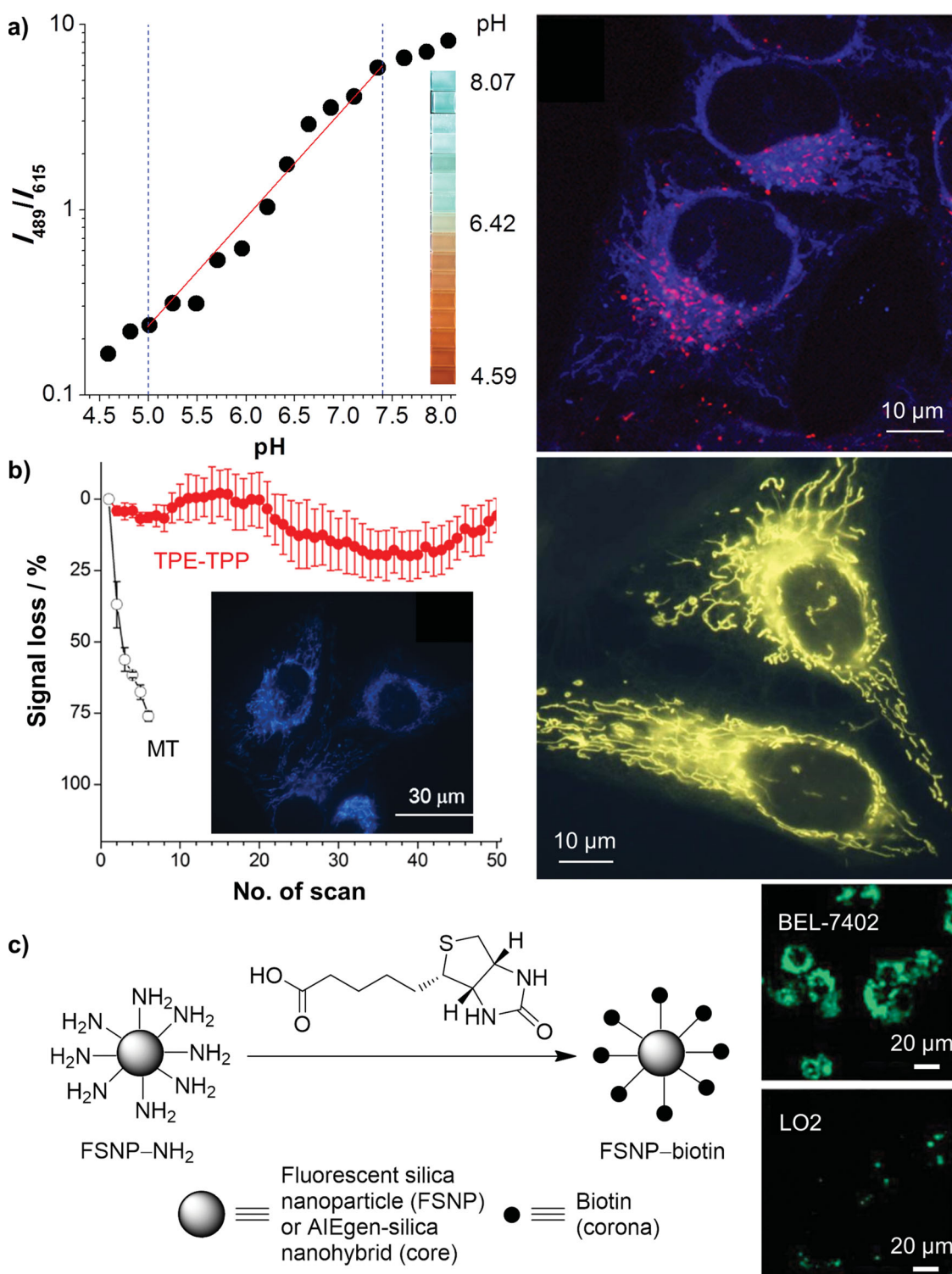


Figure 24. (a) (Left) Plot of I_{489}/I_{615} of TPE-Cy versus pH in buffer solutions in the presence of 1,2-dioleoyl-glycero-3-phosphocholine; $\lambda_{\text{ex}} = 380 \text{ nm}$. (Right) Overlay image of HeLa cells incubated with TPE-Cy for 2 h; individual confocal images taken under excitations of 405 and 488 nm. Reproduced with permission.^[208] Copyright 2013, American Chemical Society. (b) (Left) Signal loss (%) of fluorescence of TPE-TPP (solid circle) and MT (open circle) with increasing number of scans; insert: fluorescent image of living HeLa cells stained with TPE-TPP. Reproduced with permission.^[258] Copyright 2013, American Chemical Society. (Right) Fluorescent images of HeLa cells incubated with **68**. Reproduced with permission.^[197b] Copyright 2013, John Wiley and Sons. (c) (Left) Synthetic route for fabrication of biotin-functionalized fluorescent silica nanoparticles. (Right) Fluorescent images of hepatocellular carcinoma cells (BEL-7402) and normal liver cells (LO2) stained by FSNP-biotin conjugates for 3 h. Reproduced with permission.^[264] Copyright 2012, Royal Society of Chemistry.

used to sense subcellular pH and monitor pH_i vibrations in live cells.^[208] The transition point of its red-to-blue emission is shifted from extracellular pH 10 to intracellular pH 6.5. The dynamic range of TPE-Cy covers the whole pH_i range from 4.7 to 8.0, which are difficult, if not impossible, to achieve by traditional pH_i indicators. TPE-Cy enjoys good biocompatibility and cell permeability. In the live cell images shown in the right panel of Figure 24a, the red signals are from acidic organelles, while the regions with blue emissions are more alkaline. A co-staining experiment of TPE-Cy with LysoTrackerGreen inside the living cells perfectly supports this conclusion. Other AIEgen-based pH sensors with good performances have been constructed by Tong's research team.^[256]

Monitoring the dynamics of mitochondrial morphological changes is attracting increasing attention owing to its involvement in early stage apoptosis and degenerative conditions.^[257] To follow the bioprocesses, highly specific and photostable bio-probes need to be developed. Photostable AIEgens for specific mitochondrial imaging have been designed, an example of which is an adduct of TPE and triphenylphosphonium (TPE-TPP).^[258] It is prepared by a simple procedure and shows AIE feature with a strong blue emission peaked at 466 nm in solid state. The reticulum structures of mitochondria are clearly visible, thanks to its intense fluorescence. It is photostable: after 50 scans for a total irradiation time of ~7 min, its signal loss is less than 20%. No significant difference is observed between the 1st and 50th scans (Figure 24b). The slight fluctuation in the signal may be attributed to the movement of the live cells. In sharp contrast, the signals of the mitochondrial tracker (MT) drop dramatically. When exposed to the excitation light, the outermost layers of the nanoaggregates of TPE-TPP may be photobleached or photooxidized but the inner layers are protected from such damages due to dense packing of the particles. Thanks to its high specificity, superb photostability and great tolerance to microenvironment changes, TPE-TPP is an excellent bioimaging agent for mitochondrial targeting and morphological tracking.

Another example of AIEgen-based mitochondrial visualizer is a TPE-pyridinium salt (**68**). It works as an excellent fluorescent imager for specific staining of mitochondria in living cells with high photostability.^[197] Different from TPE-TPP, **68** is a yellow light emitter, which can afford higher signal-to-noise ratios. It is remarkable that very fine and detailed structures of the mitochondria can be clearly visualized by this brilliant AIE tracker. It is well-known that mitochondrion has a large negative potential on the matrix side of membrane. Fluorophores for mitochondrial visualization are thus commonly lipophilic and cationic in character.^[252,259] AIEgen **68** possesses both of these characteristics and therefore functions as an outstanding staining agent for specific targeting of mitochondria in living cells. Similarly, a conjugated phosphonium salt (**29**) synthesized by Gong, Ning, et al. has worked well as a fluorescence probe for imaging mitochondria in cells, due to its AIE characteristic, hydrophobic core, and positive charge.^[114] Accompanying the advancement in the area of AIE study, a large variety of AIEgens have been developed, which have been used to image almost all the structures in living cells. Thus, in addition to the pH_i and mitochondrial tracking discussed above, specific imaging of membrane,^[212,260] surface protein,^[211]

lysosome,^[261] cytoplasm^[262] and nucleus^[263] have all been accomplished.

Tumor targeting and imaging are important endeavors in the area of biomedical research. Specially designed AIEgen nano-aggregates have been utilized for various biomedical imaging applications, thanks to their high emission efficiency and superb photobleaching resistance. Fluorescent silica nanoparticles (FSNPs) consisting of AIEgen–silica hybrids, for instance, have served as a new platform for the development of multi-functional cellular imaging agents. Amidation of the silole-containing FSNP-NH₂ core with biotin affords a new tumor cell tracker (FSNP–biotin) with high selectivity (Figure 24c).^[264] The resultant FSNP–biotin nanoparticles are spherical in shape and uniform in diameter (or monodisperse in size distribution). Their suspensions in aqueous media emit strong green light, owing to the AIE attribute of the silole aggregates in the hybrid nanoparticles.

After being stained by the FSNP–biotin nanoparticles for a period of 3 h, strong green light is emitted from the HeLa and BEL-7402 cells, which are representative cell lines for cervical and hepatocellular carcinomas with over-expressed biotin receptors, whereas weak emission is observed from LO2 cells, which are normal liver cells with less-expressed biotin receptors (Figure 24c). This is attributed to the receptor-mediated endocytosis. For the tumor cells with over-expressed receptors on the surfaces, the FSNP–biotin nanoparticles bind the cell membranes through ligand-receptor interaction. This triggers the cell internalization into the intracytoplasmic vesicles or the formation of clathrin-coated vesicles. The nanoparticles may be further processed in vacuoles and endosomes and eventually released to cytoplasm. On the other hand, the nanoparticles without biotin coating enter the cells mainly through caveolae-dependent endocytosis, whose rate is much slower and specificity is much lower. The FSNP–biotin nanoparticles are lastingly retained inside the living cells, enabling long-term tumor cell tracking over multiple passages as well as quantitative analysis of tumor cell metastasis.

Besides biotin, folic acid is another widely used receptor for tumor-specific recognition and identification.^[265] Taking a synthetic strategy similar to that used for the fabrication of the FSNP–biotin nanoparticles discussed above, Fu, Tian, et al. have successfully prepared folate-functionalized FSNPs with silica as the shells and 9,10-distyrylanthracene as the cores.^[265a] The yellow light emitting FSNPs are utilized for targeted HeLa cell imaging. The FSNPs are mesoporous and may potentially be used as vehicles for controlled, externally activatable release of anticancer drugs. Other bio-recognition species such as antibodies and aptamers can also be incorporated into FSNPs to create specific tumor-targeting bioimaging systems.

Silica nanoparticles-loaded AIE systems can not only be applied to cell imaging but also be used to bring about desired therapeutic effects. Tao, Wei and coworkers have made the first attempt to integrate cell imaging with cancer therapy in one FSNP system.^[266] Mesoporous FSNPs are prepared via one-pot incorporation of 9,10-bis[4-(octadecyloxy)styryl]anthracene into silica nanoparticles using a cationic surfactant cetyltrimethyl ammonium bromide (CTAB) as the structure-directing template and tumor-killing agent. The resultant FSNPs exhibit a remarkable anticancer efficiency. After removal of the CTAB

surfactant, the FSNPs display excellent biocompatibility and can thus be used for cell imaging.

The quantum dots of inorganic semiconductors such as CdS and CdSe are highly emissive but cytotoxic. Nanoaggregates of AIEgens are in some sense the organic versions of quantum dots and may thus be referred to as AIE dots. The organic AIE dots enjoy such advantages as high luminescence efficiency, excellent biocompatibility and high photostability, which allow them to work as long-term non-invasive cell tracers. In collaboration with Liu's group, we have done systematic work along this direction.^[33,263,267] We have recently fabricated the red light-emitting AIE dots functionalized by HIV-1 Tat, which can readily enter living cells.^[263] The AIE dots can not only target tumor cells but also permeate into cellular nucleus, making them attractive candidates for nucleus imaging.

4.3.2. Bacterial Imaging

Investigation of microorganisms is an important subject of research because of their essential roles in medical hygiene, environmental monitoring, food processing, antibiotic development, etc.^[268] Long-term tracking of bacteria is of great importance for monitoring bacterial viability under storage or use, evaluating disinfection efficiency, and investigating pharmacokinetics and pharmacodynamics of antibacterials. However, conventional fluorophores for bacterial assays, such as propidium iodide, suffer from high toxicity and poor photostability, which makes them unsuitable for long-term tracing study. We have unveiled an important function of AIEgen **82** as a fluorescent visualizer for differentiating live and dead bacteria (Figure 25a).^[269] In comparison to commercial viability probes, **82** is highly emissive, photostable and benign to bacteria, rendering it well-suited for long-term bacterial viability tracking study.

After incubating with **82** for 3 h, no fluorescence is observed from live bacteria, but intense emission is given by dead bacteria. The AIEgen is a cell-impermeable DNA stain that binds to the groove of double-stranded DNA. For the live bacteria, their membranes are intact and the molecules of **82** cannot enter the cells to interact with the internal DNA strands. For the dead bacteria, however, their membranes are broken, which exposes their DNA strands to the molecules of **82** for interactive binding. Because of the RIR process, the AIE molecules bound onto the dead bacteria emit strong fluorescence. In other words, the bacteria with compromised membranes open the access for the molecules of **82** to reach their DNA strands, rendering them intensely luminescent. The feasibility of using **82** for screening bactericides has also been demonstrated.^[269] Plate count experiment indicates that **82** imposes negligible toxicity on bacteria over a long period of time, manifesting that it is an excellent biotracer for long-term bacterial viability assay.

4.3.3. Tissue Imaging

In vivo tissue imaging is of critical value to clinical diagnosis and medicinal therapy as well as fundamental biological research. The mature techniques in the market are X-ray imaging, cranial computer tomography (CT), type-B ultrasonic

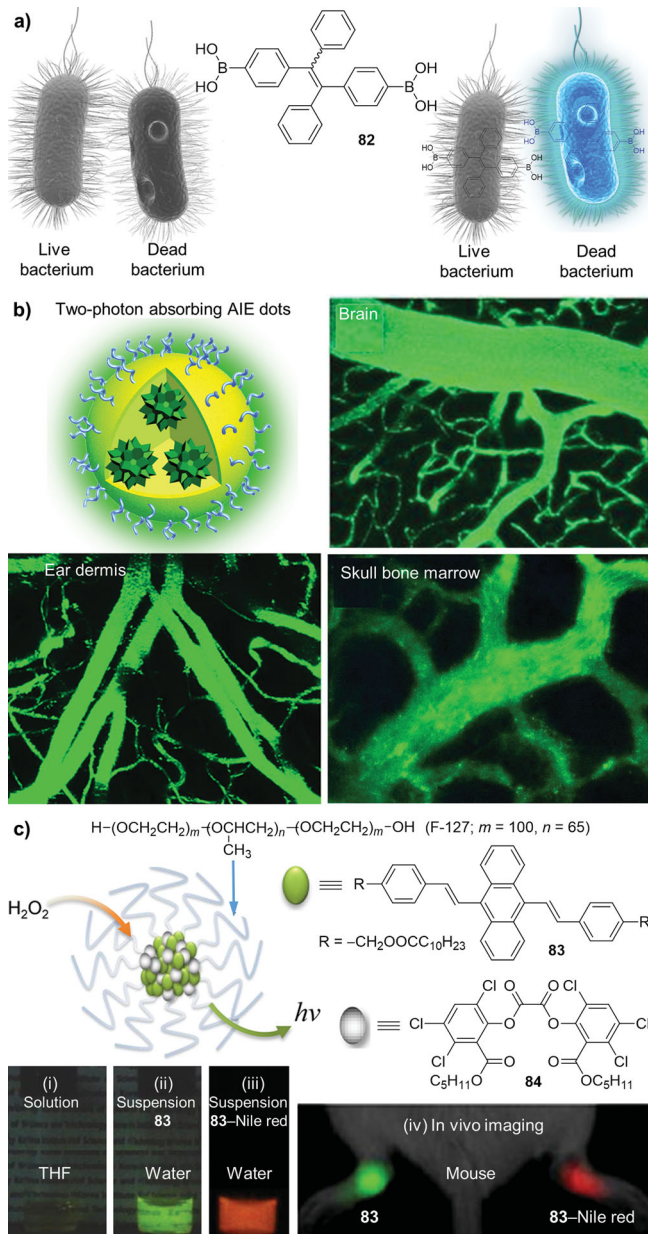


Figure 25. (a) Discrimination between live and dead bacteria by boronated TPE derivative **82**. Reproduced with permission.^[269] Copyright 2014, Wiley-VCH Verlag GmbH & Co. KGaA. (b) Intravital two-photon fluorescence imaging of blood vessels in different organs by two-photon absorbing AIE dots. Reproduced with permission.^[275] Copyright 2013, Wiley-VCH Verlag GmbH & Co. KGaA. (c) Diagrammatic illustration of AIE nanoaggregates and their components F-127, **83** and **84**. (i) Photograph of a mixture of **83**, **84** and F-127 in THF, chemiluminescence (CL) of water-dispersed (ii) nanoparticles of the mixture and (iii) nanoparticles doped with Nile red generated by addition of H_2O_2 , and (iv) in-vivo CL images of LPSO-induced arthritis model. Reproduced with permission.^[278] Copyright 2012, American Chemical Society.

scanning, and magnetic resonance imaging (MRI). Each of them, however, suffers from some drawbacks. For example, both X-ray and CT exert some detrimental influence on human body, due to the associated ionizing radiation. For type-B ultrasonic scanning, its resolution is relatively low, it is inapplicable

to intestinal cavity organ lesions, and the diagnosis result is easily affected by, or heavily relies on, operator. The sensitivity of MRI is low and it is not well suited for solid tissues such as tumors and bones or tissues with bloodstreams. New tissue imaging techniques with less or no harmful effect, high resolution, wide applicability, and great reliability are thus in great demand. Fluorescence imaging has great potential to become a new tissue imaging technique.

Thanks to their high brightness and great photostability as well as non-invasiveness, AIE dots have been utilized for *in vitro* and *in vivo* tissue imaging, whose performances in tumor imaging have been found to be superior to conventional systems.^[33,89,263,264,267,269] AIE dots, for example, have been prepared from BSA and an AIEgen consisting of TPE, triphenylamine and DCM (abbreviated as TTD). The TTD–BSA dots emit far-red/near-infrared (NIR) light and are employed for tissue imaging.^[89] The AIE dots show excellent cancer cell uptake and tumor-targeting ability *in vivo* due to the enhanced permeability and retention effect. He et al. have demonstrated the utility of the phospholipid–PEG nanomicelles encapsulating AIEgens for *in vivo* tumor targeting.^[270] Because the AIE dots-related tumor targeting and imaging studies have been summarized in one of our recent review articles,^[33] further discussions will not be carried out here to avoid duplication.

The emergence of two-photon intravital imaging technique has opened up a new avenue for tissue imaging by allowing non-invasive monitoring of cellular events at single-cell level *in vivo*. In comparison with the conventional one-photon fluorescence imaging, two-photon fluorescence imaging (TPFI) can engender high-energy visible fluorescence from low-energy irradiation in the NIR region (700–1000 nm).^[271,272] TPFI furnishes a unique and clear optical window for *in vivo* bioimaging with deep tissue penetration, minimal interference from auto-fluorescence, and low phototoxicity to living substrates.^[273,274] To realize TPFI, a good two-photon absorbing agent with a high δ value and a large two-photon action cross-section ($\Phi_F\delta$) is required. Intravital vasculature imaging is important because blood vessels are the major components of the circulatory system. Previously used organic dyes and nanoparticles for intravital imaging of vasculatures cannot fully meet the requirements of TPFI because of the limitations associated with their poor photobleaching resistance and low δ and/or $\Phi_F\delta$ values.

AIEgens have great promise in the construction of organic TPFI bioprobes with large $\Phi_F\delta$ values for high-contrast bioimaging applications. Ng, Liu, et al. have recently carried out an unprecedented work on utilizing ultrabright organic dots with AIE characteristics for real-time two-photon intravital vasculature imaging (Figure 25b).^[275] The AIE dots are fabricated by loading AIE molecules into hydrophilic PEG shells through a nanoprecipitation procedure. The AIE dots with a small size (~33 nm) show a high Φ_F (62%) and a large $\Phi_F\delta$ (6.3×10^4 GM) as well as excellent colloidal stability, great photostability, and low *in vivo* toxicity. The AIE dots do not blink, whose emission is much brighter than that of commercially available quantum dots QD655. Real-time *in vivo* two-photo imaging studies in the brain, bone marrow and ear of live mice reveal that the AIE dots act as an effective TPFI agent for *in vivo* blood vasculature imaging with deep-tissue penetration and high contrast.

In the systems discussed above, photonic energy, most frequently UV excitation, is used to activate luminescence processes of chromophores. Other energy sources can also be utilized to generate light emissions. Chemical and photonic energies are known to be interconvertible. Chemiluminescence (CL) is the light emission triggered by a chemical reaction, rather than photoexcitation. CL offers ultrahigh sensitivity due to the elimination of the noises associated with the photoexcitation-generated autofluorescence from background.^[276,277] CL processes of AIEgens have been realized and utilized for biomedical imaging applications. Kim and coworkers, for example, have fabricated AIEgen/peroxalate nanoparticles with enhanced and tunable CL for imaging biogenic hydrogen peroxide (H_2O_2).^[278] H_2O_2 is an endogenous molecular species that is involved in diverse physiological and pathological processes in the living system.^[279] Sensitive visualization of low-level H_2O_2 in cells and *in vivo* is of great importance not only for the fundamental study to understand its essential roles in cellular processes but also for the early diagnosis of inflammatory diseases.^[280] CL has been explored as the contrast signal for high-sensitivity imaging of H_2O_2 .^[281]

Non-enzymatic peroxalate-based CL (POCL) reaction is utilized for sensitive and selective *in vivo* imaging of H_2O_2 . Figure 25c shows the POCL reaction occurring in the reactant-integrated nanoreactor. The hydrophobic interior of the AIE-active nanoparticle contains a 9,10-distyrylanthracene derivative (83) as the light-emitting species and bis{3,4,6-trichloro-2-[(pentyloxy)carbonyl]phenyl}oxalate (84) as the highly reactive peroxalate, while the outer shell of the nanoparticle is made of a biocompatible polymeric surfactant, Pluronic F-127. Exposure to H_2O_2 triggers the reaction of 84 and transfers the energy to the co-loaded 83 to generate fluorescence by pure chemical excitation. Due to its AIE characteristic, 83 in the aggregate nanoparticle emits a strong green light. The CL nanoparticles with an average size of ~20 nm are capable of detecting intracellular H_2O_2 overproduced during immune response and realizing *in vivo* imaging of H_2O_2 . When a low-energy luminophore such as Nile red is used as a dopant, the dense integration in the nanoparticle facilitates intraparticle CL energy transfer to red shift the emission spectrum toward the biologically more transparent optical window, enabling highly sensitive *in-vivo* visualization of H_2O_2 associated with early stage inflammation.

4.4. Smart Materials

Many AIEgens are “intelligent” or “smart” materials, whose luminescence properties change in response to external stimuli or environmental variations, such as electric field, photonic irradiation, mechanical force, solvent polarity, heating/cooling (temperature), fuming (vapor), pH (medium) and storage (time).^[27–35] The luminescence change with mechanical force is a chromic effect commonly observed in many AIE systems. Such mechanochromic materials have great potentials to find applications in areas like pressure sensors, information storage, and security inks.^[34,282–284] The mechanochromic effects of the AIEgens are often associated with variations in their molecular packing structures. A propeller shape with a highly twisted conformation is one of the most distinct structural

features of an AIEgen. The loose packing morphology of such propeller-shaped AIE molecules is sensitive to external perturbation, thus giving rise to a chromic response. Many AIEgen-based mechanochromic systems have been covered in the review article recently published by Chi, Xu, et al.^[34] Herein, we would just pick up some typical examples of newly developed mechanochromic systems for discussion. It is noted that the mechanochromic process often coexists with other chromic

processes (e.g., thermochromism and vapochromism) in a reversible system.

TPE derivative (*E*-2 shows multiple chromic effects including mechano-, piezo-, thermo-, vapo- and chronochromisms (Figure 26a).^[49] A simple grinding of its powdery sample leads to a large bathochromic shift (from 447 to 477 nm; $\Delta\lambda = 30$ nm) in its emission color. A thermal annealing or vapor fuming by a polar solvent readily reverses the emission color

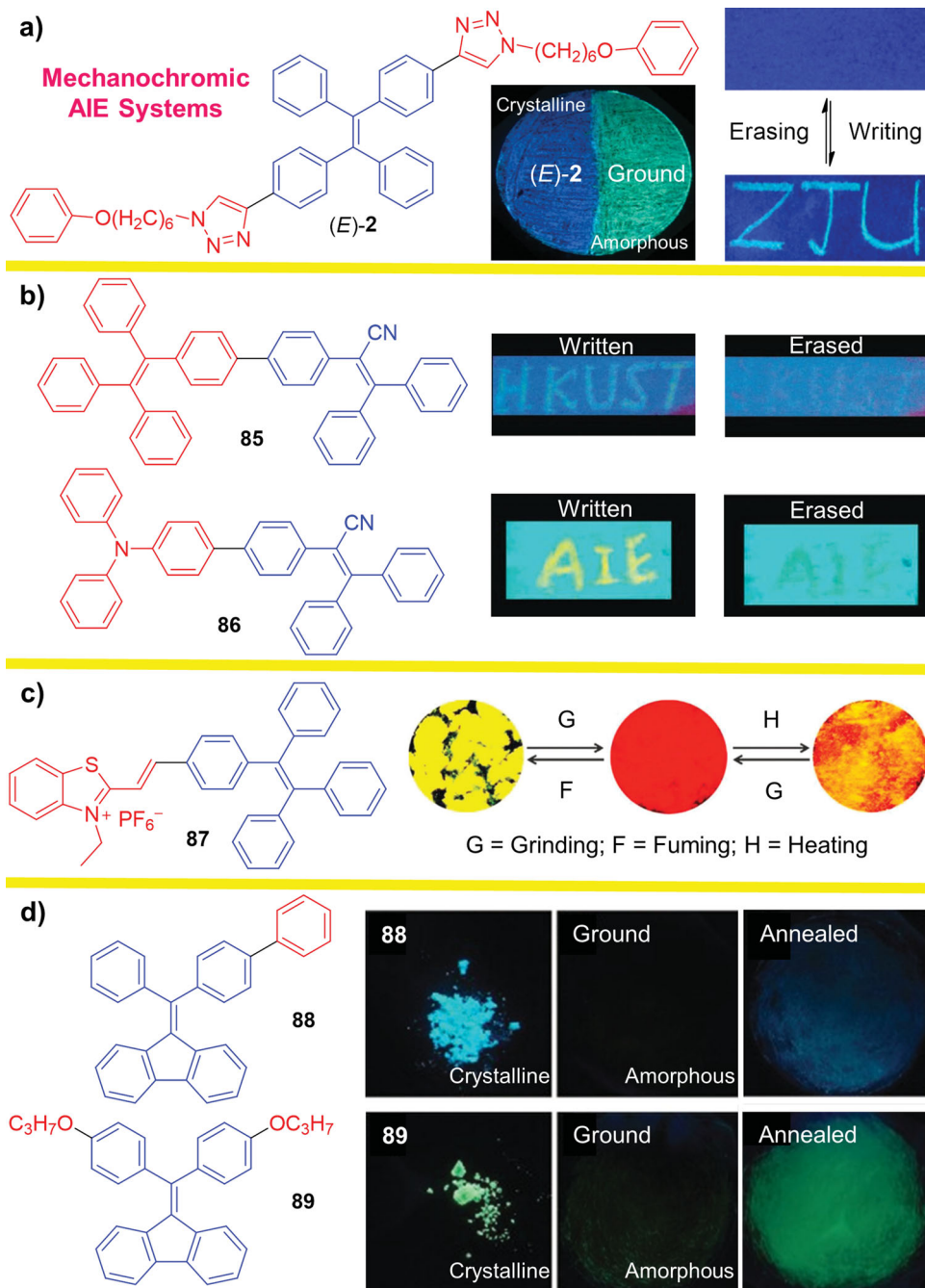


Figure 26. Fluorescent photographs of writing–erasing processes of (a) (*E*-2 (reproduced with permission;^[49] Copyright 2012, American Chemical Society) and (b) 85 and 86 (reproduced with permission;^[285] Copyright 2013, Wiley-VCH Verlag GmbH & Co. KGaA). Switching of solid-state emissions of (c) 87 (reproduced with permission;^[286] Copyright 2012, Royal Society of Chemistry) and (d) 88 and 89 by repeated grinding–fuming, grinding–heating and/or grinding–annealing processes (reproduced with permission;^[288] Copyright 2011, Wiley-VCH Verlag GmbH & Co. KGaA).

back. Pressurization can also cause a red-shift in its emission color, although to a less extent ($\Delta\lambda \sim 8$ nm). Emission restoration of the ground sample proceeds with a semilog dependence on time. The potential for real-world application of this smart material has been demonstrated by a writing–erasing process. When the powder of (E)-2 is sprayed onto a filter paper as a thin solid film, it emits a blue light upon UV excitation. When the paper is scratched with a spatula, the written letters (ZJU) emits a bluish-green light. Heating or fuming erases the letters by converting the emission color back to the original color. This suggests that (E)-2 may be used as a security ink for rewritable information storage system. The packing of the propeller-shaped AIE molecules is loose and can be readily modulated by external perturbation, which easily activates the morphological transformation or phase transition.

We have recently designed and synthesized a group of triphenylacrylonitrile derivatives, e.g., 85 and 86, with propeller-like conformation and multiple mutable interactions (Figure 26b).^[285] Synergistic interplay between the twisted molecular conformation and intra- and intermolecular interactions (van de Waals force, C–H···N, C–H···π H-bonding, dipole–dipole interaction, etc.) endows all the derivatives with strong AIE effects, high solid-state Φ_F values, and remarkable mechanochromisms with large changes in the emission colors and efficiencies. AIEgen 86 shows a stronger mechanochromic activity with a higher contrast in the emission color ($\Delta\lambda = 78$ nm) and a larger change in the emission efficiency ($\alpha_\Phi = 24\%$), in comparison to those of 85 ($\Delta\lambda = 72$ nm, $\alpha_\Phi = 11\%$), owing to the stronger D–A interaction in the former system. The planarization of the twisted molecular conformation and the destruction of the multiple intermolecular interactions by the application of mechanical force cause the phase transition from crystalline to amorphous state, leading to the observed large mechanochromic effect.

In the above discussed writing–erasing cycles, the emission colors are hopping back and forth between blue (447 nm) and bluish-green [477 nm; for (E)-2], blue (443 nm) and green (515 nm; for 85), and bluish-green (478 nm) and yellow (556 nm; for 86). The luminescence switching can be shifted to longer wavelength region through judicious structural design. For example, functionalization of TPE with benzothiazolium unit greatly red-shifts the emission color.^[286] The luminescence spectra of the crystals of the TPE–benzothiazolium adduct (87) are peaked at 565–591 nm, depending on their molecular packing structures, while those of its amorphous powders are peaked at 644–663 nm. Gently grinding the crystals of 87 readily brings about amorphization and bathochromically shifts the emission peak from 565 to 650 nm (Figure 26c). Fuming with acetone vapor for 10 min reinstalls the initial yellow emission. The conversion between the yellow and red emissions can be repeated many times without fatigue, as the physical stimuli are nondestructive in nature. Moreover, heating the ground sample of 87 at 150 °C for a short while changes its emission color from red to orange, while grinding reverts the color change, thanks to the reversible thermo- and mechanochromic processes.

In many AIEgen-based mechanochromic systems, the emission efficiencies are decreased to some extents by mechanical grinding. In some systems, the emissions can even be totally quenched. AIEgen 88 is such an example: its emission vanishes

upon grinding (Figure 26d). It has been known that 88 emits faintly in amorphous phase but intensely in crystalline phase, exhibiting a unique CIE effect.^[23,287] The grinding-caused quenching of its light emission is the reversal of the CIE process. We have recently developed another diphenyldibenzofulvene derivative with CIE attribute (89).^[288] Its single crystal emits at 500 nm with a Φ_F of 82.1%. Its amorphous powder, however, emits dimly at 580 nm with a Φ_F value as low as <1%. With more twisted and rigid conformation and stronger C–H···π and C–H···O interaction in the crystalline state, the structure of 89 is stiffened and its radiationless pathways are blocked. The CIE feature of the AIEgen endows it with the capability to switch between dark (off) and bright (on) states. Its emission is quenched by grinding, while heating recovers its emission. This on–off process can be repeated many times. The CIE effect enriches mechanochromic behaviors of AIEgens. Judicial combinations of the different chromic effects will enable the AIEgens to find a large array of high-tech applications.

5. Summary and Perspective

AIEgens are a class of functional materials that luminesce more brilliantly in the practically useful solid state than in the scholarly interested solution state. The performances of their aggregates are superior to those of their individual molecules—*the whole is more brilliant than the parts*—in sharp contrast to conventional ACQ systems.^[2,3] Because of its academic value and practical implications, AIE research has attracted much interest, with many research groups actively participating in the area of study. In this review, we have summarized the progresses made in the area in recent years. We have examined mechanistic issues of AIE processes, presented typical examples of different types of AIEgens, discussed their structure–property relationships, and demonstrated their high-tech applications as advanced materials. Through careful data scrutinization, we have gained deeper insights into AIE mechanisms and proposed RIM processes as the main cause for the AIE phenomena.

AIEgens enjoy a great diversity in molecular structure, ranging from pure hydrocarbons to heteroatom-containing compounds to organometallic complexes. Among them, the AIEgens without chromophores in classic sense are particularly intriguing. Their heterodox emission processes are rationalized to be associated with rigidification-induced emissions and their light-emitting species are attributed to the nanoaggregates or clusters of electron-rich atoms or groups. In the nanoclusters, the electron-rich groups overlap with each other to share their unpaired electrons and function as “clustered chromophores” with narrowed energy gaps. Further studies, however, are needed to fully understand the exact mechanisms for the light emission processes of this group of unique AIEgens.

The most appealing applications of AIEgens are in the areas of life science and biomedical engineering. The AIE dots, including the AIEgen-containing nanohybrids and the AIEgen-decorated nanoparticles, can be used for in-vitro and in-vivo imaging of biogenic molecules, cells, tissues, organisms, etc. The bright emission, high efficiency, great photostability,

superb biocompatibility, and large optical nonlinearity of the AIE dots make them promising for in-depth and long-term imaging and tracing applications. The development of multi-modality sensing systems (e.g., AIE + MRI) and the combination with other medication processes (e.g., controlled or targeted drug delivery) will further widen the scope of biomedical applications of the AIE dots to such important areas as clinical diagnosis and therapeutic treatment.

The AIE research is advancing so rapidly that we cannot cover all the reported data in this review article. The space limitation forces us to be highly selective in choosing examples for presentation and discussion. As a compensation to this pitiful loss, we herein provide a list of selected papers published recently by different research groups in the area in the Reference Section.^[289–313] Although much work has been done in the area, many intriguing possibilities remain to be explored. We enthusiastically look forward to new developments in this exciting area of research.

Acknowledgements

This work was partially supported by the National Basic Research Program of China (973 Program 2013CB834701), the Research Grants Council of Hong Kong (HKUST2/CRF/10, AoE/P-03/08, 604913, 604711, 602212, and N_HKUST620/11), and Guangdong Innovative Research Team Program (201101C0105067115).

Received: March 26, 2014

Revised: May 25, 2014

Published online: June 30, 2014

- [1] a) *Oxford Dictionary*, <http://www.oxforddictionaries.com/definition/english/aggregate>; retrieved on May 15, 2014; b) *Aggregate*, <http://en.wikipedia.org/wiki/Aggregate>; retrieved on May 15, 2014.
- [2] J. B. Birks, *Photophysics of Aromatic Molecules*, Wiley, London **1970**.
- [3] *Photonic Research Systems*, http://www.prbsbio.com/html/general_faq.html#q4; retrieved on May 15, **2014**.
- [4] a) X. Zhang, D. Gorl, V. Stepanenko, F. Wurthner, *Angew. Chem. Int. Ed.* **2014**, *53*, 1270; b) S. W. Thomas III, G. D. Joly, T. M. Swager, *Chem. Rev.* **2007**, *107*, 1339.
- [5] F. J. M. Hoeben, P. Jonkheijm, E. W. Meijer, A. P. H. J. Schenning, *Chem. Rev.* **2005**, *105*, 1491.
- [6] U. H. F. Bunz, *Chem. Rev.* **2000**, *100*, 1605.
- [7] F. Hide, M. A. Diaz-Garcia, B. J. Schwartz, A. J. Heeger, *Acc. Chem. Res.* **1997**, *30*, 430.
- [8] S. M. Borisov, O. S. Wolfbeis, *Chem. Rev.* **2008**, *108*, 423.
- [9] R. B. Thompson, *Fluorescence Sensors and Biosensors*, CRC, Boca Raton **2006**.
- [10] C. W. Tang, S. A. Vanslyke, *Appl. Phys. Lett.* **1987**, *51*, 913.
- [11] C. D. Geddes, J. R. Lakowicz, *Advanced Concepts in Fluorescence Sensing*, Springer, Norwell **2005**.
- [12] E. A. Jares-Erijman, T. M. Jovin, *Nat. Biotechnol.* **2003**, *21*, 1387.
- [13] H. Saigusa, E. C. Lim, *Acc. Chem. Res.* **1996**, *29*, 171.
- [14] J. Wang, Y. Zhao, Y. C. Dou, H. Sun, P. Xu, K. Ye, J. Zhang, S. Jiang, F. Li, Y. Wang, *J. Phys. Chem. B* **2007**, *111*, 5082.
- [15] S. Hecht, J. M. J. Fréchet, *Angew. Chem. Int. Ed.* **2001**, *40*, 74.
- [16] B. T. Nguyen, J. E. Gautrot, C. Ji, P.-L. Brunner, M. T. Nguyen, X. X. Zhu, *Langmuir* **2006**, *22*, 4799.
- [17] L. Chen, S. Xu, D. Mcbranch, D. Whitten, *J. Am. Chem. Soc.* **2000**, *122*, 9302.
- [18] P. N. Taylor, M. J. O'Connell, L. A. Mcneill, M. J. Hall, R. T. Aplin, H. L. Anderson, *Angew. Chem. Int. Ed.* **2000**, *39*, 3456.
- [19] J. Luo, Z. Xie, J. W. Y. Lam, L. Cheng, H. Chen, C. Qiu, H. S. Kwok, X. Zhan, Y. Liu, D. Zhu, B. Z. Tang, *Chem. Commun.* **2001**, 1740.
- [20] B. Z. Tang, X. Zhan, G. Yu, P. P. S. Lee, Y. Liu, D. Zhu, *J. Mater. Chem.* **2001**, *11*, 2974.
- [21] J. W. Chen, B. Xu, X. Y. Ouyang, B. Z. Tang, Y. Cao, *J. Phys. Chem. A* **2004**, *108*, 7522.
- [22] H. Tong, Y. Hong, Y. Dong, Y. Ren, M. Haeussler, J. W. Y. Lam, K. S. Wong, B. Z. Tang, *J. Phys. Chem. B* **2007**, *111*, 2000.
- [23] H. Tong, Y. Dong, Y. Hong, M. Haeussler, J. W. Y. Lam, H. H. Y. Sung, X. Yu, J. Sun, I. D. Williams, H. S. Kwok, B. Z. Tang, *J. Phys. Chem. C* **2007**, *111*, 2287.
- [24] Q. Zeng, Z. Li, Y. Dong, C. Di, A. Qin, Y. Hong, L. Ji, Z. Zhu, C. K. W. Jim, G. Yu, Q. Li, Z. Li, Y. Liu, J. Qin, B. Z. Tang, *Chem. Commun.* **2007**, 70.
- [25] Y. Dong, J. W. Y. Lam, A. Qin, J. Liu, Z. Li, B. Z. Tang, J. Sun, H. S. Kwok, *Appl. Phys. Lett.* **2007**, *91*, 011111.
- [26] M. Freemantle, *Chem. Eng. News* **2001**, *79*, 29.
- [27] M. Wang, G. Zhang, D. Zhang, D. Zhu, B. Z. Tang, *J. Mater. Chem.* **2010**, *20*, 1858.
- [28] Y. Hong, J. W. Y. Lam, B. Z. Tang, *Chem. Commun.* **2009**, 4332.
- [29] a) Y. Hong, J. W. Y. Lam, B. Z. Tang, *Chem. Soc. Rev.* **2011**, *40*, 5361; b) R. Hu, N. L. C. Leung, B. Z. Tang, *Chem. Soc. Rev.* **2014**, *43*, 4494.
- [30] Z. Shuang, A. Qin, J. Z. Sun, B. Z. Tang, *Prog. Chem.* **2011**, *23*, 623.
- [31] J. Liu, J. W. Y. Lam, B. Z. Tang, *J. Inorg. Organomet. Polym.* **2009**, *19*, 249.
- [32] Z. Zhao, J. W. Y. Lam, B. Z. Tang, *J. Mater. Chem.* **2012**, *22*, 23726.
- [33] D. Ding, K. Li, B. Liu, B. Z. Tang, *Acc. Chem. Res.* **2013**, *46*, 2441.
- [34] Z. Chi, X. Zhang, B. Xu, X. Zhou, C. Ma, Y. Zhang, S. Liu, J. Xu, *Chem. Soc. Rev.* **2012**, *41*, 3878.
- [35] G. Zhao, C. Shi, Z. Guo, W. Zhu, S. Zhu, *Chin. J. Org. Chem.* **2012**, *32*, 1620.
- [36] J. Chen, C. C. W. Law, J. W. Y. Lam, Y. Dong, S. M. F. Lo, I. D. Williams, D. Zhu, B. Z. Tang, *Chem. Mater.* **2003**, *15*, 1535.
- [37] X. Fan, J. L. Sun, F. Z. Wang, Z. Z. Chu, P. Wang, Y. Q. Dong, R. R. Hu, B. Z. Tang, D. C. Zou, *Chem. Commun.* **2008**, 2989.
- [38] S. Li, Q. Wang, Y. Qian, S. Wang, Y. Li, G. Yang, *J. Phys. Chem. A* **2007**, *111*, 11793.
- [39] Q. Peng, Y. Yi, Z. Shuai, J. Shao, *J. Am. Chem. Soc.* **2007**, *129*, 9333.
- [40] Q. Peng, Y. Yi, Z. Shuai, J. Shao, *J. Chem. Phys.* **2007**, *126*, 114302.
- [41] Y. Q. Dong, J. W. Y. Lam, A. Qin, Z. Li, J. Z. Sun, Y. P. Dong, B. Z. Tang, *J. Inorg. Organomet. Polym. Mater.* **2007**, *17*, 673.
- [42] J. Chen, Z. Xie, J. W. Y. Lam, C. C. W. Law, B. Z. Tang, *Macromolecules* **2003**, *36*, 1108.
- [43] a) J. Luo, K. Song, F. L. Gu, Q. Miao, *Chem. Sci.* **2011**, *2*, 2029; b) Z. Lin, A. Qin, *Nat. Sci. Rev.* **2014**, *1*, 22–24.
- [44] C. L. Schilling, E. F. Hilinski, *J. Am. Chem. Soc.* **1988**, *110*, 2296.
- [45] D. A. Shultz, M. A. Fox, *J. Am. Chem. Soc.* **1989**, *111*, 6311.
- [46] A. Simeonov, M. Matsushita, E. A. Juban, E. H. Z. Thompson, T. Z. Hoffman, A. E. Beuscher IV, M. J. Taylor, W. R. Wirsching, J. K. McCusker, R. C. Stevens, D. P. Millar, P. G. Schultz, R. A. Lerner, K. D. Janda, *Science* **2000**, *290*, 307.
- [47] D. H. Waldeck, *Chem. Rev.* **1991**, *91*, 415.
- [48] J. Saitiel, J. T. D'Agostino, *J. Am. Chem. Soc.* **1972**, *94*, 6445.
- [49] J. Wang, J. Mei, R. Hu, J. Z. Sun, A. Qin, B. Z. Tang, *J. Am. Chem. Soc.* **2012**, *134*, 9956.
- [50] N. B. Shustova, T.-C. Ong, A. F. Cozzolino, V. K. Michaelis, R. G. Griffin, M. Dinc, *J. Am. Chem. Soc.* **2012**, *134*, 15061.
- [51] A. J. Qin, J. W. Y. Lam, F. Mahtab, C. K. W. Jim, L. Tang, J. Z. Sun, H. H. Y. Sung, I. D. Williams, B. Z. Tang, *Appl. Phys. Lett.* **2009**, *94*, 253308.
- [52] J. Shi, N. Chang, C. Li, J. Mei, C. Deng, X. Luo, Z. Liu, Z. Bo, Y. Q. Dong, B. Z. Tang, *Chem. Commun.* **2012**, *48*, 10675.

- [53] C. Deng, Y. Niu, Q. Peng, A. Qin, Z. Shuai, B. Z. Tang, *J. Chem. Phys.* **2011**, *135*, 014304.
- [54] X. Gao, Q. Peng, Y. Niu, D. Wang, Z. Shuai, *Phys. Chem. Chem. Phys.* **2012**, *14*, 14207.
- [55] Q. Wu, C. Deng, Q. Peng, Y. Niu, Z. Shuai, *J. Comput. Chem.* **2012**, *33*, 1862.
- [56] Q. Wu, Q. Peng, Y. Niu, X. Gao, Z. Shuai, *J. Phys. Chem. A* **2012**, *116*, 3881.
- [57] G. Liu, M. Yang, L. Wang, J. Zheng, H. Zhou, J. Wu, Y. Tian, *J. Mater. Chem. C* **2014**, *2*, 2684.
- [58] M. Yang, D. Xu, W. Xi, L. Wang, J. Zheng, J. Huang, J. Zhang, H. Zhou, J. Wu, Y. Tian, *J. Org. Chem.* **2013**, *78*, 10344.
- [59] a) W.-b. Jia, H.-w. Wang, L.-m. Yang, H.-b. Lu, L. Kong, Y.-p. Tian, X.-t. Tao, J.-x. Yang, *J. Mater. Chem. C* **2013**, *1*, 7092; b) B. Wang, Y. Wang, J. Hua, Y. Jiang, J. Huang, S. Qian, H. Tian, *Chem. Eur. J.* **2011**, *17*, 2647.
- [60] a) M. Herman, D. S. Perry, *Phys. Chem. Chem. Phys.* **2013**, *15*, 9970; b) B. Klaumünzer, D. Kröner, H. Lischka, P. Saalfrank, *Phys. Chem. Chem. Phys.* **2012**, *14*, 8693.
- [61] L. Rossa, F. Vögtle, *Top. Curr. Chem.* **1983**, *113*, 157.
- [62] A. Schröder, H.-B. Mekelburger, F. Vögtle, *Top. Curr. Chem.* **1994**, *172*, 179.
- [63] Y.-T. Wu, J. S. Siegel, *Chem. Rev.* **2006**, *106*, 4843.
- [64] V. M. Tsefrikas, L. T. Scott, *Chem. Rev.* **2006**, *106*, 4868.
- [65] T. Kawase, H. Kurata, *Chem. Rev.* **2006**, *106*, 5250.
- [66] K. Tahara, Y. Tobe, *Chem. Rev.* **2006**, *106*, 5274.
- [67] T. Nishiuchi, K. Tanaka, Y. Kuwatani, J. Sung, T. Nishinaga, D. Kim, M. Iyoda, *Chem. Eur. J.* **2013**, *19*, 4110.
- [68] a) E. E. Jolley, *Nature* **1936**, *138*, 1009; b) G. Scheibe, *Angew. Chem.* **1936**, *49*, 563.
- [69] T. Kobayashi, *J-Aggregates*, World Scientific, Singapore **1996**.
- [70] T. J. James, *The Theory of Photographic Process*, Macmillan, New York **1977**.
- [71] F. Würthner, T. E. Kaiser, C. R. Saha-Möller, *Angew. Chem. Int. Ed.* **2011**, *50*, 3376.
- [72] *J-aggregate*: <http://en.wikipedia.org/wiki/J-aggregate>; retrieved on May 15, 2014.
- [73] X.-Q. Li, X. Zhang, S. Ghosh, F. Würthner, *Chem. Eur. J.* **2008**, *14*, 8074.
- [74] Y. Wang, T. Liu, L. Bu, J. Li, C. Yang, X. Li, Y. Tao, W. Yang, *J. Phys. Chem. C* **2012**, *116*, 15576.
- [75] B.-K. An, S.-K. Kwon, S.-D. Jung, S. Y. Park, *J. Am. Chem. Soc.* **2002**, *124*, 14410.
- [76] X. Y. Shen, W. Z. Yuan, Y. Liu, Q. Zhao, P. Lu, Y. Ma, I. D. Williams, A. Qin, J. Z. Sun, B. Z. Tang, *J. Phys. Chem. C* **2012**, *116*, 10541.
- [77] A. Douhal, F. Lahmani, A. H. Zewail, *Chem. Phys.* **1996**, *207*, 477.
- [78] S. Lochbrunner, T. Schultz, M. Schmitt, J. P. Shaffer, M. Z. Zgierski, A. Stolow, *J. Chem. Phys.* **2001**, *114*, 2519.
- [79] J. Goodman, L. E. Brus, *J. Am. Chem. Soc.* **1978**, *100*, 7472.
- [80] S. M. Ormson, R. G. Brown, *Prog. React. Kinet.* **1994**, *19*, 45.
- [81] G. Yang, S. Li, S. Wang, Y. Li, C. R. Chim. **2011**, *14*, 789.
- [82] T. Mutai, H. Sawatani, T. Shida, H. Shono, K. Araki, *J. Org. Chem.* **2013**, *78*, 2482.
- [83] Y. Shigemitsu, T. Mutai, H. Houjou, K. Araki, *J. Phys. Chem. A* **2012**, *116*, 12041.
- [84] R. Wei, P. Song, A. Tong, *J. Phys. Chem. C* **2013**, *117*, 3467.
- [85] B.-R. Gao, H.-Y. Wang, Z.-Y. Yang, H. Wang, L. Wang, Y. Jiang, Y.-W. Hao, Q.-D. Chen, Y.-P. Li, Y.-G. Ma, H.-B. Sun, *J. Phys. Chem. C* **2011**, *115*, 16150.
- [86] Z.-Q. Yan, Z.-Y. Yang, H. Wang, A.-W. Li, L.-P. Wang, H. Yang, B.-R. Gao, *Spectrochim. Acta A: Mol. Biomol. Spectr.* **2011**, *78*, 1640.
- [87] H. H. Fang, Q. D. Chen, J. Yang, H. Xia, B. R. Gao, J. Feng, Y. G. Ma, H. B. Sun, *J. Phys. Chem. C* **2010**, *114*, 11958.
- [88] R. Hu, E. Lager, A. Aguilar-Aguilar, J. Liu, J. W. Y. Lam, H. H. Y. Sung, I. D. Williams, Y. Zhong, K. S. Wong, E. Peña-Cabrera, B. Z. Tang, *J. Phys. Chem. C* **2009**, *113*, 15845.
- [89] W. Qin, D. Ding, J. Liu, W. Z. Yuan, Y. Hu, B. Liu, B. Z. Tang, *Adv. Funct. Mater.* **2012**, *22*, 771.
- [90] S. Kim, Q. Zheng, G. He, D. J. Bharali, H. E. Pudavar, A. Baev, P. N. Prasad, *Adv. Funct. Mater.* **2006**, *16*, 2317.
- [91] W. Z. Yuan, P. Lu, S. Chen, J. W. Y. Lam, Z. Wang, Y. Liu, H. S. Kwok, B. Z. Tang, *Adv. Mater.* **2010**, *22*, 2159.
- [92] H. Jiating, X. Bin, C. Feipeng, X. Haijian, L. Kunpeng, Y. Ling, T. Wenjing, *J. Phys. Chem. C* **2009**, *113*, 9892.
- [93] C. J. Bhongale, C. W. Chang, C. S. Lee, E. W. G. Diau, C. S. Hsu, *J. Phys. Chem. B* **2005**, *109*, 13472.
- [94] Y.-X. Li, Z. Chen, Y. Cui, G.-M. Xia, X.-F. Yang, *J. Phys. Chem. C* **2012**, *116*, 6401.
- [95] J. Feng, X. Chen, Q. Han, H. Wang, P. Lu, Y. Wang, *J. Lumin.* **2011**, *131*, 2775.
- [96] R. Hu, J. W. Y. Lam, Y. Liu, X. Zhang, B. Z. Tang, *Chem. Eur. J.* **2013**, *19*, 5617.
- [97] M. D. McGehee, A. J. Heeger, *Adv. Mater.* **2000**, *12*, 1655.
- [98] Z. Zhang, B. Xu, J. Su, L. Shen, Y. Xie, H. Tian, *Angew. Chem. Int. Ed.* **2011**, *50*, 11654.
- [99] L. Yang, J. Ye, L. Xu, X. Yang, W. Gong, Y. Lin, G. Ning, *RSC Adv.* **2012**, *2*, 11529.
- [100] F. Jäkle, *Chem. Rev.* **2010**, *110*, 3985.
- [101] H. Sohn, J. M. Sailor, D. Magde, W. C. Trogler, *J. Am. Chem. Soc.* **2003**, *125*, 3821.
- [102] O. Fadhel, M. Gras, N. Lemaitre, V. Deborde, M. Hissler, B. Geffroy, R. Réau, *Adv. Mater.* **2009**, *21*, 1261.
- [103] K. Xiao, Y. Liu, T. Qi, W. Zhang, F. Wang, J. Gao, W. Qiu, Y. Ma, G. Cui, S. Chen, X. Zhan, G. Yu, J. Qin, W. Hu, D. Zhu, *J. Am. Chem. Soc.* **2005**, *127*, 13281.
- [104] J. Ferman, J. P. Kakareka, W. T. Klooster, J. L. Mullin, J. Quattrucci, J. S. Ricci, H. J. Tracy, W. J. Vining, S. Wallace, *Inorg. Chem.* **1999**, *38*, 2464.
- [105] H. J. Tracy, J. L. Mullin, W. T. Klooster, J. A. Martin, S. W. Haug, I. Rudloe, K. Watts, *Inorg. Chem.* **2005**, *44*, 2003.
- [106] L. Mullin, H. J. Tracy, J. R. Ford, S. R. Keenan, F. Fridman, *J. Inorg. Organometal. Polym. Mat.* **2007**, *17*, 201.
- [107] K. Shiraishi, T. Sanji, M. Tanaka, *ACS Appl. Mater. Interfaces* **2009**, *1*, 1379.
- [108] K. Shiraishi, T. Sanji, M. Tanaka, *J. Mol. Eng. Mater.* **2013**, *1*, 1340001.
- [109] Y. Ren, W. H. Kan, M. A. Henderson, P. G. Bomben, C. P. Berlinguet, V. Thangadurai, T. Baumgartner, *J. Am. Chem. Soc.* **2011**, *133*, 17014.
- [110] T. L. Bandrowsky, J. B. Carroll, J. Braddock-Wilking, *Organometallics* **2011**, *30*, 3559.
- [111] T. Han, X. Feng, B. Tong, J. Shi, L. Chen, J. Zhi, Y. Dong, *Chem. Commun.* **2012**, *48*, 416.
- [112] X. Shi, H. Wang, T. Han, X. Feng, B. Tong, J. Shi, J. Zhi, Y. Dong, *J. Mater. Chem.* **2012**, *22*, 19296.
- [113] Z. T. Wang, Y. Fang, J. Z. Sun, A. J. Qin, B. Z. Tang, *Sci. China Chem.* **2013**, *56*, 1187.
- [114] W. Chen, D. Zhang, W. Gong, Y. Lin, G. Ning, *Spectro. Acta Part A: Mol. Biomol. Spectro.* **2013**, *110*, 471.
- [115] K. Namitharan, K. Pitchumani, *Org. Biomol. Chem.* **2012**, *10*, 2937.
- [116] X. Chen, Y. Xiang, P.-S. Song, R. Wei, Z. Zhou, K. Li, A. Tong, *J. Lumin.* **2011**, *131*, 1453.
- [117] M. Shellaiah, Y.-H. Wu, A. Singh, M. V. R. Raju, H.-C. Lin, *J. Mater. Chem. A* **2013**, *1*, 1310.
- [118] Z. Yu, Y. Duan, L. Cheng, Z. Han, Z. Zheng, H. Zhou, J. Wu, Y. Tian, *J. Mater. Chem.* **2012**, *22*, 16927.
- [119] M. Matsui, T. Shibata, M. Fukushima, Y. Kubota, K. Funabiki, *Tetrahedron* **2012**, *68*, 9936.

- [120] Q. Dai, W. Liu, L. Zeng, C.-S. Lee, J. Wu, P. Wang, *Cryst. Eng. Comm.* **2011**, *13*, 4617.
- [121] B. Wang, N. He, B. Li, S. Jiang, Y. Qu, S. Qu, J. Hua, *Aust. J. Chem.* **2012**, *65*, 387.
- [122] T. Ishii-i, K. Ikeda, Y. Kichise, M. Ogawa, *Chem. Asian J.* **2012**, *7*, 1553.
- [123] Z.-F. An, C. Zheng, R.-F. Chen, J. Yin, J.-J. Xiao, H.-F. Shi, Y. Tao, Y. Qian, W. Huang, *Chem. Eur. J.* **2012**, *18*, 15655.
- [124] E. Cogné-Laage, J. F. Allemand, O. Ruel, J. B. Baudin, V. Croquette, M. Blanchard-Desce, L. Jullien, *Chem. Eur. J.* **2004**, *10*, 1445.
- [125] R. Yoshii, A. Nagai, K. Tanaka, Y. Chujo, *Chem. Eur. J.* **2013**, *19*, 4506.
- [126] J. Liu, Q. Meng, X. Zhang, X. Lu, P. He, L. Jiang, H. Dong, W. Hu, *Chem. Commun.* **2013**, *49*, 1199.
- [127] A. Nandakumar, P. T. Perumal, *Org. Lett.* **2013**, *15*, 382.
- [128] I. Javed, T. Zhou, F. Muhammad, J. Guo, H. Zhang, Y. Wang, *Langmuir* **2012**, *28*, 1439.
- [129] R. Gómez, C. Seoane, J. L. Segura, *Chem. Soc. Rev.* **2007**, *36*, 1305.
- [130] A. B. Flynn, W. W. Ogilvie, *Chem. Rev.* **2007**, *107*, 4698.
- [131] a) T. He, X. Tao, J. Yang, D. Guo, H. Xia, J. Jia, M. Jiang, *Chem. Commun.* **2011**, *47*, 2907; b) R. Hu, S. Li, Y. Zeng, J. Chen, S. Wang, Y. Li, G. Yang, *Phys. Chem. Chem. Phys.* **2011**, *13*, 2044.
- [132] Y. Qian, S. Li, Q. Wang, X. Sheng, S. Wu, S. Wang, J. Li, G. Yang, *Soft Matter* **2012**, *8*, 757.
- [133] Y. Qian, M. Cai, X. Zhou, Z. Gao, X. Wang, Y. Zhao, X. Yan, W. Wei, L. Xie, W. Huang, *J. Phys. Chem. C* **2012**, *116*, 12187.
- [134] A. Bernet, R. Q. Albuquerque, M. Behr, S. T. Hoffmann, H.-W. Schmidt, *Soft Matter* **2012**, *8*, 66.
- [135] D. Xu, X. Liu, R. Lu, P. Xue, X. Zhang, H. Zhou, J. Jia, *Org. Biomol. Chem.* **2011**, *9*, 1523.
- [136] M. P. Lightfoot, F. S. Mair, R. G. Pritchard, J. E. Warren, *Chem. Commun.* **1999**, *19*, 1945.
- [137] T.-Q. Nguyen, R. Martel, P. Avouris, M. L. Bushey, L. Brus, C. Nuckolls, *J. Am. Chem. Soc.* **2004**, *126*, 5234.
- [138] M. A. Baldo, D. F. O'Brien, Y. You, A. Shoustikov, S. Sibley, M. E. Thompson, S. R. Forrest, *Nature* **1998**, *395*, 151.
- [139] Q. Zhao, C. Huang, F. Li, *Chem. Soc. Rev.* **2011**, *40*, 2508.
- [140] W. Z. Yuan, X. Y. Shen, H. Zhao, J. W. Y. Lam, L. Tang, P. Lu, C. Wang, Y. Liu, Z. Wang, Q. Zheng, J. Z. Sun, Y. Ma, B. Z. Tang, *J. Phys. Chem. C* **2010**, *114*, 6090.
- [141] Y. Y. Gong, Y. Q. Tan, J. Mei, Y. R. Zhang, W. Z. Yuan, Y. M. Zhang, J. Z. Sun, B. Z. Tang, *Sci. China Chem.* **2013**, *56*, 1178.
- [142] Y. Y. Gong, Y. Q. Tan, H. Li, Y. R. Zhang, W. Z. Yuan, Y. M. Zhang, J. Z. Sun, B. Z. Tang, *Sci. China Chem.* **2013**, *56*, 1183.
- [143] O. Bolton, K. Lee, H. J. Kim, K. Y. Lin, J. Kim, *Nat. Chem.* **2011**, *3*, 205.
- [144] D. Lee, O. Bolton, B. C. Kim, J. H. Youk, S. Takayama, J. Kim, *J. Am. Chem. Soc.* **2013**, *135*, 6325.
- [145] S. Hirata, K. Totani, J. Zhang, T. Yamashita, H. Kaji, S. R. Marder, T. Watanabe, C. Adachi, *Adv. Funct. Mater.* **2013**, *23*, 3386.
- [146] C. M. Xing, J. W. Y. Lam, A. Qin, Y. Dong, M. Haussler, W. T. Yang, B. Z. Tang, *Polym. Mater. Sci. Eng.* **2007**, *96*, 418.
- [147] A. Pucci, R. Rausa, F. Ciardelli, *Macromol. Chem. Phys.* **2008**, *209*, 900.
- [148] M. Boominathan, V. Sathish, M. Nagaraj, N. Bhuvanesh, S. Muthusubramanian, S. Rajagopal, *RSC Adv.* **2013**, *3*, 22246.
- [149] Q. Zhu, L. Huang, Z. Chen, S. Zheng, L. Lv, Z. Zhu, D. Cao, H. Jiang, S. Liu, *Chem. Eur. J.* **2013**, *19*, 1268.
- [150] L. Huang, J. Su, D. Zhong, H. Wang, R. Liu, L. Yu, Q. Zhu, S. Liu, *RSC Adv.* **2013**, *3*, 13286.
- [151] B. Manimaran, P. Thanasekaran, T. Rajendran, R. J. Lin, I. J. Chang, G. H. Lee, S. M. Peng, S. Rajagopal, K. L. Lu, *Inorg. Chem.* **2002**, *41*, 5323.
- [152] Y.-Z. Xie, G.-G. Shan, P. Li, Z.-Y. Zhou, Z.-M. Su, *Dyes Pigments* **2013**, *96*, 467.
- [153] G.-G. Shan, H.-B. Li, H.-Z. Sun, D.-X. Zhu, H.-T. Cao, Z.-M. Su, *J. Mater. Chem. C* **2013**, *1*, 1440.
- [154] G.-G. Shan, L.-Y. Zhang, H.-B. Li, S. Wang, D.-X. Zhu, P. Li, C.-G. Wang, Z.-M. Su, Y. Liao, *Dalton Trans.* **2012**, *41*, 523.
- [155] G.-G. Shan, H.-B. Li, J.-S. Qin, D.-X. Zhu, Y. Liao, Z.-M. Su, *Dalton Trans.* **2012**, *41*, 9590.
- [156] G.-G. Shan, D.-X. Zhu, H.-B. Li, P. Li, Z.-M. Su, Y. Liao, *Dalton Trans.* **2011**, *40*, 2947.
- [157] N. Zhao, Y.-H. Wu, J. Luo, L.-X. Shi, Z.-N. Chen, *Analyst* **2013**, *138*, 894.
- [158] S. Liu, H. Sun, Y. Ma, S. Ye, X. Liu, X. Zhou, X. Mou, L. Wang, Q. Zhao, W. Huang, *J. Mater. Chem.* **2012**, *22*, 22167.
- [159] Z. Luo, X. Yuan, Y. Yu, Q. Zhang, D. T. Leong, J. Y. Lee, J. Xie, *J. Am. Chem. Soc.* **2012**, *134*, 16662.
- [160] J. Liang, Z. Chen, J. Yin, G.-A. Yu, S. H. Liu, *Chem. Commun.* **2013**, *49*, 3567.
- [161] K. Fujisawa, Y. Izumi, A. Nagamatsu, K. Uno, O. Tsutsumi, *Mol. Cryst. Liq. Cryst.* **2012**, *563*, 50.
- [162] I. O. Koshevoy, Y.-C. Chang, A. J. Karttunen, J. R. Shakirova, J. Jänis, M. Haukka, T. Pakkanen, P.-T. Chou, *Chem. Eur. J.* **2013**, *19*, 5104.
- [163] J. Kuwabara, Y. Ogawa, A. Taketoshi, T. Kanbara, *J. Organomet. Chem.* **2011**, *696*, 1289.
- [164] C. Zhu, S. Li, M. Luo, X. Zhou, Y. Niu, M. Lin, J. Zhu, Z. Cao, X. Lu, T. Wen, Z. Xie, P. V. R. Schleyer, H. Xia, *Nat. Chem.* **2013**, *5*, 698.
- [165] Y. Kawamura, K. Goushi, J. Brooks, J. J. Brown, H. Sasabe, C. Adachi, *Appl. Phys. Lett.* **2005**, *86*, 071104.
- [166] R. Jin, *Nanoscale* **2010**, *2*, 343.
- [167] J. C. Sanchez, W. C. Troglar, *J. Mater. Chem.* **2008**, *18*, 3143.
- [168] M. A. Baldo, M. E. Thompson, S. R. Forrest, *Nature* **2000**, *403*, 750.
- [169] K. C. Wu, P. J. Ku, C. S. Lin, H. T. Shih, F. I. Wu, M. J. Huang, J. J. Lin, I. C. Chen, C. H. Cheng, *Adv. Funct. Mater.* **2008**, *18*, 67.
- [170] T. P. I. Saragi, T. Spehr, A. Siebert, T. Fuhrmann-Lieker, J. Salbeck, *Chem. Rev.* **2007**, *107*, 1011.
- [171] Y.-H. Kim, H.-C. Jeong, S.-H. Kim, K. Yang, S.-K. Kwon, *Adv. Funct. Mater.* **2005**, *15*, 1799.
- [172] C.-C. Wu, Y.-T. Lin, K.-T. Wong, R.-T. Chen, Y.-Y. Chien, *Adv. Mater.* **2004**, *16*, 61.
- [173] M.-T. Lee, C.-H. Liao, C.-H. Tsai, C. H. Chen, *Adv. Mater.* **2005**, *17*, 2493.
- [174] Z. Zhao, C. Y. K. Chan, S. Chen, C. Deng, J. W. Y. Lam, C. K. W. Jim, Y. Hong, P. Lu, Z. Chang, X. Chen, P. Lu, H. S. Kwok, H. Qiu, B. Z. Tang, *J. Mater. Chem.* **2012**, *22*, 4527.
- [175] J. Huang, X. Yang, J. Wang, C. Zhong, L. Wang, J. Qin, Z. Li, *J. Mater. Chem.* **2012**, *22*, 2478.
- [176] J. Huang, N. Sun, J. Yang, R. Tang, Q. Li, D. Ma, J. Qin, Z. Li, *J. Mater. Chem.* **2012**, *22*, 12001.
- [177] J. Huang, N. Sun, Y. Dong, R. Tang, P. Lu, P. Cai, Q. Li, D. Ma, J. Qin, Z. Li, *Adv. Funct. Mater.* **2013**, *23*, 2329.
- [178] S. Xue, L. Yao, S. Liu, C. Gu, F. Shen, W. Li, H. Zheng, H. Wu, Y. Ma, *J. Mater. Chem.* **2012**, *22*, 21502.
- [179] J. Zhou, Z. Chang, Y. Jiang, B. He, M. Du, P. Lu, Y. Hong, H. S. Kwok, A. Qin, H. Qiu, Z. Zhao, B. Z. Tang, *Chem. Commun.* **2013**, *49*, 2491.
- [180] J. Mei, J. Wang, J. Z. Sun, H. Zhao, W. Yuan, C. Deng, S. Chen, H. H. Y. Sung, P. Lu, A. Qin, H. S. Kwok, Y. Ma, I. D. Williams, B. Z. Tang, *Chem. Sci.* **2012**, *3*, 549.
- [181] H. Li, Z. Chi, X. Zhang, B. Xu, S. Liu, Y. Zhang, J. Xu, *Chem. Commun.* **2011**, *47*, 11273.
- [182] C. T. Chen, *Chem. Mater.* **2004**, *16*, 4389.

- [183] X. Du, J. Qi, Z. Zhang, D. Ma, Z. Y. Wang, *Chem. Mater.* **2012**, *24*, 2178.
- [184] M. Grell, D. D. C. Bradley, *Adv. Mater.* **1999**, *11*, 895.
- [185] M. Bertolotti, G. Sansoni, F. Scudieri, *Appl. Opt.* **1979**, *18*, 528.
- [186] S. Sergeyev, W. Pisula, Y. H. Geerts, *Chem. Soc. Rev.* **2007**, *36*, 1902.
- [187] M. O'Neill, S. M. Kelly, *Adv. Mater.* **2003**, *15*, 1135.
- [188] K. Binnemans, C. Görller-Walrand, *Chem. Rev.* **2002**, *102*, 2303.
- [189] S. H. Chen, H. Shi, B. M. Conger, J. C. Mastrangelo, T. Tsutsui, *Adv. Mater.* **1996**, *8*, 998.
- [190] A. C. Sentman, D. L. Gin, *Adv. Mater.* **2001**, *13*, 1398.
- [191] J.-H. Wan, L.-Y. Mao, Y.-B. Li, Z.-F. Li, H.-Y. Qiu, C. Wang, G.-Q. Lai, *Soft Matter* **2010**, *6*, 3195.
- [192] W. Z. Yuan, Z.-Q. P. Lu, C. Deng, J. W. Y. Lam, Z. Wang, E.-Q. Chen, Y. Ma, B. Z. Tang, *J. Mater. Chem.* **2012**, *22*, 3323.
- [193] Y. F. Chen, J. S. Lin, W. Z. Yuan, Z. Q. Yu, J. W. Y. Lam, B. Z. Tang, *Sci. China Chem.* **2013**, *56*, 1191.
- [194] S.-J. Yoon, J. H. Kim, K. S. Kim, J. W. Chung, B. Heinrich, F. Mathevet, P. Kim, B. Donnio, A.-J. Attias, D. Kim, S. Y. Park, *Adv. Funct. Mater.* **2012**, *22*, 61.
- [195] J. Liu, H. Su, L. Meng, Y. Zhao, C. Deng, J. C. Y. Ng, P. Lu, M. Faisal, J. W. Y. Lam, X. Huang, H. Wu, K. S. Wong, B. Z. Tang, *Chem. Sci.* **2012**, *3*, 2737.
- [196] X. Gu, J. Yao, G. Zhang, Y. Yan, C. Zhang, Q. Peng, Q. Liao, Y. Wu, Z. Xu, Y. Zhao, H. Fu, D. Zhang, *Adv. Funct. Mater.* **2012**, *22*, 4862.
- [197] a) N. Zhao, M. Li, Y. Yan, J. W. Y. Lam, Y. L. Zhang, Y. S. Zhao, K. S. Wong, B. Z. Tang, *J. Mater. Chem. C* **2013**, *1*, 4640; b) *Aggregation-Induced Emission: Applications*, (Ed: A. Qin, B. Z. Tang), Wiley, Singapore, **2013**.
- [198] C. Shi, Z. Guo, Y. Yan, S. Zhu, Y. Xie, Y. S. Zhao, W. Zhu, H. Tian, *ACS Appl. Mater. Interfaces* **2013**, *5*, 192.
- [199] S. H. Chen, D. Katsis, A. W. Schmid, J. C. Mastrangelo, T. Tsutsui, T. N. Blanton, *Nature* **1999**, *397*, 506.
- [200] A. Montali, C. Bastiaansen, P. Smith, C. Weder, *Nature* **1998**, *392*, 261.
- [201] E. Peeters, M. P. T. Christiaans, R. A. J. Janssen, H. F. M. Schoo, H. P. J. M. Dekkers, E. W. Meijer, *J. Am. Chem. Soc.* **1997**, *119*, 9909.
- [202] L. Heng, X. Wang, D. Tian, J. Zhai, B. Z. Tang, L. Jiang, *Adv. Mater.* **2010**, *22*, 4716.
- [203] S. Chen, J. Liu, Y. Liu, H. Su, Y. Hong, C. K. W. Jim, R. T. K. Kwok, N. Zhao, W. Qin, J. W. Y. Lam, K. S. Wong, B. Z. Tang, *Chem. Sci.* **2012**, *3*, 1804.
- [204] D. Li, J. Liu, R. T. K. Kwok, Z. Liang, B. Z. Tang, J. Yu, *Chem. Commun.* **2012**, *48*, 7167.
- [205] Y. Liu, Y. Tang, N. N. Barashkov, I. S. Irgibaeva, J. W. Y. Lam, R. Hu, D. Birimzhanova, Y. Yu, B. Z. Tang, *J. Am. Chem. Soc.* **2010**, *132*, 13951.
- [206] T. Han, J. W. Y. Lam, N. Zhao, M. Gao, Z. Yang, E. Zhao, Y. Dong, B. Z. Tang, *Chem. Commun.* **2013**, *49*, 4848.
- [207] X. Chen, X. Y. Shen, E. Guan, Y. Liu, A. Qin, J. Z. Sun, B. Z. Tang, *Chem. Commun.* **2013**, *49*, 1503.
- [208] S. Chen, Y. Hong, Y. Liu, J. Liu, C. W. T. Leung, M. Li, R. T. K. Kwok, E. Zhao, J. W. Y. Lam, Y. Yu, B. Z. Tang, *J. Am. Chem. Soc.* **2013**, *135*, 4926.
- [209] a) H. Shi, R. T. K. Kwok, J. Liu, B. Xing, B. Z. Tang, B. Liu, *J. Am. Chem. Soc.* **2012**, *134*, 17972; b) H. Shi, J. Liu, J. Geng, B. Z. Tang, B. Liu, *J. Am. Chem. Soc.* **2012**, *134*, 9569.
- [210] a) J. Mei, J. Tong, J. Wang, A. Qin, J. Z. Sun, B. Z. Tang, *J. Mater. Chem.* **2012**, *22*, 17063; b) J. Mei, Y. Wang, J. Tong, J. Wang, A. Qin, J. Z. Sun, B. Z. Tang, *Chem. Eur. J.* **2013**, *19*, 612; c) H. Shi, N. Zhao, D. Ding, J. Liang, B. Z. Tang, B. Liu, *Org. Biomol. Chem.* **2013**, *11*, 7289; d) Y. Yuan, R. T. K. Kwok, B. Z. Tang, B. Liu, *J. Am. Chem. Soc.* **2014**, *136*, 2546; e) D. Ding, J. Liang, H. Shi, R. T. K. Kwok, M. Gao, G. Feng, Y. Yuan, B. Z. Tang, B. Liu, *J. Mater. Chem. B* **2014**, *2*, 231.
- [211] a) Y. Yuan, R. T. K. Kwok, G. Feng, J. Liang, J. Geng, B. Z. Tang, B. Liu, *Chem. Commun.* **2014**, *50*, 295; b) H. Shi, J. Liu, J. Geng, B. Z. Tang, B. Liu, *J. Am. Chem. Soc.* **2012**, *134*, 9569; c) H. Wang, J. Liu, A. Han, N. Xiao, Z. Xue, G. Wang, J. Long, D. Kong, B. Liu, Z. Yang, D. Ding, *ACS Nano* **2014**, *8*, 1475.
- [212] a) Y. Li, R. T. K. Kwok, B. Z. Tang, B. Liu, *RSC Adv.* **2013**, *3*, 10135; b) X. Xu, S. Yan, Y. Zhou, R. Huang, Y. Chen, J. Wang, X. Weng, X. Zhou, *Bioorg. Med. Chem. Lett.* **2014**, *24*, 1654; c) Y. Li, R. T. K. Kwok, B. Z. Tang, B. Liu, *RSC Adv.* **2013**, *3*, 10135.
- [213] Y. Liu, C. Deng, L. Tang, A. Qin, R. Hu, J. Z. Sun, B. Z. Tang, *J. Am. Chem. Soc.* **2011**, *133*, 660.
- [214] Y. Yu, A. Qin, C. Feng, P. Lu, K. M. Ng, K. Q. Luo, B. Z. Tang, *Analyst* **2012**, *137*, 5592.
- [215] Y. Hong, L. Meng, S. Chen, C. W. T. Leung, L.-T. Da, M. Faisal, D.-A. Silva, J. Liu, J. W. Y. Lam, X. Huang, B. Z. Tang, *J. Am. Chem. Soc.* **2012**, *134*, 1680.
- [216] X. Wang, J. Hu, T. Liu, G. Zhang, S. Liu, *J. Mater. Chem.* **2012**, *22*, 8622.
- [217] C. Krause, T. Werner, C. Huber, O. S. Wolfbeis, *Anal. Chem.* **1999**, *71*, 1544.
- [218] W. Kaim, B. Schwederski, *Bioinorganic Chemistry: Inorganic Elements in the Chemistry of Life*, John Wiley & Sons Ltd., England, **1991**, p. 208.
- [219] X. Huang, X. Gu, G. Zhang, D. Zhang, *Chem. Commun.* **2012**, *48*, 12195.
- [220] V. Bhalla, A. Gupta, M. Kumar, *Dalton Trans.* **2013**, *42*, 4464.
- [221] T. Sanji, M. Nakamura, M. Tanaka, *Tetrahedron Lett.* **2011**, *52*, 3283.
- [222] H. Zhang, Y. Qu, Y. Gao, J. Hua, J. Li, B. Li, *Tetrahedron Lett.* **2013**, *54*, 909.
- [223] F. Sun, G. Zhang, D. Zhang, L. Xue, H. Jiang, *Org. Lett.* **2011**, *13*, 6378.
- [224] J.-H. Ye, L. Duan, C. Yan, W. Zhang, W. He, *Tetrahedron Lett.* **2012**, *53*, 593.
- [225] G. Huang, G. Zhang, D. Zhang, *Chem. Commun.* **2012**, *48*, 7504.
- [226] J. I. Steinfeld, J. Wormhoudt, *Annu. Rev. Phys. Chem.* **1998**, *49*, 203.
- [227] J. Wang, J. Mei, W. Yuan, P. Lu, A. Qin, J. Z. Sun, Y. Ma, B. Z. Tang, *J. Mater. Chem.* **2011**, *21*, 4056.
- [228] *Criminalistics: An Introduction to Forensic Science*, (Ed: R. Saferstein), Prentice Hall, Inc, Upper Saddle River, NJ, 9th edn, **2006**.
- [229] B. Wilshire, *Endeavour* **1996**, *20*, 12.
- [230] Y. Li, L. Xu, B. Su, *Chem. Commun.* **2012**, *48*, 4109.
- [231] Y.-S. Zheng, Y.-J. Hu, *J. Org. Chem.* **2009**, *74*, 5660.
- [232] D.-M. Li, Y.-S. Zheng, *Chem. Commun.* **2011**, *47*, 10139.
- [233] D.-M. Li, H. Wang, Y.-S. Zheng, *Chem. Commun.* **2012**, *48*, 3176.
- [234] S. K. Tripathy, J. Kumar, H. S. Nalwa, *Handbook of Polyelectrolytes and Their Applications*, American Scientific Publishers, Los Angeles, **2002**.
- [235] J. Duhamel, *Acc. Chem. Res.* **2006**, *39*, 953.
- [236] S. Zhang, J. M. Yan, A. J. Qin, J. Z. Sun, B. Z. Tang, *Sci. China Chem.* **2013**, *56*, 1253.
- [237] a) A. Pucci, G. Iasilli, F. Tantussi, F. Fuso, G. Ruggeri, *AIP Conf. Proc.* **2012**, *1459*, 89; b) F. Ciardelli, G. Ruggeri, A. Pucci, *Chem. Soc. Rev.* **2013**, *42*, 857.
- [238] C. Li, T. Wu, C. Hong, G. Zhang, S. Liu, *Angew. Chem. Int. Ed.* **2012**, *51*, 455.
- [239] B. J. Lawrence, R. H. Singer, L. M. Marselle, *Cell (Cambridge, Mass.)* **1989**, *57*, 493.
- [240] M. Hocek, M. Fojta, *Org. Biomol. Chem.* **2008**, *6*, 2233.
- [241] R. B. Mujumdar, L. S. Ernst, S. R. Mujumdar, C. J. Lewis, A. S. Waggoner, *Bioconj. Chem.* **1993**, *4*, 105.
- [242] Y. Yu, J. Liu, Z. Zhao, K. M. Ng, K. Q. Luo, B. Z. Tang, *Chem. Commun.* **2012**, *48*, 6360.

- [243] a) J. Liang, R. T. K. Kwok, H. Shi, B. Z. Tang, B. Liu, *ACS Appl. Mater. Interfaces* **2013**, *5*, 8784; b) Z. Song, Y. Hong, R. T. K. Kwok, J. W. Y. Lam, B. Liu, B. Z. Tang, *J. Mater. Chem. B* **2014**, *2*, 1717; c) X. Gu, G. Zhang, Z. Wang, W. Liu, L. Xiao, D. Zhang, *Analyst* **2013**, *138*, 2427.
- [244] T. Noguchi, T. Shiraki, A. Dawn, Y. Tsuchiya, L. T. N. Lien, T. Yamamoto, S. Shinkai, *Chem. Commun.* **2012**, *48*, 8090.
- [245] T. Kato, K. Hatanaka, *J. Biosci. Bioeng.* **2011**, *112*, 202.
- [246] K. Dhara, Y. Hori, R. Baba, K. Kikuchi, *Chem. Commun.* **2012**, *48*, 11534.
- [247] X.-M. Hu, Q. Chen, J.-X. Wang, Q.-Y. Cheng, C.-G. Yan, J. Cao, Y.-J. He, B.-H. Han, *Chem. Asian J.* **2011**, *6*, 2376.
- [248] M. Nakamura, T. Sanji, M. Tanaka, *Chem. Eur. J.* **2011**, *17*, 5344.
- [249] X. Shen, Q. Jiang, J. Wang, L. Dai, G. Zou, Z.-G. Wang, W.-Q. Chen, W. Jiang, B. Ding, *Chem. Commun.* **2012**, *48*, 11301.
- [250] I. Johnson, M. T. Z. Spence, *Molecular Probes Handbook, a Guide to Fluorescent Probes and Labeling Technologies*, 11th edn, Life Technologies, Paisley, **2010**.
- [251] Y. Wang, J. Y. J. Shyy, S. Chien, *Annu. Rev. Biomed. Eng.* **2008**, *10*, 1.
- [252] Y. Yu, C. Feng, Y. N. Hong, J. Z. Liu, S. J. Chen, K. M. Ng, K. Q. Luo, B. Z. Tang, *Adv. Mater.* **2011**, *23*, 3298.
- [253] F. Mahtab, Y. Yu, J. W. Y. Lam, J. Z. Liu, B. Zhang, P. Lu, X. X. Zhang, B. Z. Tang, *Adv. Funct. Mater.* **2011**, *21*, 1733.
- [254] J. R. Casey, S. Grinstein, J. Orlowski, *Nat. Rev. Mol. Cell Biol.* **2010**, *11*, 50.
- [255] A. Roos, W. F. Boron, *Physiol. Rev.* **1981**, *61*, 296.
- [256] P. Song, X. Chen, Y. Xiang, L. Huang, Z. Zhou, R. Wei, A. Tong, *J. Mater. Chem.* **2011**, *21*, 13470.
- [257] Y.-L. P. Ow, D. R. Green, Z. Hao, T. W. Mak, *Nat. Rev. Mol. Cell Biol.* **2008**, *9*, 532.
- [258] C. W. T. Leung, Y. Hong, S. Chen, E. Zhao, J. W. Y. Lam, B. Z. Tang, *J. Am. Chem. Soc.* **2013**, *135*, 62.
- [259] G. Masanta, C. S. Lim, H. J. Kim, J. H. Han, H. M. Kim, B. R. Cho, *J. Am. Chem. Soc.* **2011**, *133*, 5698.
- [260] Y. Li, Y. Wu, J. Zhang, M. Chen, R. Liu, F. Li, *Chem. Commun.* **2013**, *49*, 11335.
- [261] R. Hu, C. F. A. Gómez-Durán, J. W. Y. Lam, J. L. Belmonte-Vázquez, C. Deng, S. Chen, R. Ye, E. Peña-Cabrera, Y. Zhong, K. S. Wong, B. Z. Tang, *Chem. Commun.* **2012**, *48*, 10099.
- [262] Z. Zhao, J. Geng, Z. Chang, S. Chen, C. Deng, T. Jiang, W. Qin, J. W. Y. Lam, H. S. Kwok, H. Qiu, B. Liu, B. Z. Tang, *J. Mater. Chem.* **2012**, *22*, 11018.
- [263] a) W. Qin, K. Li, G. Feng, M. Li, Z. Yang, B. Liu, B. Z. Tang, *Adv. Funct. Mater.* **2013**, *24*, 635; b) Q. Zhao, K. Li, S. Chen, A. Qin, D. Ding, S. Zhang, Y. Liu, B. Liu, J. Z. Sun, B. Z. Tang, *J. Mater. Chem.* **2012**, *22*, 15128; c) D. Ding, K. Li, W. Qin, R. Zhan, Y. Hu, J. Liu, B. Z. Tang, B. Liu, *Adv. Healthc. Mater.* **2013**, *2*, 500.
- [264] M. Li, J. W. Y. Lam, F. Mahtab, S. Chen, W. Zhang, Y. Hong, J. Xiong, Q. Zheng, B. Z. Tang, *J. Mater. Chem. B* **2013**, *1*, 676.
- [265] a) Z. Wang, B. Xu, L. Zhang, J. Zhang, T. Ma, J. Zhang, X. Fu, W. Tian, *Nanoscale* **2013**, *5*, 2065; b) K. Li, Y. Jiang, D. Ding, X. Zhang, Y. Liu, J. Hua, S.-S. Feng, B. Liu, *Chem. Commun.* **2011**, *47*, 7323; c) J. Geng, K. Li, D. Ding, X. Zhang, W. Qin, J. Liu, B. Z. Tang, B. Liu, *Small* **2012**, *8*, 3655; d) K. Li, D. Ding, Q. Zhao, J. Sun, B. Z. Tang, B. Liu, *Sci. China Chem.* **2013**, *56*, 1228.
- [266] X. Zhang, X. Zhang, S. Wang, M. Liu, Y. Zhang, L. Tao, Y. Wei, *ACS Appl. Mater. Interfaces* **2013**, *5*, 1943.
- [267] a) K. Li, W. Qin, D. Ding, N. Tomczak, J. Geng, R. Liu, J. Liu, X. Zhang, H. Liu, B. Liu, B. Z. Tang, *Sci. Rep.* **2013**, *3*, 1150; b) K. Li, Z. Zhu, P. Cai, R. Liu, N. Tomczak, D. Ding, J. Liu, W. Qin, Z. Zhao, Y. Hu, X. Chen, B. Z. Tang, B. Liu, *Chem. Mater.* **2013**, *25*, 4181; c) J. Geng, Z. Zhu, W. Qin, L. Ma, Y. Hu, G. G. Gurzadyan, B. Z. Tang, B. Liu, *Nanoscale* **2014**, *6*, 939; d) Y. Huang, F. Hu, R. Zhao, G. Zhang, H. Yang, D. Zhang, *Chem. Eur. J.* **2014**, *20*, 158.
- [268] F. Oukacine, J. P. Quirino, L. Garrelly, B. Romestand, T. Zou, H. Cottet, *Anal. Chem.* **2011**, *83*, 4949.
- [269] E. Zhao, Y. Hong, S. Chen, C. W. T. Leung, C. Y. K. Chan, R. T. K. Kwok, J. W. Y. Lam, B. Z. Tang, *Adv. Healthc. Mater.* **2014**, *3*, 88.
- [270] D. Wang, J. Qian, S. He, J. S. Park, K.-S. Lee, S. Han, Y. Mu, *Biomaterials* **2011**, *32*, 5880.
- [271] D. R. Larson, W. R. Zipfel, R. M. Williams, S. W. Clark, M. P. Bruchez, F. W. Wise, W. W. Webb, *Science* **2003**, *300*, 1434.
- [272] K. Schenke-Layland, I. Riemann, O. Damour, U. A. Stock, K. Konig, *Adv. Drug Deliv. Rev.* **2006**, *58*, 878.
- [273] F. Helmchen, W. Denk, *Nat. Methods* **2005**, *2*, 932.
- [274] G. He, L. S. Tan, Q. Zheng, P. N. Prasad, *Chem. Rev.* **2008**, *108*, 1245.
- [275] D. Ding, C. C. Goh, G. Feng, Z. Zhao, J. Liu, R. Liu, N. Tomczak, J. Geng, B. Z. Tang, L. G. Ng, B. Liu, *Adv. Mater.* **2013**, *25*, 6083.
- [276] *Chemiluminescence in Analytical Chemistry* (Ed: A. M. Garcia-Campana, W. R. G. Baeyens), Marcel Dekker, New York, **2001**.
- [277] A. Roda, M. Guardigli, P. Pasini, M. Mirasoli, E. Michelini, M. Musiani, *Anal. Chim. Acta* **2005**, *541*, 25.
- [278] Y.-D. Lee, C.-K. Lim, A. Singh, J. Koh, J. Kim, I. C. Kwon, S. Kim, *ACS Nano* **2012**, *6*, 6759.
- [279] M. Giorgio, M. Trinei, E. Migliaccio, P. G. Pelicci, *Nat. Rev. Mol. Cell Biol.* **2007**, *8*, 722.
- [280] K. Zhang, R. J. Kaufman, *Nature* **2008**, *454*, 455.
- [281] C. Lu, G. Song, J.-M. Lin, *Trends Anal. Chem.* **2006**, *25*, 985.
- [282] S. J. Toal, K. A. Jones, D. Magde, W. C. Trogler, *J. Am. Chem. Soc.* **2005**, *127*, 11661.
- [283] M. Irie, T. Fukaminato, T. Sasaki, N. Tamai, T. Kawai, *Nature* **2002**, *420*, 759.
- [284] A. Kishimura, T. Yamashita, K. Yamaguchi, T. Aida, *Nat. Mater.* **2005**, *4*, 546.
- [285] W. Z. Yuan, Y. Tan, Y. Gong, P. Lu, J. W. Y. Lam, X. Y. Shen, C. Feng, H. H.-Y. Sung, Y. Lu, I. D. Williams, J. Z. Sun, Y. Zhang, B. Z. Tang, *Adv. Mater.* **2013**, *25*, 2837.
- [286] N. Zhao, Z. Yang, J. W. Y. Lam, H. H. Y. Sung, N. Xie, S. Chen, H. Su, M. Gao, I. D. Williams, K. S. Wong, B. Z. Tang, *Chem. Commun.* **2012**, *48*, 8637.
- [287] Y. Q. Dong, J. W. Y. Lam, A. J. Qin, Z. Li, J. Z. Sun, H. H. Y. Sung, I. D. Williams, B. Z. Tang, *Chem. Commun.* **2007**, *40*.
- [288] X. Luo, J. Li, C. Li, L. Heng, Y. Q. Dong, Z. Liu, Z. Bo, B. Z. Tang, *Adv. Mater.* **2011**, *23*, 3261.
- [289] a) X. Xue, Y. Zhao, L. Dai, X. Zhang, X. Hao, C. Zhang, S. Huo, J. Liu, C. Liu, A. Kumar, W.-Q. Chen, G. Zou, X.-J. Liang, *Adv. Mater.* **2014**, *26*, 712; b) A. Pérez, J. L. Serrano, T. Sierra, A. Ballesteros, D. de Saá, J. Barluenga, *J. Am. Chem. Soc.* **2011**, *133*, 8110; c) P. S. Salini, A. P. Thomas, R. Sabarinathan, S. Ramakrishnan, K. C. G. Sreedevi, M. L. P. Reddy, A. Srinivasan, *Chem. Eur. J.* **2011**, *17*, 6598.
- [290] a) Z. Shi, J. Davies, S.-H. Jang, W. Kaminsky, A. K. -Y. Jen, *Chem. Commun.* **2012**, *48*, 7880; b) T. Kato, K. Naka, *Chem. Lett.* **2012**, *41*, 1445; c) C.-C. Chang, M.-C. Hsieh, J.-C. Lin, T.-C. Chang, *Biomaterials* **2012**, *33*, 897.
- [291] a) K. A. N. Upamali, L. A. Estrada, P. K. De, X. Cai, J. A. Krause, D. C. Neckers, *Langmuir* **2011**, *27*, 1573; b) E. Cariati, V. Lanzeni, E. Tordin, R. Ugo, C. Botta, A. G. Schieroni, A. Sironi, D. Pasini, *Phys. Chem. Chem. Phys.* **2011**, *13*, 18005; c) J. R. Berenguer, E. Lalinde, M. T. Moreno, S. Sánchez, J. Torroba, *Inorg. Chem.* **2012**, *51*, 11665.
- [292] a) P. P. Kapadia, M. A. Magnus, D. C. Swenson, F. C. Pigge, *J. Mol. Struct.* **2011**, *1003*, 82; b) F. Anariba, L. L. Chng, N. S. Abdullah, F. E. H. Tay, *J. Mater. Chem.* **2012**, *22*, 19303; c) T. Tian, X. Chen, H. Li, Y. Wang, L. Guo, L. Jiang, *Analyst* **2013**, *138*, 991.
- [293] a) P. Alam, M. Karanam, A. R. Choudhury, I. R. Laskar, *Dalton Trans.* **2012**, *41*, 9276; b) Y. Yang, X. Su, C. N. Carroll, I. Aprahamian,

- Chem. Sci.* **2012**, *3*, 610; c) T. C. Bozeman, K. A. Edwards, K. M. Fecteau, M. G. Verde Jr., A. Blanchard, D. L. Woodall, N. Benfarero, J. R. Ford, J. L. Mullin, C. K. Prudente, H. J. Tracy, *J. Inorg. Organomet. Polym.* **2011**, *21*, 316.
- [294] a) X. Wang, A. R. Morales, T. Urakami, L. Zhang, M. V. Bondar, M. Komatsu, K. D. Belfield, *Bioconjug. Chem.* **2011**, *22*, 1438; b) M. K. Nayak, *J. Photochem. Photobiol. A: Chem.* **2012**, *241*, 26; c) P. Spearman, S. Tavazzi, L. Silvestri, A. Burini, A. Borghesi, P. Mercandelli, M. Panigati, G. D'Alfonso, A. Sironi, L. De Cola, *Proc. SPIE* **2012**, *8435*, 84352D.
- [295] a) S. Bhattacharya, S. K. Samanta, *Chem. Eur. J.* **2012**, *18*, 16632; b) M. Shimizu, Y. Asai, Y. Takeda, A. Yamatani, T. Hiyama, *Tetrahedron Lett.* **2011**, *52*, 4084; c) S. Kamino, A. Muranaka, M. Murakami, A. Tatsumi, N. Nagaoka, Y. Shirasaki, K. Watanabe, K. Yoshida, J. Horigome, S. Kameda, M. Uchiyama, S. Enomoto, *Phys. Chem. Chem. Phys.* **2013**, *15*, 2131.
- [296] a) J. Chahine, N. Saffon, M. Cantuel, S. Fery-Forgues, *Langmuir* **2011**, *27*, 2844; b) Y. M. Chabre, R. Roy, *Chem. Soc. Rev.* **2013**, *42*, 4657; c) S. Mukherjee, P. Thilagar, *Chem. Commun.* **2013**, *49*, 7292.
- [297] a) S. Odabas, E. Tekin, F. Turksoy, C. Tanyeli, *J. Mater. Chem. C* **2013**, *1*, 7081; b) J. B. Carroll, J. Braddock-Wilking, *Organometallics* **2013**, *32*, 1905; c) J. Y. Kim, T. Yasuda, Y. S. Yang, C. Adachi, *Adv. Mater.* **2013**, *25*, 2666.
- [298] a) S. Kumar, P. Singh, A. Mahajan, S. Kumar, *Org. Lett.* **2013**, *15*, 3400; b) N. B. Shustova, A. F. Cozzolino, S. Reineke, M. Baldo, M. Dincă, *J. Am. Chem. Soc.* **2013**, *135*, 13326; c) A. Singh, C.-K. Lim, Y.-D. Lee, J.-h. Maeng, S. Lee, J. Koh, S. Kim, *ACS Appl. Mater. Interfaces* **2013**, *5*, 8881.
- [299] a) S. Pogodin, N. Assadi, I. Agranal, *Struct. Chem.* **2013**, *24*, 1747; b) A. Bolzoni, L. Viglianti, A. Bossi, P. R. Mussini, S. Cauteruccio, C. Baldoli, E. Licandro, *Eur. J. Org. Chem.* **2013**, 7489; c) P. Zhang, W. Dou, Z. Ju, X. Tang, W. Liu, C. Chen, B. Wang, W. Liu, *Adv. Mater.* **2013**, *25*, 6112.
- [300] a) S. Guieu, J. Rocha, A. M.S. Silva, *Tetrahedron* **2013**, *69*, 9329; b) V. Sathish, A. Ramdass, Z.-Z. Lu, M. Velayudham, P. Thanasekaran, K.-L. Lu, S. Rajagopal, *J. Phys. Chem. B* **2013**, *117*, 14358; c) S. Fery-Forgues, S. Veesler, W. B. Fellows, L. M. Tolbert, K. M. Solntsev, *Langmuir* **2013**, *29*, 14718.
- [301] a) Y. Shigemitsu, M. Hagimori, N. Mizuyama, B.-C. Wang, Y. Tominaga, *Dyes Pigments* **2013**, *99*, 940; b) F. Canfarotta, M. J. Whitcombe, S. A. Piletsky, *Biotechnol. Adv.* **2013**, *31*, 1585; c) M. Kurita, M. Momma, K. Mizuguchi, H. Nakano, *Chem. Phys. Chem.* **2013**, *14*, 3898.
- [302] a) D. Zhao, G. Li, D. Wu, X. Qin, P. Neuhaus, Y. Cheng, S. Yang, Z. Lu, X. Pu, C. Long, J. You, *Angew. Chem. Int. Ed.* **2013**, *52*, 13676; b) T. Virgili, A. Forni, E. Cariati, D. Pasini, C. Botta, *J. Phys. Chem. C* **2013**, *117*, 27161; c) J. Hatai, S. Bandyopadhyay, *Chem. Commun.* **2014**, *50*, 64.
- [303] a) S.-L. Tou, G.-J. Huang, P.-C. Chen, H.-T. Chang, J.-Y. Tsai, J.-S. Yang, *Chem. Commun.* **2014**, *50*, 620; b) K. S. Bejoymohandas, T. M. George, S. Bhattacharya, S. Natarajan, M. L. P. Reddy, *J. Mater. Chem. C* **2014**, *2*, 515; c) S. Choi, J. Bouffard, Y. Kim, *Chem. Sci.* **2014**, *5*, 751.
- [304] a) S. Ozturk, S. Atilgan, *Tetrahedron Lett.* **2014**, *55*, 70; b) T. Noguchi, B. Roy, D. Yoshihara, Y. Tsuchiya, T. Yamamoto, S. Shinkai, *Chem. Eur. J.* **2014**, *20*, 381; c) X. Li, K. Ma, S. Zhu, S. Yao, Z. Liu, B. Xu, B. Yang, W. Tian, *Anal. Chem.* **2014**, *86*, 298.
- [305] a) I. S. Turan, F. P. Cakmak, F. Sozmen, *Tetrahedron Lett.* **2014**, *55*, 456; b) C. W. T. Leung, Y. Hong, J. Hanske, E. Zhao, S. Chen, E. V. Pletneva, B. Z. Tang, *Anal. Chem.* **2014**, *86*, 1263; c) Y. Yu, Z. Luo, D. M. Chevrier, D. T. Leong, P. Zhang, D.-E. Jiang, J. Xie, *J. Am. Chem. Soc.* **2014**, *136*, 1246.
- [306] a) S. Sharma, A. Dhir, C. P. Pradeep, *Sensor Actuat. B Chem.* **2014**, *191*, 445; b) N. Abid-Jarraya, H. Turki-Guermazi, K. Khemakhem, S. Abid, N. Saffon, S. Fery-Forgues, *Dyes Pigments* **2014**, *101*, 164; c) K. Tanabe, D. Kodama, M. Hasegawa, T. Kato, *Chem. Lett.* **2014**, *43*, 184.
- [307] a) L. Yao, S. Zhang, R. Wang, W. Li, F. Shen, B. Yang, Y. Ma, *Angew. Chem. Int. Ed.* **2014**, *53*, 2119; b) J. Jayabharathi, V. Thanikachalam, V. Kalaiarasi, K. Jayamoorthy, *Spectrochim. Acta A* **2014**, *120*, 389; c) K. Ariga, T. Mori, M. Akamatsu, J. P. Hill, *Thin Solid Films* **2014**, *554*, 32.
- [308] a) E. P. J. Parrott, N. Tan, R. Hu, J. A. Zeitler, B. Z. Tang, E. MacPherson, *Mater. Horiz.* **2014**, *1*, 251; b) T.-S. Hsiao, S.-L. Deng, K.-Y. Shih, J.-L. Hong, *J. Mater. Chem. C* **2014**, *2*, 4828; c) H. Shi, W. Zhang, X. Dong, X. Wu, Y. Wu, L. Fang, Y. Miao, H. Wang, *Dyes Pigments* **2014**, *104*, 34.
- [309] a) C. Zhang, C. Liu, X. Xue, X. Zhang, S. Huo, Y. Jiang, W.-Q. Chen, G. Zou, X.-J. Liang, *ACS Appl. Mater. Interfaces* **2014**, *6*, 757; b) P. Wang, X. Yan, F. Huang, *Chem. Commun.* **2014**, *50*, 5017.
- [310] a) Z. Liu, W. Xue, Z. Cai, G. Zhang, D. Zhang, *J. Mater. Chem. B* **2011**, *21*, 14487; b) X. Shen, G. Zhang, D. Zhang, *Org. Lett.* **2012**, *14*, 1744; c) F. Hu, Y. Huang, G. Zhang, R. Zhao, D. Zhang, *Tetrahedron Lett.* **2014**, *55*, 1471.
- [311] a) Y. Li, X. Hu, S. Tian, Y. Li, G. Zhang, S. Liu, *Biomaterials* **2014**, *35*, 1618; b) X.-L. Xin, M. Chen, Y.-b. Ai, F.-l. Yang, X.-L. Li, F. Li, *Inorg. Chem.* **2014**, *53*, 2922.
- [312] a) D. Wang, J. Qian, W. Qin, A. Qin, B. Z. Tang, S. He, *Sci. Rep.* **2014**, *4*, 4279; b) X. Zhang, X. Zhang, B. Yang, Y. Zhang, Y. Wei, *ACS Appl. Mater. Interfaces* **2014**, *6*, 3600; c) X. Zhang, X. Zhang, B. Yang, J. Hui, M. Liu, Z. Chi, S. Liu, J. Xu, Y. Wei, *Polym. Chem.* **2014**, *5*, 683; d) X. Zhang, X. Zhang, B. Yang, J. Hui, M. Liu, W. Liu, Y. Chen, Y. Wei, *Polym. Chem.* **2014**, *5*, 689.
- [313] a) X. Wang, H. Liu, J. Li, K. Ding, Z. Lv, Y. Yang, H. Chen, X. Li, *Chem. Asian J.* **2014**, *9*, 784; b) R. E. Scalise, P. A. Caradonna, H. J. Tracy, J. L. Mullin, A. E. Keirstead, *J. Inorg. Organomet. Polym.* **2014**, *24*, 431; c) M. Zhang, G. Feng, Z. Song, Y.-P. Zhou, H.-Y. Chao, D. Yuan, T. T. Y. Tan, Z. Guo, Z. Hu, B. Z. Tang, B. Liu, D. Zhao, *J. Am. Chem. Soc.* **2014**, *136*, 7241.